Supersymmetric dark matter at the LHC and in non-collider experiments.

Olga Bessidskaia

Master's Thesis

Supervisors: Johan Lundberg and Christophe Clement
Elementary Particle Physics Group
Fysikum
Stockholm University

April 3, 2012

Stockholms universitet

Abstract

Supersymmetry is a theory of elementary particle physics that can resolve several theoretical problems associated with the Standard Model of particle physics. Supersymmetry also provides a possible solution to the dark matter puzzle, by providing a plausible dark matter particle candidate.

A set of supersymmetric models, studied by the ATLAS experiment at the Large Hadron Collider (LHC), is examined in the first part of this work. The compatibility of the models investigated by ATLAS with existing constraints on the relic dark matter density and on the Higgs boson mass are examined. Modifications to these models are proposed in order to ensure compatibility with these experimental constraints. In the second part of this work, a large set of supersymmetric models, which could be detectable at the LHC, is considered. Using this set of models, we investigate the complementarity of the dark matter searches at the LHC with other direct and indirect dark matter searches.

Sammanfattning

Supersymmetri är en teori för ny fysik som kan lösa flera teoretiska problem med nuvarande standardmodell för partikelfysik. Supersymmetri medför även en möjlig lösning på gåtan om den mörka materian, genom att framföra en rimlig partikelkandidat för mörk materia.

I den första delen av rapporten undersöks en uppsättning supersymmetriska modeller, som har studerats i ATLAS-experimentet vid LHC. Vi undersöker hur förenliga dessa modeller är med experimentella begränsningar för densiteten för mörk materia och Higgs bosonens massa. Justeringar till modellerna föreslås med syftet att göra dem kompatibla med dessa experimentella begränsningar. I andra delen behandlas ett stort antal supersymmetriska modeller som skulle kunna upptäckas med LHC. Med dessa modeller som utgångspunkt undersöks hur komplementära sökningar efter mörk materia vid LHC är med sökningar vid andra direkta och indirekta detektionsexperiment.

Contents

1 Introduction

The Standard Model (SM) of particle physics describes the interactions of all known elementary particles through the strong, electromagnetic and weak forces. Despite the accuracy of predictions of the SM [ADL$^+$06], some theoretical problems remain unresolved and new physics on the TeV scale is expected. For instance, the Standard Model does not include dark matter, which constitutes the major part of the matter content of the Universe [LDH$^+$11].

Supersymmetry (SUSY) postulates that the laws of physics are invariant under a symmetry that transforms bosons into fermions and vice versa. The main implication of this is an extension of the SM particle spectrum: for each boson, there is a fermion superpartner; for each fermion, there is a boson superpartner. The lightest of the superpartners has properties that make it a plausible candidate for the cold dark matter in the Universe. Moreover, SUSY can resolve the hierarchy or naturalness problem, by introducing natural cancellations to otherwise diverging loop corrections to the Higgs boson mass.

While supersymmetric particles have not yet been discovered, experimental results have put limits on different SUSY parameters. There is in general a large number of parameters in SUSY models and it is impossible to know which of the infinitely many models is the correct one without experimental input. One strategy in addressing this problem is creating a model framework, by specififying a set of parameters, and fix all but a few, typically two, scanning over the non-frozen parameters. When comparing predictions from SUSY to experimental data, exclusion limits can be set in two-dimensional parameter space for that particular model framework.

At the Large Hadron Collider (LHC), SUSY particles could be produced and detected in high-energy proton-proton collisions. Other searches for dark matter are conducted by detectors, which aim to either interact directly with dark matter particles (direct detection) or to infer the presence of dark matter particles via detection of their annihilation products (indirect detection).

This work is composed of two parts. The first part (Sec. 3) is based on a set of supersymmetric models that have been searched for by the ATLAS collaboration at the LHC. The models predict values for physical observables, such as the amount of supersymmetric relic dark matter. These predicted values are compared to current observational limits and modifications to the models are introduced to better fit observational constraints. The second part (Sec. 4) is a study of the complementarity of the LHC experiments with other direct and indirect dark matter searches.

2 Theory

2.1 The Standard Model

The standard model of particle physics is the theory that describes the known elementary particles and their interactions. It is experimentally confirmed to a very high precision [ADL$^+$06]. The Standard Model addresses the following questions: What are the basic particles that constitute all matter? How do these particles interact? How can the rates of various elementary particle reactions be predicted? The particle content, or spectrum, of the SM is given below.

2.1.1 The Standard Model particle spectrum

According to the SM, all the matter in the Universe consists of elementary spin-$\frac{1}{2}$ fermions, which interact by exchanging bosonic force fields. The fermions are divided into three families, or generations, as shown in Table 1. The families differ from each other by their mass: the first family being the lightest and the third family the heaviest. There are two types of fermions: leptons and quarks. There are six types or "flavours" of quarks, three flavours of leptons and three flavours of neutrinos.

	1st family	2nd family	3rd family	charge
Quarks	up (u)	charm (c)	top (t)	$+2/3$
	down (d)	strange (s)	bottom (b)	$-1/3$
Neutrinos	ν_e	ν_μ	ν_τ	0
Leptons	electron (e)	muon (μ)	tauon (τ)	-1

Table 1: The fermions of the Standard Model, grouped in three families. The different particle species are referred to as flavours.

Quarks are confined to bound states, "hadrons", such as protons and neutrons. A proton consists of three valence quarks: two up-quarks and one down quark, which are held together by gluons - mediators of the strong force. In addition, there is a number of sea quarks in the proton, which appear and disappear continuously. Quarks carry a baryon number $B = 1/3$. They can interact through the strong, electromagnetic and weak force.

An example of charged leptons are electrons, which are bound to atomic nuclei by exchanging the quanta of the electromagnetic force: photons. The carriers of the weak force are the charged $W^\pm$ bosons and neutral Z^0 bosons. Charged leptons interact electromagnetically and by the weak force. Neutrinos interact by the weak force only. The spin 1 force carriers are presented in Table 2, together with their masses. Charged leptons and neutinos carry a lepton number $L = 1$. For the purpose of this text, only charged particles

SM particle	Notation	Force mediated	Mass
Gluon	g	Strong	0 GeV
Photon	γ	Electromagnetic	0 GeV
Z^0 boson	Z	Weak (neutral current)	91.2 GeV
$W^{\pm}$ boson	$W^{\pm}$	Weak (charged currents)	80.4 GeV

Table 2: The force carriers in the Standard Model.

with non-zero lepton number are referred to as "leptons".

The SM predicts the existence of one Higgs boson, with spin 0. The Higgs boson is required within the SM to explain how elementary particles acquire mass.

Each elementary particle has an antiparticle in the SM. The antiparticles have the same properties such as mass and spin, except that they have opposite charge and opposite baryon or lepton number.

The helicity of a particle is a measure of the relation between its spin and momentum. The projection of the spin on the momentum of a particle can either take a positive or a negative value. Particles with a spin projection in the same direction as its momentum have right-handed helicity. Particles with a spin projection opposite to the momentum are called left-handed. The weak force only couples to left-handed fermions. Only left-handed neutrinos and right-handed anti-neutrinos have been observed in Nature.

2.2 Problems with the Standard Model

The SM is a very good description of particle physics as we know it, having excellent agreement with high precision electroweak data [ADL$^+$06]. Nevertheless, there are some fundamental problems associated with the SM, a few of which are listed below.

One problem is related to the Higgs mechanism, called the hierarchy problem or naturalness problem. Another shortcoming of the SM is that it must be incomplete since there is no SM particle that can explain the dark matter in our Universe. New physics is required to resolve both of these questions.

2.2.1 The naturalness problem

The Standard Model relies on the existence of a Higgs field to explain that elementary particles have mass. After electroweak symmetry breaking, the vacuum expectation value (v.e.v.) of the Higgs field is non-zero, which gives mass to the SM fermions and the W and Z^0 bosons, while preserving the gauge invariance of the gauge boson [MS93]. A consequence of the Higgs mechanism is the existence of a massive Higgs boson.

From fits to electroweak data, the Higgs boson should have a mass of at most a few hundred GeV [Erl10], [ADL$^+$06]. However, higher order radiative corrections to the Higgs mass squared diverge. This divergence is proportional to Λ^2 [JKG96], where Λ is the highest energy scale in the theory. Often, Λ is assumed to be $\Lambda \sim 10^{16}$ GeV, the so-called "Grand Unification Scale" at which the strong, electromagnetic and weak couplings become of similar strength. Hence there is an incompability between electroweak fits, which predict a low Higgs mass, and the theory that produces an enormous Higgs mass. It would be possible to enormously fine tune the SM parameters to achieve cancellation of the corrections of the Higgs mass, but such an enormous fine tuning is considered unlikely unless it is generated by a new symmetry of Nature.

2.2.2 Dark matter

The first evidence for dark matter was the analysis of rotation curves of spiral galaxies. Circular velocities of clouds of neutral hydrogen can be measured as a function of R, the distance from the center of the galaxy. By Kepler's law, the circular velocity v of a body orbiting a galaxy at a distance R from it's center is given by:

$$v = \sqrt{\frac{GM(R)}{R}} \quad , \tag{1}$$

where $M(R)$ is the mass of the galaxy contained inside a radius R [Lid03]. Once R is large enough to enclose almost the entire galaxy mass, the velocity of orbiting bodies should decrease with increasing distance as $R^{-1/2}$. However, in almost all cases, the velocities rise quickly for small R and they stay constant as far as can be measured [Lid03], as shown in Fig. 1.

One way to explain these rotation curves is by the presence of a large amount of invisible mass, termed dark matter, which interacts only through gravity and possibly the weak force. The dark matter is believed to form a spherical halo, enclosing the visible disc-like part of the spiral galaxy. From measured velocities of orbiting hydrogen clouds and the predicitons on rotation velocities from ordinary matter, the contribution to rotational velocity from dark matter can be inferred, as shown in Fig. 1 for the galaxy NGC 6503.

A strong piece of evidence for dark matter is the so-called Bullet Cluster [CBG$^+$06], a cluster merger located 3.4 billion light years away. As shown in the composite image in Fig. 2, hot gas from the clusters collides and emits X-rays, shown in red. The gas constitutes the major part of the baryonic content of the clusters. However, from gravitational lensing, it is found that the mass of the Bullet Cluster is concentrated to the blue areas in Fig. 2. This mass has passed through the collision zone without interacting

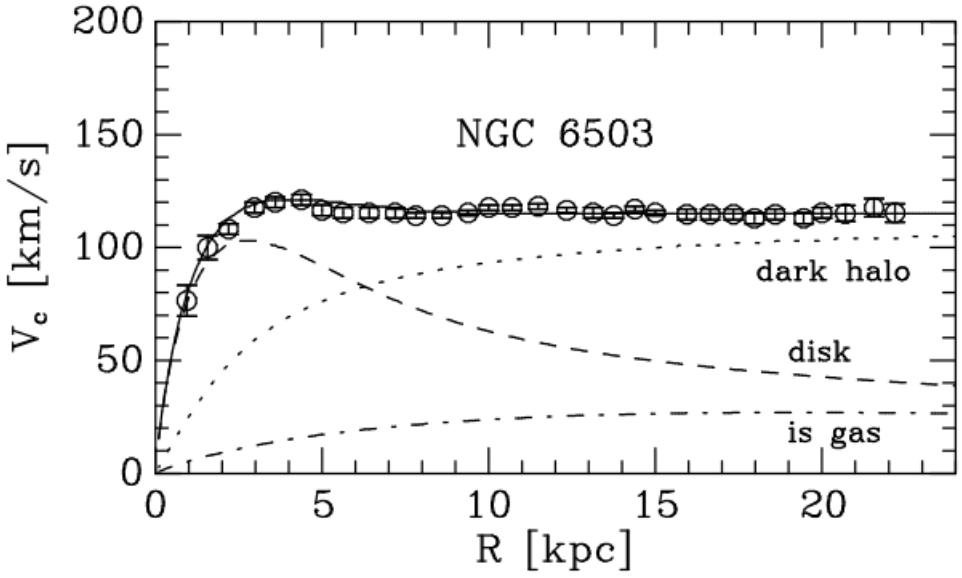

Figure 1: Rotation curves for the galaxy NGC 6503. The circular velocity V_c is shown as a function of the radius R in kpc. Velocities corresponding to data are shown as circles. Contributions to the velocity from interstellar gas, the galactic disc and dark matter halo are inferred. The image is obtained from [Fuc00].

electromagnetically. Observations of the Bullet Cluster show that it consists mainly of non-baryonic matter that only interacts by gravity and possibly the weak force.

Another piece of evidence for dark matter comes from precise measurements of the Cosmic Microwave Background (CMB) performed by the Wilkinson Microwave Anisotropy Probe (WMAP) satellite. The CMB image from WMAP is shown in Fig. 3. The CMB originates from the era when the Universe became transparent to light, when the age of the Universe was a few hundred thousand years. It is very uniform: the difference between so called hot spots and cold spots is only 400 μK, while the average temperature of the CMB is 2.7K. From the overdensities (hot spots) observed in the CMB, the galaxy clusters later developed. During this era, matter would contract by gravity and dilute by the radiation pressure exerted by the baryonic matter upon contraction. From the properties of the temperature fluctuations, it is concluded that the major part of dark matter is cold [BG04], or non-relativistic. From fits of the WMAP measurements of the CMB to a cosmological model, it is inferred that more than 80% of the total matter content in the Universe is constituted by non-baryonic cold dark matter [LDH$^+$11] .

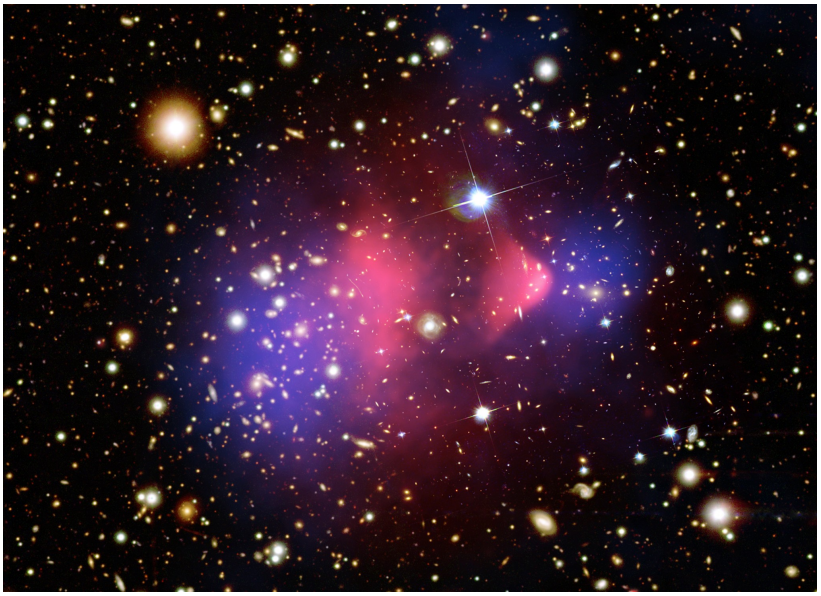

Figure 2: A composite image showing the galaxy cluster merger NGC 6503, known as the Bullet Cluster. The distribution of mass, as measured by gravitational lensing, is shown in blue. The distribution of heated baryonic matter, as measured by X-ray emission, is shown in red. The image is obtained from Ref. [NAS].

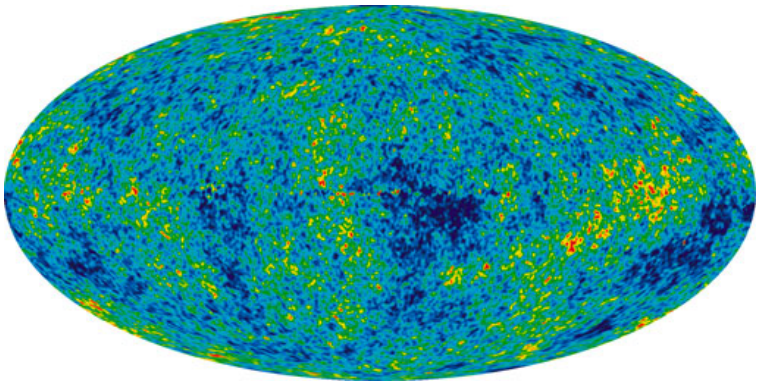

Figure 3: Measurements of the Cosmic Microwave Background from seven years of data from WMAP over the whole sky in galactic coordinates. The image shows temperature fluctuations from 13.7 billion years ago as differences in colour. The red areas are so-called hot spots, the blue areas are cold spots. The temperature fluctuations are of the size ± 200 μK, whereas the mean temperature is 2.7 K. The image was obtained from Ref. [CMB].

In summary, a valid dark matter candidate should be stable over cosmological time scales, not interact by the strong and electromagnetic forces and be non-baryonic and non-relativistic. There is no particle in the SM that can explain dark matter. Most of the dark matter is believed to consist of elementary particles which may not have been discovered yet. One of the leading candidates beyond the SM are Weakly Interacting Massive Particles (WIMPs), with masses in the range 10 GeV to some TeV. WIMP dark matter is well motivated by both cosmology and particle physics. Motivation for WIMPs constituting cold dark matter, and an overview and comparison with other cold dark matter candidates is given in Ref. [JKG96].

2.3 Supersymmetry

Supersymmetry [Mar97], [Fay76], [FF78], [DK98] is the idea that the laws of physics are invariant under exchange of bosons and fermions. Supersymmetry must be a broken rather than a perfect symmetry, otherwise the SUSY particles would have the same mass as their partners and should have been observed already.

In the Minimal Supersymmetric extension of the Standard Model (MSSM), which we are considering, there are 124 free parameters [Mar97], which include the masses of SUSY particles (sparticles), couplings and Higgs parameters. The SM particle spectrum is greatly extended in the MSSM, as each SM particle should have a superpartner. Some features of SUSY is an elegant solution to the naturalness problem and the prediction of the existence of a particle that could consitute cold dark matter.

2.3.1 The particle spectrum of the MSSM

The superpartners have the same properties, such as couplings and quantum numbers as their twin particles, but their spin differs by 1/2. In the MSSM, every SM spin 1/2 fermion has a bosonic superpartner of spin 0 with a prefix "s" (sfermion, selectron). Every SM spin 1 boson has a fermionic superpartner of spin 1/2 with an "ino" suffix (gluino, higgsino). The superpartners are labelled with a $\sim$: $\tilde{e}$ for selectrons, $\tilde{g}$ for gluinos etc. A summary of the SUSY particle spectrum is given in Table 3.

The MSSM requires two Higgs doublets to provide for masses to all SM and SUSY particles. This results in five physical Higgs bosons. Two of them are CP-even and neutral, denoted h^0 (the lighter) and H^0 (the heavier). In addition, there is a neutral CP-odd higgs A^0 and two oppositely charged higgses, $H^{\pm}$.

In the MSSM, there is one fermionic degree of freedom for each bosonic degree of freedom [JKG96]. This has consequences for the MSSM particle spectrum and is related to helicity. SM leptons have spin 1/2, which allows for two helicities. On the other hand, sleptons have spin 0 and can only

SM particle	Spin	Superpartner	Spin
quarks (q)	1/2	squarks ($\tilde{q}$)	0
neutrinos (ν)	1/2	sneutrinos ($\tilde{\nu}$)	0
leptons (l)	1/2	sleptons ($\tilde{l}$)	0
gluons (g)	1	gluinos ($\tilde{g}$)	1/2
photon (γ)	1	neutralinos	1/2
Z^0 boson (Z^0)	1	($\tilde{\chi}_1^0, \tilde{\chi}_2^0, \tilde{\chi}_3^0, \tilde{\chi}_4^0$)	
Neutral Higgs bosons (h^0, H^0)	0		
$W^\pm$ boson ($W^\pm$)	1	charginos	1/2
Charged Higgs boson ($H^\pm$)	1	($\tilde{\chi}_1^\pm, \tilde{\chi}_2^\pm$)	
Neutral Higgs boson (A^0)	0		

Table 3: The SM particles and their superpartners in the MSSM. The neutralinos $\tilde{\chi}_i^0$ are linear combinations of neutral binos, winos and higgsinos. The charginos $\tilde{\chi}_i^\pm$ are linear combinations of charged winos and higgsinos.

have one helicity. Therefore, there are two sleptons for each charged SM lepton, one corresponding to left-handed leptons and one corresponding to right-handed leptons. As SM neutrinos can only have left-handed helicity, there are no right-handed sneutrinos. The right-handed sfermions do not interact by the weak force and can have a mass that is different from the corresponding left-handed sparticle.

In the SM, linear combinations of the interaction fields B^0 and W_i form the mass eigenstates known as photons, Z^0 bosons and $W^\pm$ bosons. The interaction fields have superpartners called binos and winos, with the corresponding mass parameters M_1 and M_2.

Charged winos and higgsinos of the MSSM mix after electroweak symmetry breaking, forming mass eigenstates called charginos: $\tilde{\chi}_1^\pm, \tilde{\chi}_2^\pm$. By convention, $\tilde{\chi}_1^\pm$ is the lightest chargino and $\tilde{\chi}_2^\pm$ is the heaviest. The mass and interaction eigenstates are related by the chargino mixing matrix $\mathbf{M}_C$:

$$\mathbf{M_C} = \begin{pmatrix} M_2 & \sqrt{2}M_W \sin\beta \\ \sqrt{2}M_W \cos\beta & \mu \end{pmatrix}. \tag{2}$$

Here μ is a Higgs parameter, M_2 is the wino mass, M_W is the mass of the $W^\pm$ boson and $\sin\beta$ is related to the Higgs parameter $\tan\beta$. The mass eigenstates correspond to particles which may be detected and whose masses can be measured. Their content in terms of the interaction fields determines how the charginos will interact.

For neutral sparticles, there are four interaction fields: bino, neutral wino, and two neutral higgsino fields. Linear combinations of these fields form mass eigenstates that are called neutralinos and denoted $\tilde{\chi}_1^0, \tilde{\chi}_2^0, \tilde{\chi}_3^0, \tilde{\chi}_4^0$. By convention, the subscript 1 denotes the lightest neutralino, the subscript 2 the second lightest and so forth. The neutralinos are related to the inter-

action eigenstates through the neutralino mixing matrix $\mathbf{M}_N$:

$$\mathbf{M_N} = \begin{pmatrix} M_1 & 0 & -M_Z \sin\theta_W \cos\beta & M_Z \sin\theta_W \sin\beta \\ 0 & M_2 & M_Z \cos\theta_W \cos\beta & -M_Z \cos\theta_W \sin\beta \\ -M_Z \sin\theta_W \cos\beta & M_Z \cos\theta_W \cos\beta & 0 & -\mu \\ M_Z \sin\theta_W \sin\beta & -M_Z \cos\theta_W \sin\beta & -\mu & 0 \end{pmatrix} \quad (3)$$

In this matrix, θ_W is the Weinberg angle, one of the fundamental parameters of the SM [MS93]. The parameters M_Z and M_W are masses of the Z^0 and $W^\pm$ bosons. On the diagonal, M_1 is the bino mass and M_2 is the wino mass. The elements $\cos\beta$ and $\sin\beta$ can be seen as ways of expressing a Higgs parameter; μ is the Higgs mixing parameter. In this work, we use the term "gaugino" to label the superpartners of the electroweak gauge bosons, which will be $\tilde{\chi}_1^0$, $\tilde{\chi}_2^0$, $\tilde{\chi}_1^\pm$ for our models. The heavier chargino $\tilde{\chi}_2^\pm$ and neturalinos $\tilde{\chi}_3^0$, $\tilde{\chi}_4^0$ will be higgsino-like in our models.

2.3.2 Phenomenological MSSM

Within the MSSM, different assumptions, for example on the supersymmetrybreaking mechanism, can be made in order to reduce the 124-dimensional parameter space to a more manageable number of dimensions. For example, assumptions of the supersymmetry breaking mechanism can be made. The advantage of the phenomenological Minimal Supersymmetric Standard Model (pMSSM) is that no assumption about the supersymmetry breaking mechanism is made, as such assumptions generally strongly constrain the SUSY mass hierarchies. To reduce the number of free parameters, phenomenological constraints are applied to the MSSM. The constraints are that there is no additional source of CP-violation to the SM from SUSY and that there is no neutral particle that can mediate a flavour changing process. These constraints reduce the number of free parameters to 25 [Mar97]. The parameters are different SUSY mass parameters, masses for Higgs bosons, trlinilear couplings, the top quark mass and the ratio of Higgs doublet v.e.v.s $\tan\beta$. All SUSY models considered in this work are within the pMSSM framework.

2.3.3 R-parity

Without additional restrictions, SUSY contains baryon and lepton number violating interactions, which imply predictions of proton decays. As protons are stable over a time scale of 10^{32} years [Nak10], an additional conserved quantum number is introduced, to remove these interactions from the theory. This discrete quantity is called R-parity and is given by:

$$R = (-1)^{3(B-L)+2S}. \quad (4)$$

Here B is the baryon number, L is the lepton number and S is the spin.

R-parity has value $R = 1$ for all SM particles and $R = -1$ for SUSY particles. It is a multiplicative symmetry: the R-parity of a system is the product of the R-parity of its components. Therefore, if R-parity is conserved, a SUSY particle can never decay into only SM particles. This implies that the Lightest Supersymmetric Particle (LSP) must be absolutely stable. If SUSY particles are produced from SM particles in accelerators, they must be created in pairs to preserve R-parity. In this work, it is always assumed that R-parity is conserved.

2.3.4 SUSY and the SM problems

If the LSP is neutral, this particle would not interact electromagnetically. Assuming conservation of R-parity, the LSP will be stable over cosmological timescales. The most commonly considered LSP is the lightest neutralino [JKG96], a linear combination of neutral gauginos and higgsinos. Neutralinos carry no baryon number. A neutralino with a mass on the GeV scale would thus provide a massive neutral non-baryonic elementary particle as a candidate for Weakly Interacting Massive Particles. In this work, only neutralino LSPs are considered.

SUSY resolves the naturalness problem by introducing additional corrections to the Higgs mass squared. These corrections are related to the diverging terms by a factor of -1: in SUSY, for every boson loop there is a fermion loop that cancels it. This implies a natural cancellation of the diverging Higgs loop corrections. The quadratic dependence of corrections to the Higgs mass squared on $\Lambda \sim 10^{16}$ GeV is reduced to at most a logarithmic dependence [JKG96]. In this way, the artificial fine-tuning is avoided and the naturalness problem is solved. For the cancellation to occur, the mass difference between SM particles and their superpartners should not be much greater a few TeV.

2.4 Experimental constraints on SUSY models

For the supersymmetric models considered in this work, three experimental constraints are applied. The three constraints are upper limits on the dark matter density from WMAP, lower limits on the Higgs mass from LEP and existing measurements on the branching ratio $\mathrm{Br}(b \to s + \gamma)$. These three constraints are described in detail below.

2.4.1 The dark matter constraint

If there is a stable particle, such as a stable neutralino LSP, it would exist in equilibrium abundance in the early hot dense Universe, while the temperature of the Universe is greater than the particle's mass ($kT > mc^2$). As neutralinos are their own anti-particles, two neutralino LSPs could pair

annihilate, producing standard model particles only. The equilibrium abundance is maintained by the annihilation of the heavier LSPs into lighter SM fermions f and vice versa: $\tilde{\chi}_1^0\tilde{\chi}_1^0 \leftrightarrow f\bar{f}$. In thermal equilibrium, the forward and backward reactions occur at the same rate.

As the Universe expands and cools below the LSP mass, LSP annihilation becomes favoured above production and the equilibrium abundance drops exponentially, as shown in Fig. 4. The dilution and cooling of the Universe terminates LSP annihilation once the rate of the annihilation reaction ($\tilde{\chi}_1^0\tilde{\chi}_1^0 \rightarrow f\bar{f}$) becomes lower than the expansion rate of the Universe. This is called freeze-out. The neutralino LSPs essentially stop annihilating and a so-called relic density of LSPs remains.

In Fig. 4, the equilibrium density N_{EQ} for different annihilation cross sections σ_A is shown, where $\langle\sigma_A v\rangle$ is the cross section for the process $\tilde{\chi}_1^0\tilde{\chi}_1^0 \rightarrow f\bar{f}$, multiplied by the velocity of the LSP. The brackets denote that an average is calculated over the LSP velocities. The temperature decreases as the Universe evolves towards the right in Fig. 4. For a higher $\langle\sigma_A v\rangle$, the WIMPs stay in equilibrium longer, leaving a smaller relic abundance.

The model discussed above is described by the Boltzmann equation, which can be solved numerically, as is done in DarkSUSY [GEU+04] for different SUSY models. The relic dark matter density calculated by DarkSUSY can be compared with experimental limits from WMAP, given a certain SUSY model.

Another process that could decrease the dark matter density is coannihilations. Coannihilations can occur when the LSP and another sparticle with the same quantum number are close in mass. In this case, scattering of the LSP off a SM particle can convert the LSP into the heavier sparticle [JKG96]. If the annihilation cross section of this sparticle is larger for the LSP, the effect is a lower relic dark matter density. In addition, the two different sparticles can annihilate with each other, further decreasing the relic dark matter density.

The fits to 7 years of WMAP data with a model that includes a cosmological constant and dark matter, give a relic dark matter density [LDH+11] of:

$$\Omega_c h^2 = 0.1109 \pm 0.0056, \tag{5}$$

where h is the reduced Hubble constant in units of 100 km s^{-1} Mpc^{-1}. The cosmological density of cold dark matter Ω_c is given in terms of $\Omega = \rho_c/\rho_{\mathrm{crit}}$, where ρ_c is the average cosmological density of the cold dark matter and ρ_{crit} is the critical density. In Sec. 3, an upper bound of two standard deviations above the WMAP7 central value is used. Thus we demand:

$$\Omega_c h^2_{\mathrm{max}} \leq 0.1221. \tag{6}$$

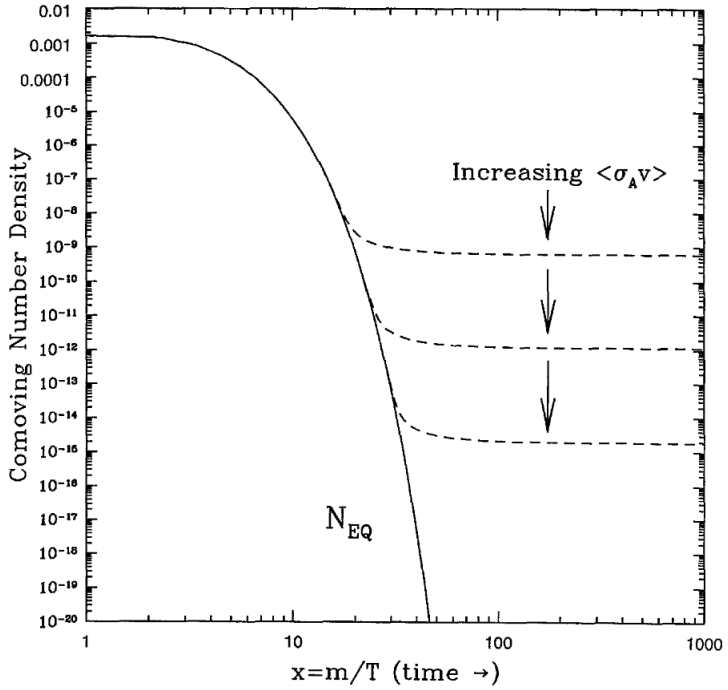

Figure 4: The relic LSP density for different velocity averaged annihilation cross sections $\langle \sigma_A v \rangle$ are shown as broken lines. The equilibrium density is shown by the solid curve. The mass m represents the $\tilde{\chi}_1^0$ mass and T is the temperature of the Universe in the same units. The paramter $x = m/T$ increases with time, as the Universe cools. The image is obtained from Ref. [Fuc00].

In Sec. 4, an upper bound of three standard devations is demanded:

$$\Omega_c h^2_{\max} \leq 0.1277. \tag{7}$$

No lower limit is applied to the dark matter density, allowing the SUSY LSPs to constitute only part of the total cold dark matter in the Universe.

2.4.2 The Higgs boson mass constraint

The constraint from LEP experiments on the mass of the Standard Model Higgs is $m_h > 114.4$ GeV [tag03]. The exact exclusion mass limits on the Higgs boson mass from LEP rely on the combination of different search channels and thus depend on the different decay branching ratios. In SUSY models, these branching ratios are altered as well as the Higgs production cross sections. Thus, for each SUSY model, the lower limit of 114.4 GeV needs to be recomputed and may in fact be lower.

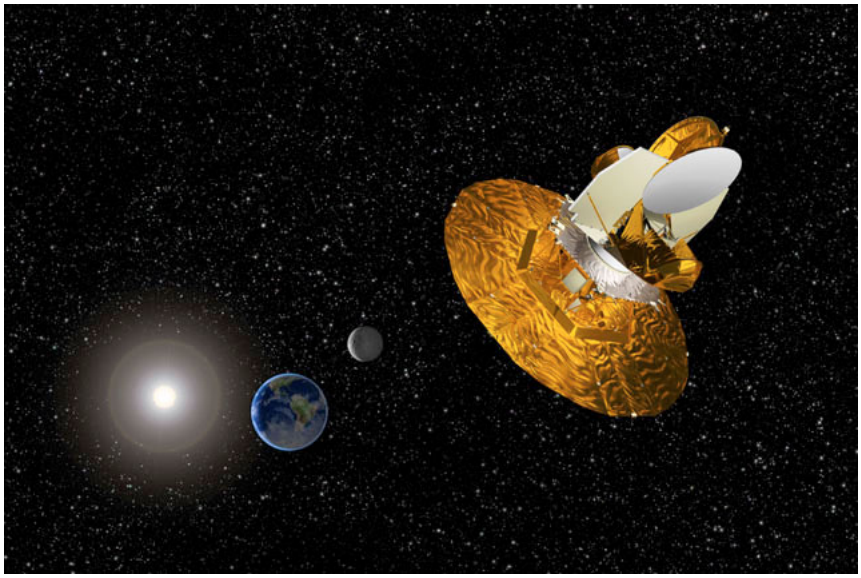

Figure 5: An artist impression of WMAP satellite. The image is obtained from Ref. [WMA].

The SUSY parameter that determines the Higgs boson mass at lowest order in the MSSM is $\tan\beta$, the ratio of the vacuum expectation values (v.e.v.s) for the two Higgs doublets:

$$\tan\beta = \frac{v_u}{v_d}. \tag{8}$$

The vacuum expectation value v_d refers to the Higgs doublet that gives a mass to down-type particles, v_u refers to the Higgs doublet that gives mass to up-type particles. At lowest order, the Higgs boson mass is bounded from above by the following [Mar97] expression:

$$m_{h^0} \leq m_Z |\cos 2\beta|. \tag{9}$$

This lowest order approximation is always smaller than the mass of the Z^0 boson, which is 91.2 GeV [Nak10]. However, significant corrections at next to leading order raise this value. The largest radiative correction [Zer10] at next to leading order is:

$$m_{h^0}^2 \leq m_Z^2(\cos 2\beta)^2 \; + \; \frac{3G_F}{\sqrt{2}\pi^2} m_t^4 \left[\log\left(\frac{m_{\tilde{t}}^2}{m_t^2}\right) + \frac{X_t^2}{m_{\tilde{t}}^2}\left(1 - \frac{1}{12}\frac{X_t^2}{m_{\tilde{t}}^2}\right)\right]. \tag{10}$$

Here G_F is the Fermi coupling constant, $G_F = 1.166 \cdot 10^{-5}$ GeV^{-2}, m_t is the mass of the standard model top quark, and $m_{\tilde{t}}$ is the mass of the stop squark. The quantity X_t is:

$$X_t = A_t - \mu/\tan\beta. \tag{11}$$

In this expression, A_t is the top quark trilinear coupling.

Considering Eq. (10) as a function of $\frac{X_t^2}{m_{\tilde{t}}^2}$, the Higgs mass correction has a maximum at $\frac{X_t^2}{m_{\tilde{t}}^2} = 6$. This condition is referred to as "maximum stop mixing", which is achieved by setting $A_t = \mu/\tan\beta + \sqrt{6}m_{\tilde{t}}$. The condition $X_t = 0$ is called "minimum stop mixing" and occurs at $A_t = \mu/\tan\beta$.

The values of $\tan\beta$, the stop mass $m_{\tilde{t}}$ and the coupling parameter A_t play an important role in determining the Higgs boson mass m_{h^0} in the MSSM.

2.4.3 The $\mathrm{Br}(b \to s + \gamma)$ constraint

One of the strictest constraints on pMSSM comes from FCNC processes, in particular the decay $b \to s + \gamma$ [JKG96], where a bottom quark radiates a photon and becomes a strange quark. The branching ratio has been measured experimentally and has a predicted value from the standard model [MAB+07] via penguin diagrams:

$$\mathrm{Br}(b \to s + \gamma)_{\mathrm{SM}} = (3.15 \pm 0.23) \cdot 10^{-2}\ \%. \tag{12}$$

The Feynman diagram for this process at lowest order involves the exchange of a charged W^- boson, as shown in Fig. 6.

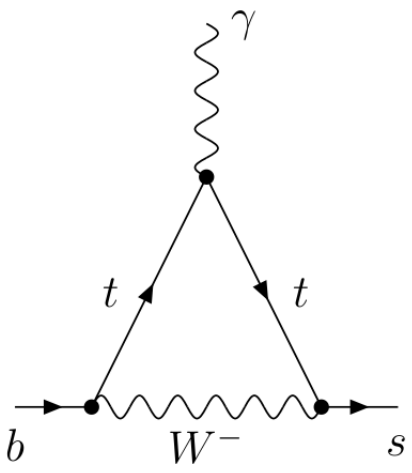

Figure 6: A diagram at lowest order for the process $b \to s + \gamma$ in the SM [MPR98].

The experimental value [(HFAG)07] for $\mathrm{Br}(b \to s + \gamma)$ agrees with the standard model prediction, which puts constraints on the pMSSM. The main SUSY contribution to the process comes from diagrams with a charged Higgs and up-type squarks. The second main contribution involves a chargino and up-type squarks [MPR98]. The Feynman diagrams for these two processes are shown in Fig. 7.

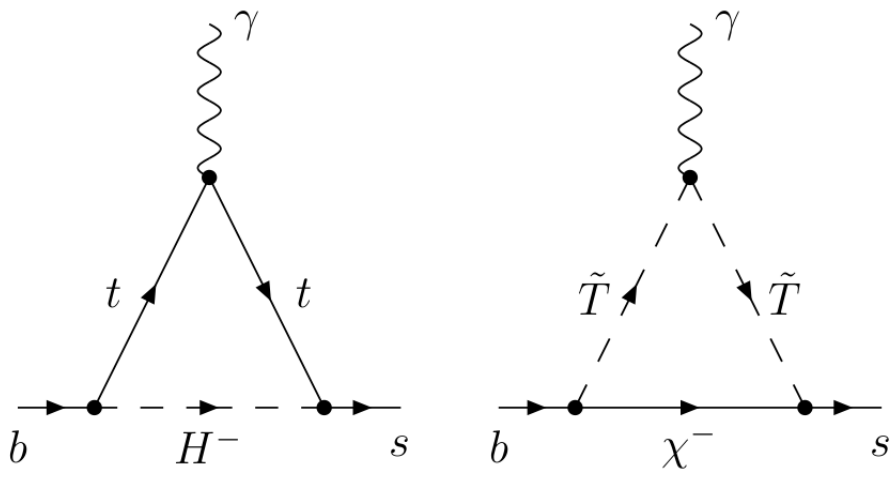

Figure 7: Feynman diagrams for the main MSSM processes for $b \to s + \gamma$ at lowest order. The charged Higgs boson H^- boson serves as an intermediate particle in the diagramt to the left. The chargino $\tilde{\chi}^-$ acts as an intermediate particle in the diagram to the right. The image is obtained from [MPR98].

The mathematical expressions for the SUSY contribution include terms containing $\tan\beta$, the mass of the charged Higgs, the squark masses and the chargino masses [JKG96]. Varying these parameters within SUSY will give different values for $\mathrm{Br}(b \to s + \gamma)$.

In this work, the range

$$2.71 \cdot 10^{-2}\ \% \leq \mathrm{Br}(b \to s + \gamma) \leq 4.39 \cdot 10^{-2}\ \%, \tag{13}$$

is used in DarkSUSY [GEU+04] to accept models as compatible with experiments. This interval is obtained by adding the theoretical uncertainty from [MAB+07] for the SM prediction as well as for the SUSY prediction to the experimental uncertainty from [(HFAG)07]. The central value is the experimental value from [(HFAG)07].

2.5 Software

Computation of the the SUSY particle masses, their decay branching ratios and the Higgs boson mass for each SUSY model is performed with Isajet 7.80 [BPPT09]. The relic dark matter density corresponding to each SUSY

model is calculated in DarkSUSY 5.0.5 [GEU+04]. The upper bound on the relic dark matter density, as defined in Sec. 2.4.1, is applied by hand.

DarkSUSY 5.0.5 also computes the value of the branching ratio $\mathrm{Br}(b \to s + \gamma)$ and tests whether it is within the limits given in Eq. (13).

The lower bound from LEP on the Higgs boson mass m_{h^0} is recalculated for each SUSY model with HiggsBounds [BBH+10], integrated in DarkSUSY.

FeynHiggs 2.8.6 [HHRW07] is employed to compute quantities related to MSSM Higgs bosons.

The program Prospino2.1 [BHS96] is used to calculate different SUSY production cross sections at the LHC.

3 Search for SUSY at ATLAS and Dark Matter Constraints

3.1 Introduction

ATLAS has published results [ATLAS11] on searches for SUSY within the pMSSM with production of squarks and gluinos and dilepton final states. The purpose of the search was to examine models with dilepton signature, which were not excluded by zero- and one-lepton SUSY searches. We focus on the model set referred to as Light Neutralino Grid in Ref. [ATLAS11]. Different points in the model grid correspond to SUSY models with different masses of squarks and gluinos, which are of the order several hundred GeV. Exclusion limits were set in the gluino mass - squark mass plane.

In this chapter, it is investigated what kind of constraints the ATLAS exclusion implies for some models of SUSY. The models presented in Ref. [ATLAS11] were developed without regards to several experimental constraints. The three constraints we wish to add are the upper bound on the relic dark matter density, given by equation (6) in Sec. 2.4.1, a lower bound on the Higgs mass, as described in Sec. 2.4.2, and a branching ratio within the limits given in equation (13) in Sec. 2.4.3. We propose a modified version of the Light Neutralino Grid and call it phenoGrid 2c. It is constructed to be similar to the Light Neutralino Grid in terms of dilepton signature at ATLAS. The challenge is to change some parameters in the grid to make it meet the three experimental constraints, without changing the LHC phenomenology.

3.2 The LHC

The Large Hadron Collider (LHC) is the largest particle accelerator in the world with a circular circumference of 27 km. It is located around 100 meters under ground, below Swiss-French border at CERN. The LHC scatters protons inelastically, resulting in production of many strongly interacting particles. The protons are accelerated in bunches, with 10^{11} protons in each bunch, and collided against each other head-on at a rate of 40 million bunch crossings each second. With about 20 collisions per bunch crossing, there are around 1 billion proton-proton inelastic collisions per second. The data collected at the LHC can give us information on physics beyond the Standard Model.

3.2.1 ATLAS

Several experiments are positioned along the LHC. One of them is ATLAS, A large Toroidal LHC ApparatuS. The cynlindrical device is 47 m long, has a diameter of 25 meters and weighs 7000 tonnes.

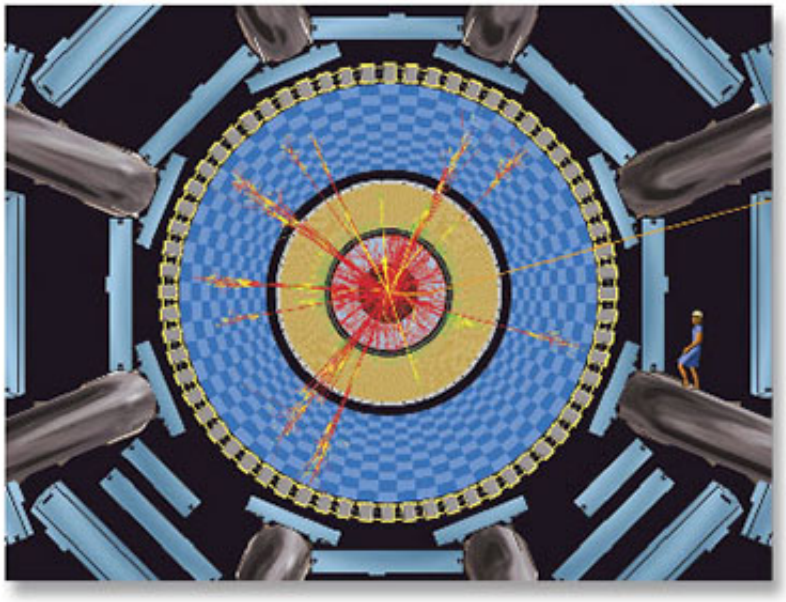

Figure 8: An illustration of a cross section of the ATLAS detector during a collision. The beam pipe, where the collision occurs, is surrounded by the inner detector (bluish-gray). Around the inner detector is Liquid Argon Calorimeter (in yellow). The next layer (shown in blue) is the Tile Calorimeter. The blue areas outside the circular part are muon spectrometers. A person is shown at the right of the image to set the scale. The image is obtained from Ref. [ATL].

The ATLAS collaboration consists of more than 3000 physicists from 174 institutions in 38 countries. Tests are performed at ATLAS to determine if the standard model describes high energy physics satisfactorily, or if new exotic particles can be found. Predictions from Monte Carlo simulations of the SM background and of supersymmetric events are compared to the number and characteristics of collision events selected by the experiment.

The ATLAS experiment consists of several sub-detectors. The inner tracking detector measures the momentum of each charged particle. Tile and Liquid Argon calorimeters measure energies of electrons, photons and hadrons produced in collisions. A muon spectrometer identifies muons and measures their momenta. A cross section of the ATLAS experiment is shown is Fig. 8.

3.2.2 Experimental signature of SUSY

If there is enough energy involved in the proton-proton collisions, SUSY particles might be pair produced. The produced sparticles go through a

sequence of decays resulting in SM particles and the neutralino LSP in the final state. Charged SM leptons and hadrons (quarks) produced in the process will register in the inner tracking detector and the calorimeters. Neutrinos and the lightest supersymmetric particle only interact weakly so they will not be observed in the detectors. The presence of neutrinos or LSPs can be deduced from the conservation of momentum. When protons are collided head-on, they have no momentum in the transverse plane. From conservation of momentum, the net momentum of leptons and quarks from a collision should be zero in the transverse plane. The so-called missing transverse energy $E_{\mathrm{T}}^{\mathrm{miss}}$ is the energy one would need to introduce in order to cancel any net transverse momentum of the detected hadrons and leptons. The transverse energy is related to the transverse momentum p_T by $E_T = \sqrt{m^2 + p_T^2}$. A non-zero $E_{\mathrm{T}}^{\mathrm{miss}}$ can arise from experimental uncertainty or from the presense of a neutrino or an LSP. SUSY events are expected to have a high missing transverse energy, since there would be two LSPs in the final state.

3.3 The ATLAS Light Neutralino Grid search

In this section, the ATLAS SUSY search [ATLAS11] within the pMSSM model set called Light Neutralino Grid is summarized.

3.3.1 Grid parameter values

The light Neutralino Grid is a set of pMSSM models that were examined at ATLAS. The name "Light Neutralino" comes from assigning the neutralino LSP a mass of 100 GeV, which is only 9 GeV above than the mass of the Z^0 boson. Scans in the two dimensional squark mass - gluino mass parameter space are performed, scanning the two masses independently of each other in the mass range 300 GeV $-$ 800 GeV. The masses of sleptons and the gauginos $\tilde{\chi}_2^0$, $\tilde{\chi}_1^{\pm}$ are related to the squark and gluino masses. All third generation sfermion masses are set to 2 TeV. The value $\tan\beta$ is set to $\tan\beta = 4$. The parameters of the models in the Light Neutralino Grid are given in Tab. 4.

3.3.2 Dilepton event selection

In Ref. [ATLAS11], SUSY models with dilepton final states are examined. In selecting collision events for the analysis, the requirement is that exactly two (charged) leptons with a transverse momentum of $p_T > 20$ GeV are present in the final state. These leptons can be electrons ($e^{\pm}$) or muons ($\mu^{\pm}$) in any combination. Exclusion limits are are computed for same sign (SS) dilepton signature and opposite sign (OS) dilepton signature separately.

For the SS analysis, the limits are calculated for the sum of the three channels $(e^{\pm}e^{\pm}), (e^{\pm}\mu^{\pm}), (\mu^{\pm}\mu^{\pm})$. For the OS analysis, the limits are calculated separately for the channels $(e^{+}e^{-}), (e^{\pm}\mu^{\mp}), (\mu^{+}\mu^{-})$ and then combined statistically.

The defining selection criteria for the signal region is a transverse missing momentum of $E_{\mathrm{T}}^{\mathrm{miss}} > 150$ GeV for the OS signature and $E_{\mathrm{T}}^{\mathrm{miss}} > 100$ GeV for the SS signature. A large missing transverse energy is possible for SUSY events with two LSPs of 100 GeV in the final state. The cut is employed to reduce the SM background, especially from Z^0 boson production.

The main SM background for the SS analysis comes from SM processes with so-called fake leptons, an example of which is charged hadrons that are mistaken for electrons in the detector. For the OS analysis, the main background comes from $t\bar{t}$ production, with subsequent leptonic decays.

3.3.3 Dilepton search results

The SUSY models of the Light Neutralino Grid have been tested against the full ATLAS dataset from 2010 [ATLAS11]. The data was collected at a centre-of mass energy of $\sqrt{s} = 7$ TeV with a total integrated luminosity of $L = 35\mathrm{pb}^{-1}$.

In the ATLAS analysis, Monte Carlo simulations of the standard model background were added to simulations of SUSY processes corresponding to the models in question. The number of events predicted by the simulations was compared to the number of events observed in ATLAS. In case the predictions from SUSY were inconsistent with the data, the corresponding models in the Light Neutralino Grid were excluded.

Parameter	Symbol	Value
Gluino mass	M_3	$[300, 800]$ GeV
Squark mass	$m_{\tilde{u}} = m_{\tilde{d}} = m_{\tilde{c}} = m_{\tilde{s}}$	$[300, 800]$ GeV
Bino (LSP) mass	M_1	100 GeV
Wino $(\tilde{\chi}_2^0, \tilde{\chi}_1^{\pm})$ mass	M_2	$M - 100$ GeV
Slepton mass	$m_{\tilde{l}_L} = m_{\tilde{\nu_L}} = m_{\tilde{l}_R}$	$M/2$
Higgs v.e.v.s ratio	$\tan\beta$	4
Third generation	$m_{\tilde{t}} = m_{\tilde{b}} = m_{\tilde{\tau}} = m_{\tilde{\nu_\tau}}$	2 TeV
Top quark mass	m_t	172.5 GeV
Higgs parameter	μ	$1.5 \cdot M$
Tril. couplings	$A_l,\ A_b$	$\mu \cdot \tan\beta$
Top tril. coupling	A_t	$\mu / \tan\beta$

Table 4: The parameters for the Light Neutralino Grid. The parameter M is defined as $M = \min(m_{\tilde{q}}, m_{\tilde{g}})$. The wino mass M_2 determines the masses of $\tilde{\chi}_2^0, \tilde{\chi}_1^{\pm}$. The bino mass M_1 sets the mass of the LSP. Tril. is an abbreviation for "trilinear".

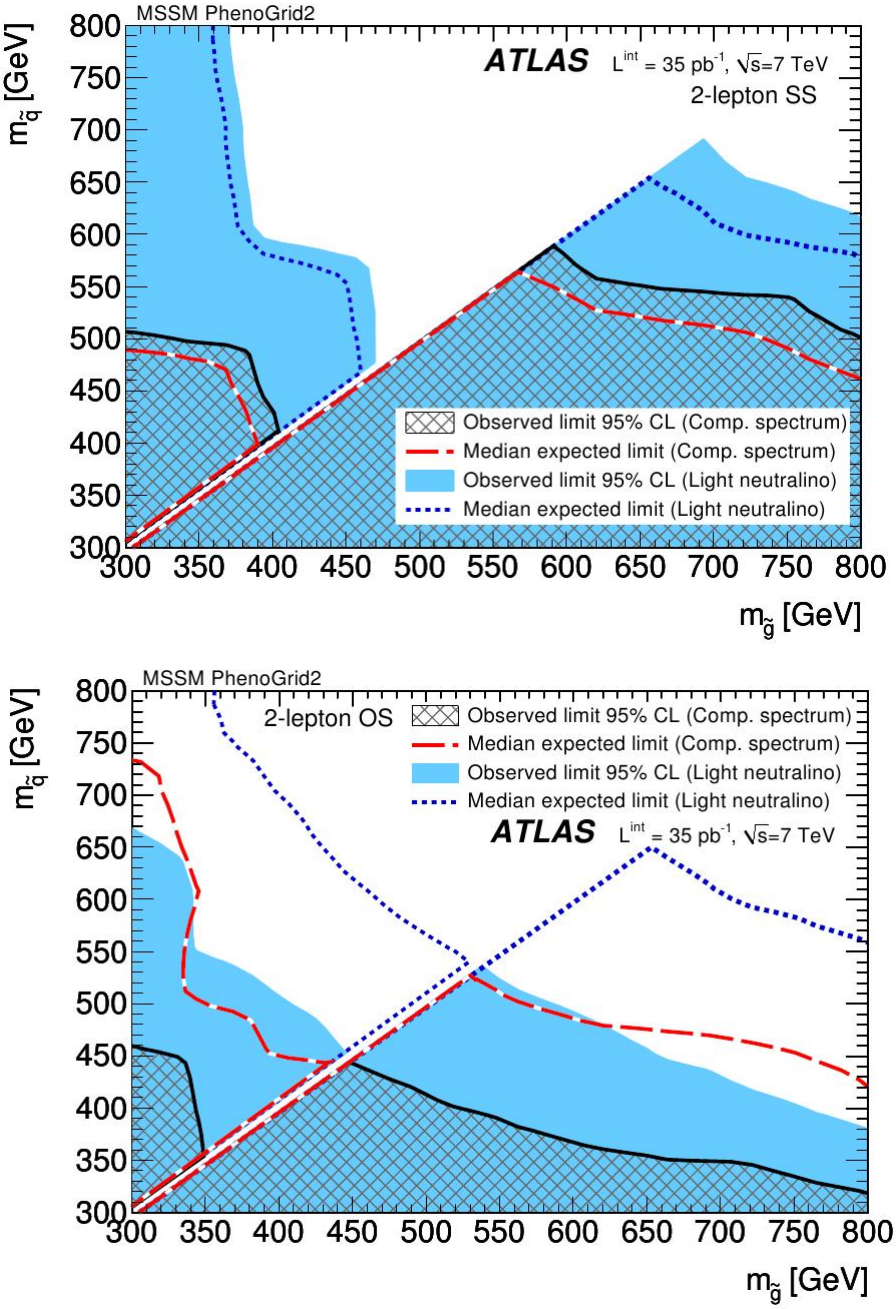

Figure 9: ATLAS exclusion limits for the Light Neutralino Grid (in blue) at 95% confidence level. Gluino masses are varied along the x-axis, squark masses along the y-axis. Results from the dilepton analysis with leptons in the final state of the same sign are shown in the upper plot. Results from searches with leptons of opposite sign are shown in the lower plot. The blue broken lines show the expected limits for the Light Neutralino Grid. The figure was obtained from Ref. [ATLAS11].

The predicted number of events in the signal region are compared to the number of events observed in ATLAS 2010 data. Depending on the number of observed events compared to number of predicted events and the experimental uncertainties, the suggested SUSY models can either be discovered, be excluded (in which case the parameter space is constrained), or be allowed.

In Ref. [ATLAS11], a 95% confidence level is used in the exclusion. The total uncertainty in the signal region, with contribution from both theory and experiment, was calculated for each model and found to be between 20% and 30%.

The ATLAS exclusion limits are shown in Fig. 9. The two graphs in Fig. 9 represent exclusion limits from analysis with SS dilepton final states ($l^{\pm}l^{\pm}$) and with OS dilepton final states ($l^{\pm}l^{\mp}$). Scanning independently over different masses of squarks and gluinos in the range $300 - 800$ GeV results in a two-dimensional grid. The blue areas in Fig. 9 correspond to models in the Light Neutralino Grid that have been excluded with a 95% confidence level. White areas correspond to models that have not been excluded in the ATLAS analysis. The lower limits for squark masses and gluino masses within the Light Neutralino model set can be read off the graphs.

The ATLAS exclusion can be summarized as follows. The SS analysis provides tighter limits on both squark and gluino masses than the OS analysis. For models where $m_{\tilde{g}} = m_{\tilde{q}} + 10$ GeV, the lower limits on the squark mass are $m_{\tilde{q}} \geq 550$ GeV from the OS analysis and $m_{\tilde{q}} \geq 690$ GeV from the SS analysis. In the region where squarks are heavier than gluinos, squark masses are excluded up to $450 - 690$ GeV (from the OS analysis), depending on the gluino mass. All models with $m_{\tilde{q}} \lesssim 450$ GeV and $m_{\tilde{g}} \lesssim 450$ GeV are excluded by the SS analysis. Models with $m_{\tilde{q}} = m_{\tilde{g}}$ are not accessible with this analysis.

3.4 Study of a modified dilepton grid

In this section, the Light Neutralino Grid is tested against the three experimental constraints in Sec. 3.4.1. A modified grid, called phenoGrid 2c, is proposed in Sec. 3.4.2. In Sec. 3.4.3 - 3.4.3.4, the ATLAS phenomenology of the Light Neutralino Grid and phenoGrid 2c is compared. The modified grid is tested against the three experimental constraints in Sec. 3.4.4.

3.4.1 The Light Neutralino Grid and non-LHC constraints

The relic dark matter density for the Light Neutralino grid, with the neutralino LSP as the dark matter particle, is computed with DarkSUSY. For the purpose of our analysis, in generating the Light Neutralino models, scans are made for squark masses and gluino masses in the range 300 GeV $-$

800 GeV in steps of 100 GeV. This results in 36 models. Instead of generating models with $m_{\tilde{g}} = m_{\tilde{q}}$, for which the conducted ATLAS analysis is not sensitive, we break the mass degeneracy by setting $m_{\tilde{g}} = m_{\tilde{q}} + 10$ GeV. The relic dark matter density corresponding to the 36 generated models is shown in Fig. 10 together with the upper limit from WMAP7 (the red line). The computed dark matter density exceeds the WMAP upper bound by a factor of 3-30 for the different models in the grid. The WMAP central value and upper bound can not be resolved from each other on the scale of this figure, the dark matter density of the Light Neutralino Grid are very many standard deviations away from the WMAP7 central value. The models in the Light Neutralino Grid are judged to be inconsistent with the world we live in.

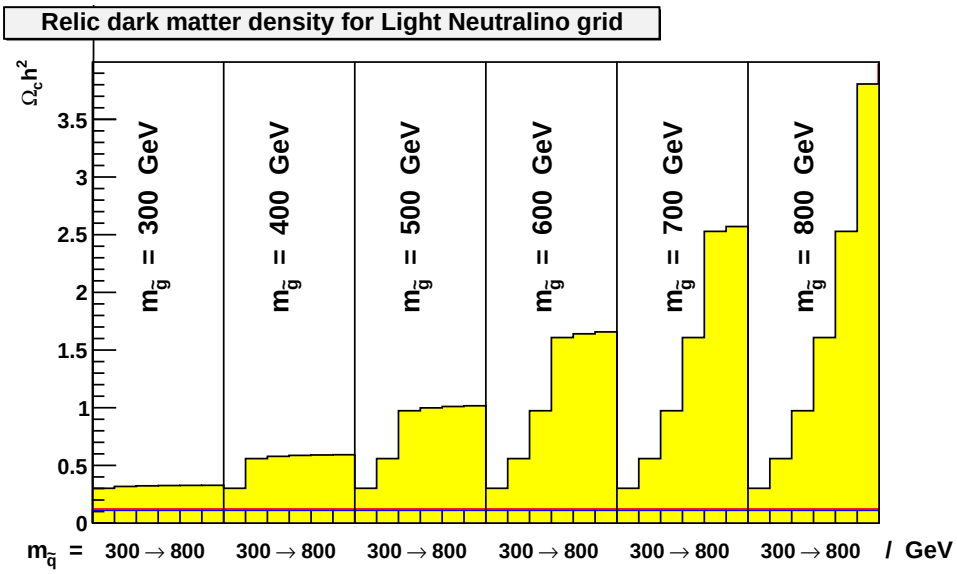

Figure 10: The dark matter density as given by the Light Neutralino Grid, computed with DarkSUSY [GEU+04]. The WMAP7 central value is $\Omega_c h^2 = 0.1109$. The red line shows the upper bound from WMAP7 at 0.1221. The 36 analyzed models are grouped as follows. In each of the six wide bins, the gluino mass is constant. The wide bins are sorted in increasing order from a gluino mass of 300 GeV to a gluino mass of 800 GeV. Within each wide bin, there are six thin bins, corresponding to six squark masses: from 300 GeV to 800 GeV in increasing order.

The Higgs mass for each SUSY model is computed and tested against LEP data. The result is $m_{h^0} = 105.4$ GeV for all the models, which is excluded by searches at LEP. The branching ratio $\mathrm{Br}(b \to s + \gamma)$ has allowed values for all models in the Light Neutralino grid.

3.4.2 Modified grid: phenoGrid 2c

Some modifications to the Light Neutralino Grid are introduced to make it consistent with cosmological observations of dark matter and LEP searches for the Higgs boson, described in Sec. 2.4. Three model parameters are modified and the resulting model grid is named phenoGrid 2c.

The main difference in the mass spectra between Light Neutralino Grid and PhenoGrid 2c is that the right-handed sleptons are much lighter in phenoGrid 2c: $m_{\tilde{l}_R} = 111$ GeV. The motivation for having a light sfermion is as follows. As described in Sec. 2.4.1, the relic dark matter density was determined by the cross section for the LSP pair annihilation in the early Universe. In the annihilation $\tilde{\chi}_1^0 + \tilde{\chi}_1^0 \rightarrow f + \bar{f}$, a sfermion $\tilde{f}$ can act as an intermediate particle in a t-channel exchange, as shown in Fig. 11.

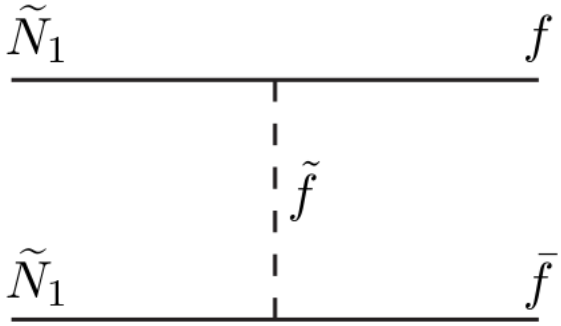

Figure 11: An illustration showing one of the processes of LSP pair annihilation. The neutralino LSP, which is called $\tilde{\chi}_1^0$ in this text is named $\tilde{N}_1$ in the figure. The SM fermions are denoted by f, sfermions by $\bar{f}$. The image has been obtained from Ref. [Mar97].

The cross section σ for the process shown in Fig. 11 is dependent on the sfermion mass $m_{\tilde{f}}$ as following [PS95]:

$$\sigma \propto \frac{1}{(t - m_{\tilde{f}}^2)^2}, \qquad t = (p_3 - p_1)^2. \tag{14}$$

Here p_1 is the four-vector of the neutralino on the top of Fig. 11 and p_3 is the four-vector of the SM fermion f. The square of the difference of these four-momenta is the Mandelstam variable t. As $\tilde{\chi}_1^0$ is a cold (non-relativistic) dark matter particle, its momentum is set to zero in the calculation of t. The sfermion considered here can be either selectron or smuon, so the SM fermions produced will be electrons or muons. As the masses of SM electrons and muons are 512 keV and 106 MeV respectively [Nak10], compared to the neutralino mass of 100 GeV, they are negligible. Under these ap-

proximations, the Mandelstam variable t has the value $t = -m^2_{\tilde{\chi}^0_1}$, which gives

$$\sigma \propto \frac{1}{(m^2_{\tilde{\chi}^0_1} + m^2_{\tilde{f}})^2}. \tag{15}$$

Therefore, decreasing the mass of the sfermion $m_{\tilde{f}}$ will increase the annihilation cross section. A high annihilation cross section results in a lower relic dark matter density, as shown in Fig. 4. We decrease the mass of the right-handed slepton from the value in the Light Neutralino Grid to meet the upper bound on dark matter density.

The mass of right-handed sleptons only is changed for phenoGrid 2c, while the mass of the left-handed sleptons are kept unchanged. The reasoning for this is the following. Right-handed sleptons do not couple to the Z and $W^{\pm}$ bosons or their superpartners. Since the wino mass is higher than the bino mass $M_2 > M_1$ in our models and $|\mu| > M_2$, the interaction content of the neutralino $\tilde{\chi}^0_2$, as given by the neutralino mixing matrix in Eq. (3), is mostly wino. Similarly, the chargino is also be wino-like. Therefore $\tilde{\chi}^0_2$ and $\tilde{\chi}^{\pm}_1$ will not couple to right-handed sleptons. No right-handed sleptons will be produced from squarks and gluinos as no sparticle can mediate these decays. The dilepton phenomenology for ATLAS will therefore not be influenced by the mass of right-handed sleptons.

In phenoGrid 2c, the value of $\tan\beta$ is raised from $\tan\beta = 4$ to $\tan\beta = 7$. This parameter is changed to easier meet lower experimental limits on the Higgs mass from LEP. At lowest order, the Higgs mass is given by $m_{h^0} \approx m_Z|\cos 2\beta|$. This value is plotted as a function of $\tan\beta$ in Fig. 12. As $\tan\beta$ grows, $\beta \to \pi/2$ and $|\cos 2\beta|$ approaches the maximum value: $|\cos 2\beta| \to 1$. So, the Higgs mass at lowest order approaches the mass of the Z^0 boson (91.2 GeV) from below as $\tan\beta$ grows. The value $|\cos 2\beta|$ grows rather rapidly at low values of $\tan\beta$ and then planes out, as seen in Fig. 12. For $\tan\beta = 4$, $m_Z|\cos 2\beta| = 80.5$ GeV. For $\tan\beta = 7$, $m_Z|\cos 2\beta| = 87.5$ GeV. So, at lowest order, changing $\tan\beta$ from 4 to 7 increases the Higgs boson mass by 7 GeV.

In order to further increase the Higgs mass corresponding to the SUSY models, the main contribution to the Higgs mass at next to leading order is modified. In the Light Neutralino grid, $A_t = \mu/\tan\beta$, which corresponds to minimum top mixing ($X_t = 0$), as discussed in Sec. 2.4.2. With this condition, the expression for the Higgs mass reduces from equation (10) to:

$$m^2_{h^0} \leq m^2_Z|\cos 2\beta|^2 \; + \; \frac{3G_F}{\sqrt{2}\pi^2} m_t^4 \log(\frac{m^2_{\tilde{t}}}{m^2_t}). \tag{16}$$

Raising the mass of the stop quark $m_{\tilde{t}}$ should increase the positive contribution to the Higgs mass. All third generation sfermions are set to 10 TeV in

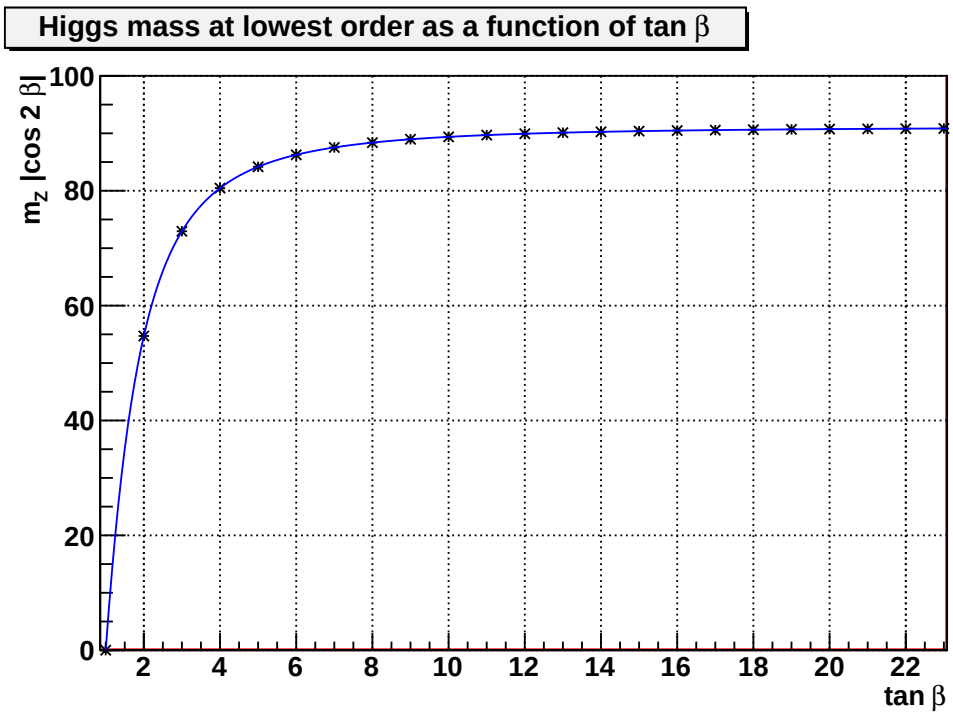

Figure 12: The analytical expression for the Higgs mass at lowest order $m_{h^0} = m_Z|\cos 2\beta|$ is plotted as a function of $\tan\beta$. For the Light Neutralino Grid, $\tan\beta = 4$ and $m_Z|\cos 2\beta| = 80.5$ GeV. For phenoGrid 2c, $\tan\beta = 7$ and $m_Z|\cos 2\beta| = 87.5$ GeV.

phenoGrid 2c, compared to 2 TeV for Light Neutralino Grid. This increases the second term in equation (16) by a factor of $\log(5^2) = 3.2$. The three modifications to Light Neutralino Grid are summarized in Table 5.

Parameter	Light Neutralino	phenoGrid 2c
l_R	M/2 (150 – 400 GeV)	111 GeV
$\tan\beta$	4	7
$m_{\tilde{t}}, m_{\tilde{b}}, m_{\tilde{\tau}}, m_{\tilde{\nu_\tau}}$	2 TeV	10 TeV

Table 5: The modifications that distinguish phenoGrid 2c from the Light Neutralino Grid. The input mass parameter for the right-handed slepton before electroweak symmetry breaking is 102 GeV. After electroweak symmetry breaking, the mass of the right-handed slepton becomes 111 GeV.

3.4.3 Sources of dilepton production

PhenoGrid 2c is constructed to have the same LHC phenomenology as the Light Neutralino Grid, with the purpose of having the ATLAS exclusion limits applicable to phenoGrid 2c as well. To confirm that the phenomenology is similar, we test the agreement of branching ratios, which correspond to dilepton production, between the Light Neutralino Grid and phenoGrid 2c.

As the masses of the strongly interacting squarks and gluinos in our models are of the same order of magnitude as the other sparticles, production of SUSY will be mainly through squarks and gluinos. Decay chains that produce leptons are those with sleptons or sneutrinos created at intermediate stages. Squarks and gluinos do not couple to sleptons and sneutrinos directly, therefore decays into these sparticles occurs via intermediate gauginos: $\tilde{\chi}_1^{\pm}, \tilde{\chi}_2^0$.

The analysis of branching ratios described below is carried out in the following steps:

- The branching ratios for lepton production from the gauginos $\tilde{\chi}_1^{\pm}, \tilde{\chi}_2^0$ are calculated for both grids.
- The branching ratios for gaugino production from squarks and gluinos are computed for both grids.
- For each squark type of the first two families and for gluinos, the branching ratios for the main decay chains that result in the production of exactly one lepton are added, and similarly for production of two leptons.
- All possible pairs of squarks and gluinos that result in a particular signature (e.g. same sign) are multiplied by their production cross section at the LHC and then added. The resulting quantity is called $LP(ll)$ and is defined in equation (17).
- The relative difference in lepton production $\Delta LP(ll)$ between the Light Neutralino Grid and phenoGrid 2c is calculated for each grid point.

These are the basic steps that will be taken to test if the acceptance of the ATLAS analysis is affected. The quantity $LP(ll)$ is the sum of all the branching ratios that give the dilepton signature, weighed by the corresponding production cross section:

$$LP(ll) = \sum_{\tilde{A},\tilde{B}} \sigma_{(p+p\to\tilde{A}+\tilde{B})} \cdot \mathrm{Br}(\tilde{A}+\tilde{B} \to l+l+X), \qquad (17)$$

$$\tilde{A}, \tilde{B} = \tilde{g}, \tilde{u}, \tilde{d}, \tilde{s}, \tilde{c}, \tilde{\bar{u}}, \tilde{\bar{d}}, \tilde{\bar{s}}, \tilde{\bar{c}}.$$

In Eq. (17), $\tilde{A}$ and $\tilde{B}$ can denote gluinos, or any of the eight squarks and anti-squarks of the first and second generation. All the different combinations of $\tilde{A}$ and $\tilde{B}$ are summed over. In the final state, X denotes the two LSPs and any additional SM final states particles, which are not charged leptons. The variable l can refer to either electrons or muons of any charge. The signature can be specified by assigning a charge and flavour to l. Each term in Eq. (17) contains the branching ratio for the decay process of $\tilde{A}$ and $\tilde{B}$ into a final states with exactly two leptons ll. These branching ratios are weighed by the cross section $\sigma_{p+p\to\tilde{A}+\tilde{B}}$ to produce $\tilde{A}$ and $\tilde{B}$ in in proton-proton collisions at the LHC. It is the relative difference $\Delta LP(ll)$ between the Light Neutralino Grid and phenoGrid 2c that is a measure of the change in phenomenology at the LHC. If $\Delta LP(ll)$ for the different dilepton signatures is small, compared to the experimental uncertainties, the ATLAS exclusion limits can be applied to our models.

In the sections below, branching ratios that are related to each other by charge conjugation will have the same value. Only branching ratios involving squarks ($\tilde{q}$) and positive charginos ($\tilde{\chi}_1^{\pm}$) are presented, not the corresponding expressions for anti-squarks ($\bar{\tilde{q}}$) and negative charginos ($\tilde{\chi}_1^{-}$). The second squark family has the same branching ratios as the first, so terms with the second squark and quark families are omitted from the text. In decay chains where either a lepton and a neutrino or two leptons are produced, both of these are of the same family and one of them carries a negative lepton number.

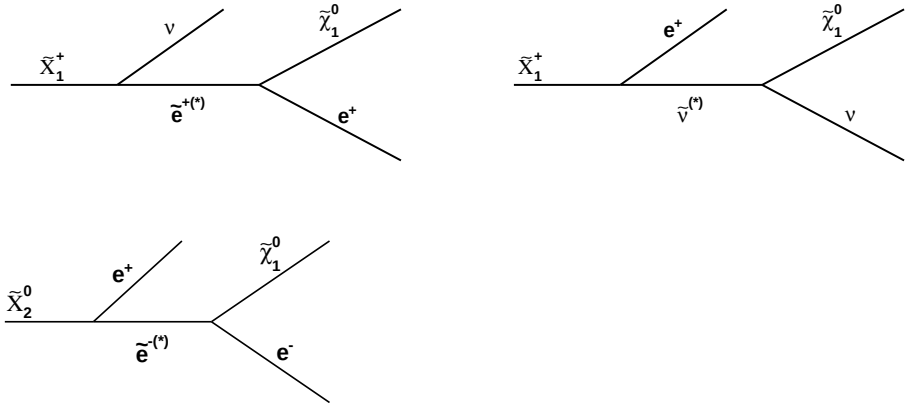

Figure 13: Selected illustrations of the decay chains of gauginos that produce leptons are shown above. The intermediate particle (selectron or snuerino) can be either virtual (off-shell), in which case it is denoted by a *, or on-shell. Decays of $\tilde{\chi}_1^+$ result in one electron e^+. Decays of $\tilde{\chi}_2^0$ can result in two electrons e^+e^-.

3.4.3.1 Lepton production from gauginos

The lepton production from charginos $\tilde{\chi}_1^+$ and neutralinos $\tilde{\chi}_2^0$ in the Light Neutralino Grid occurs via decay chains such as those shown in Fig. 13. For the chargino $\tilde{\chi}_1^+$, the branching ratios that could give visible electrons e^+ are:

1. $\mathrm{Br}(\tilde{\chi}_1^+ \to \tilde{\chi}_1^0 + e^+ + \nu)$
2. $\mathrm{Br}(\tilde{\chi}_1^+ \to \tilde{e}_L^+ + \nu) \cdot \mathrm{Br}(\tilde{e}_L^+ \to e^+ + \tilde{\chi}_1^0)$
3. $\mathrm{Br}(\tilde{\chi}_1^+ \to \tilde{\nu}_L + e^+) \cdot \mathrm{Br}(\tilde{\nu}_L \to \nu + \tilde{\chi}_1^0)$
4. $\mathrm{Br}(\chi_1^+ \to W^+ + \tilde{\chi}_1^0) \cdot \mathrm{Br}(W \to e^+ + \nu)$

All of the chargino ($\tilde{\chi}_1^+$) decays listed above give one charged electron.

Branching ratio 1 represents a three-body decay. It will occur if the mass difference between the initial $\tilde{\chi}_1^+$ and the final products is less than the mass of any intermediate particle. In all our models, however, due to the mass difference relation

$$m_{\tilde{\chi}_1^+} - m_{\tilde{\chi}_1^0} \; > \; m_{\tilde{l}_L},\, m_{\nu_L},\, m_W, \tag{18}$$

these three-body decays are absent in the model grids. Instead, decay chains with real intermediate particles, corresponding to branching ratios 2-4, produce the leptons.

Figure 14 shows the values of branching ratio 2 for the models in the Light Neutralino Grid, calculated with ISAJET [BPPT09]. Here a slepton $\tilde{l}_L$ acts as an intermediate particle. Red areas in the figure correspond to relatively large branching ratios, blue areas to small branching ratios. Decay channel 2 in the final state accounts for $14 - 24\%$ of all chargino decays, depending on the model.

Figure 15 shows branching ratio 3, with an intermediate sneutrino. This channel corresponds to $26\% - 36\%$ of all chargino decays.

The sum of branching ratios 2 and 3 is shown in Fig. 16. All combined branching ratios correspond to $49.4\% - 49.9\%$. Together with equal branching ratios for muon production, $99 - 100\%$ of all branching ratios of $\tilde{\chi}_1^+$ have been accounted for. Branching ratio 4 is negligible.

We now turn to neutralino ($\tilde{\chi}_2^0$) decays. The main branching ratios of $\tilde{\chi}_2^0$ that can give rise to electrons are:

1. $\mathrm{Br}(\tilde{\chi}_2^0 \to \tilde{\chi}_1^0 + e^- + e^+)$
2. $\mathrm{Br}(\tilde{\chi}_2^0 \to \tilde{e}_L^\pm + e^\mp) \cdot \mathrm{Br}(\tilde{e}_L^\pm \to e^\pm + \tilde{\chi}_1^0)$
3. $\mathrm{Br}(\tilde{\chi}_2^0 \to Z + \tilde{\chi}_1^0) \cdot \mathrm{Br}(Z \to e^+ + e^-)$.

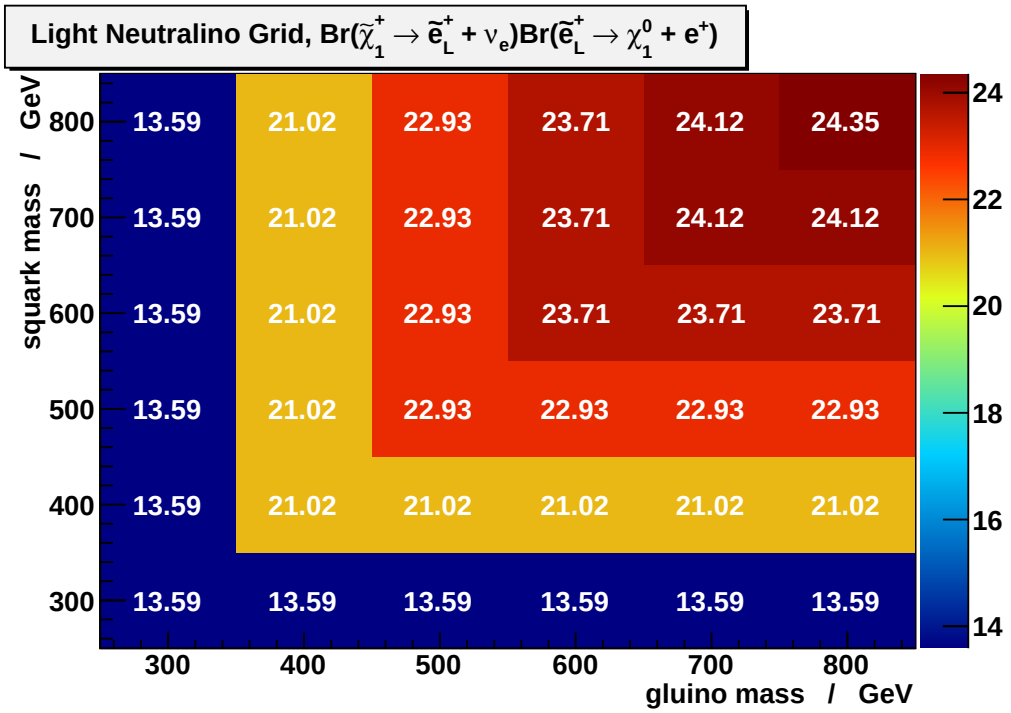

Figure 14: Branching ratio 2 for $\tilde{\chi}_1^+$ decays in % for the Light Neutralino Grid. A selectron acts as an intermediate particle and one charged lepton e^+ is produced. Gluino masses are varied along the x-axis, squark masses along the y-axis. The numbers in the grid and the colour coding show the value of the branching ratio for each model. Red corresponds to a high branching ratio, blue to a low, orange, yellow and green to intermediate.

These chains result in production of two charged electrons of opposite sign. The first term is zero, by the same argument as for the non-existence of chargino three-body decays. Branching ratios 2 and 3 for $\tilde{\chi}_2^0$ involve a real intermediate particle, which can be a slepton or a Z^0 boson.

Figure 17 shows the value of branching ratio 2 for the models in the Light Neutralino Grid. As seen in Fig. 17, $\tilde{\chi}_2^0$ decays into two electrons of opposite charge $17\% - 25\%$ of the time, with an equal probability to decay into two muons. Branching ratio 3, through a Z^0 boson, is found to be of the order of 10^{-4} % for the Light Neutralino Grid models and phenoGrid 2c models and is not considered further. Together with $\tilde{\chi}_2^0$ decays into muons, branching ratio 2 accounts for $33\% - 49\%$ of all $\tilde{\chi}_2^0$ decays. The remaining decays of the $\tilde{\chi}_2^0$ result in an LSP and two neutrinos, with no production of charged leptons.

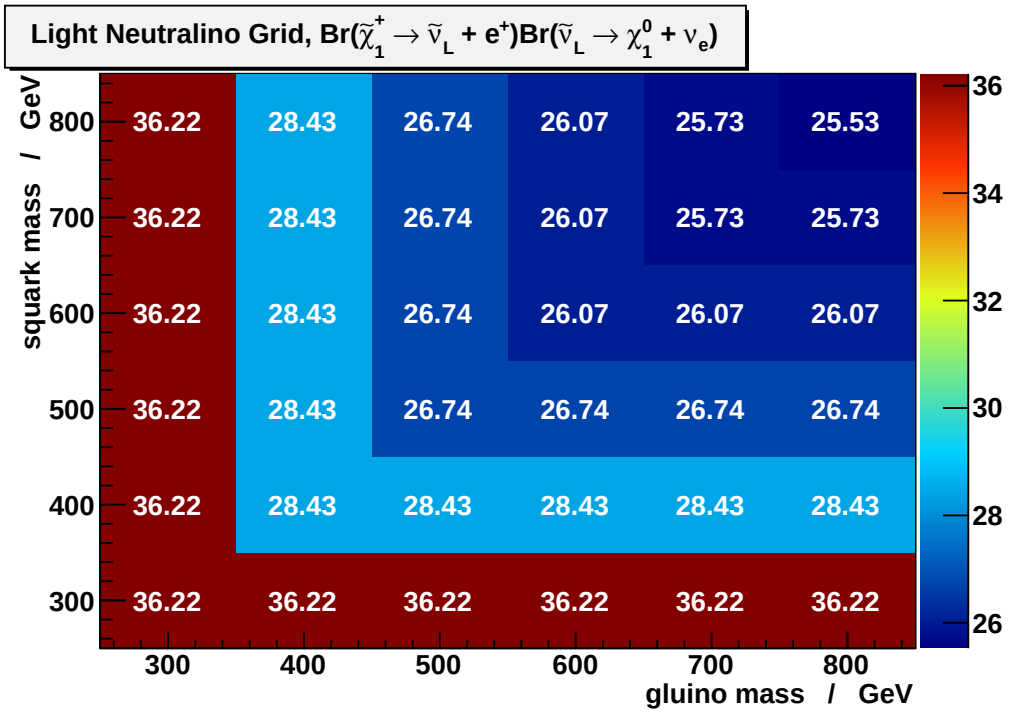

Figure 15: Branching ratio 3 for $\tilde{\chi}_1^+$ decays in % for the Light Neutralino Grid. A sneutrino acts as an intermediate particle and one electron e^+ is produced. Gluino masses are varied along the x-axis, squark masses along the y-axis. The numbers in the grid and the colour coding show the value of the branching ratio. Red corresponds to a high branching ratio, blue to a low, orange, yellow and green to intermediate.

Based on the investigations of the different terms performed here, the branching ratios for the gauginos that are used for calculations in Sec. 3.4.3.4 are

$$\begin{aligned} \mathrm{Br}(\tilde{\chi}_1^+ \to e^+ + X) &= \mathrm{Br}(\tilde{\chi}_1^+ \to \tilde{e}_L^+ + \nu_e) \cdot \mathrm{Br}(\tilde{e}_L^+ \to e^+ + \tilde{\chi}_1^0) + \\ &+ \mathrm{Br}(\tilde{\chi}_1^+ \to \tilde{\nu}_{eL} + e^+) \cdot \mathrm{Br}(\tilde{\nu}_{eL} \to \nu_e + \tilde{\chi}_1^0) \quad (19) \end{aligned}$$

for $\tilde{\chi}_1^+$ and

$$\begin{aligned} \mathrm{Br}(\tilde{\chi}_2^0 \to e^+ + e^- + X) &= \mathrm{Br}(\tilde{\chi}_2^0 \to \tilde{e}_L^+ + e^-) \cdot \mathrm{Br}(\tilde{e}_L^+ \to e^+ + \tilde{\chi}_1^0) + \\ &+ \mathrm{Br}(\tilde{\chi}_2^0 \to \tilde{e}_L^- + e^+) \cdot \mathrm{Br}(\tilde{e}_L^- \to e^- + \tilde{\chi}_1^0) \quad (20) \end{aligned}$$

for $\tilde{\chi}_2^0$.

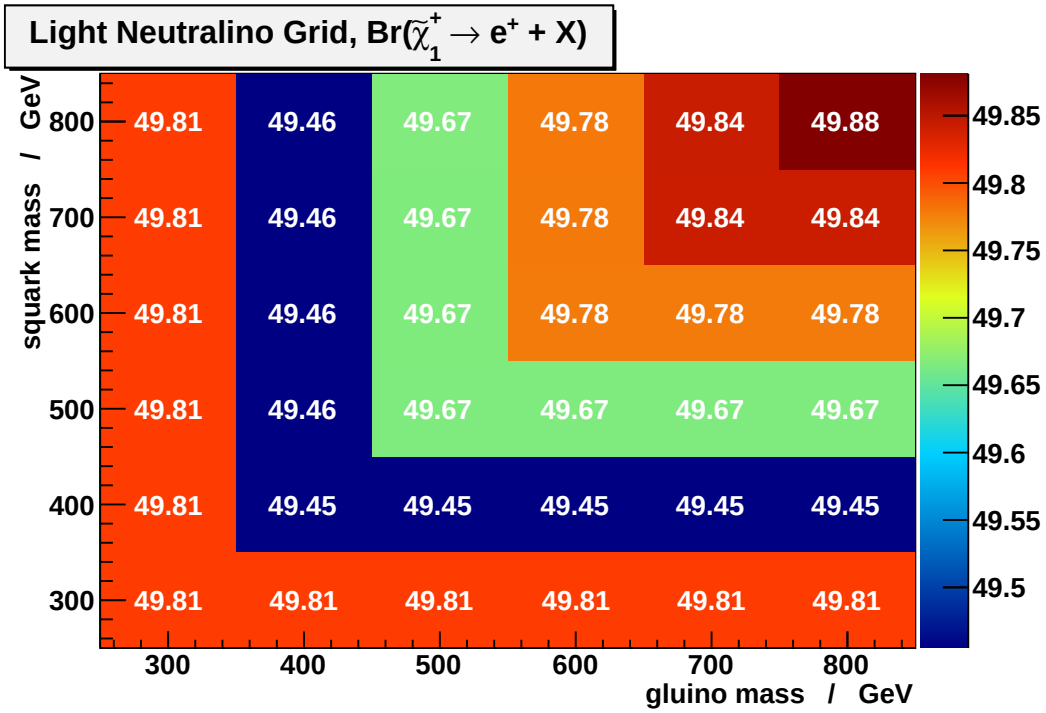

Figure 16: The main branching ratios for $\tilde{\chi}_1^+$ (branching ratios 2 and 3) in % into a final state with one electron e^+ for the Light Neutralino Grid. Gluino masses are varied along the x-axis, squark masses along the y-axis. The numbers in the grid and the colour coding show the value of the branching ratio. Red corresponds to a high branching ratio, blue to a low, orange yellow and green to intermediate.

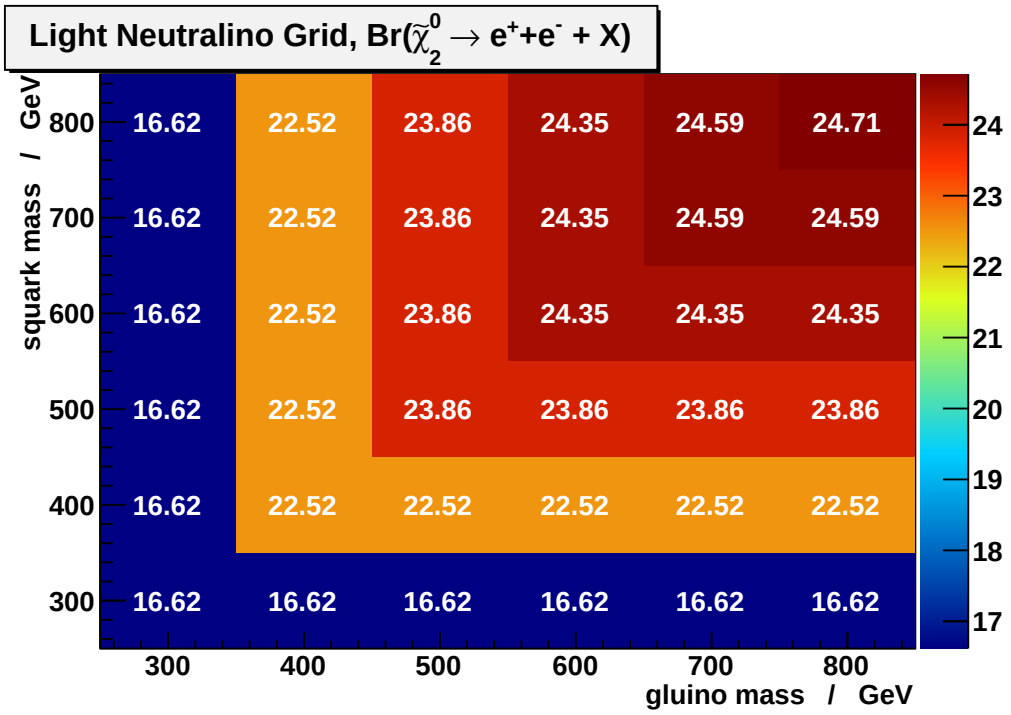

Figure 17: Term 2 for the branching ratio of $\tilde{\chi}_2^0$ into e^+e^- in % for the Light Neutralino Grid. Gluino masses are varied along the x-axis, squark masses along the y-axis. The numbers in the grid and and the colour coding show the size of the branching ratio. Red corresponds to a high branching ratio, blue to a low, orange, yellow and green to intermediate. Red corresponds to a high branching ratio, blue for a low, orange yellow and green to intermediate.

3.4.3.2 Gaugino production from squarks and gluinos

The decay chains of gluinos and squarks that lead to lepton production are examined. The dominant branching ratios for these processes. The expressions for $\tilde{\chi}_1^-$ production are similar to those for $\tilde{\chi}_1^+$ production. For a full list of the branching ratios for gaugino production included in calculations, see the Appendix A.1.

1. $\mathrm{Br}(\tilde{g} \to \tilde{\chi}_1^+ + d + \bar{u})$
2. $\mathrm{Br}(\tilde{u} \to \tilde{\chi}_1^+ + d)$
3. $\mathrm{Br}(\tilde{d} \to \tilde{g} + d) \cdot \mathrm{Br}(\tilde{g} \to \tilde{\chi}_1^+ + d + \bar{u})$
4. $\mathrm{Br}(\tilde{g} \to \tilde{d}_L + \bar{d}) \cdot \mathrm{Br}(\tilde{d}_L \to \tilde{\chi}_2^0 + d)$
5. $\mathrm{Br}(\tilde{u} \to \tilde{\chi}_2^0 + u)$
6. $\mathrm{Br}(\tilde{d} \to \tilde{\chi}_2^0 + d)$

Gluinos can not decay into gauginos in a two-body decay since they do not carry weak or electromagnetic charge. To produce gauginos, gluinos either undergo a three-body decay (branching ratio 1), or they go through a sequence of two decays with an on-shell intermediate squark (as in branching ratio 4). A condition for a chain of two decays, such as number 4, is that the mass of the decaying sparticle (here a gluino) is greater than the mass of the intermediate sparticle (sdown). The only way to produce a charged lepton from a squark of the opposite charge is for the squark to decay in a sequence of two steps with an intermediate gluon, as in branching ratio 3.

3.4.3.3 Squark and gluino production from proton collisions

During 2010, colliding protons at the LHC had an energy of 3.5 TeV each. At these energies, partons that that participate in a process with another proton are either gluons or sea quarks. The sea quarks can have any flavour and include anti-quarks. This implies that processes such as the production of two antisquarks and production two squarks from different sfermion families in a collision are possible. Since the first two sfermion families have the same masses in our models, the branching ratios for the second generation squarks have the same values as the corresponding branching ratios of the first generation. Branching ratios for decays of antisquarks have the same values as for squark decays that are related by a charge transformation.

SUSY particles are always produced in pairs. There are many different possible combinations to pick two particles $\tilde{A}, \tilde{B}$ out of gluinos, squarks and antisquarks of the first two generations for a SUSY production process, which is not covered in this text. The cross section for the pair production of $\tilde{A} + \tilde{B}$ in proton-proton collisions at the LHC with $\sqrt{s} = 7$ TeV is calculated with Prospino [BHS96]. The production of squarks of the third generation

is not considered, as their masses are an order of magnitude higher than the masses of the other squarks.

3.4.3.4 SS and OS signature

Following Ref. [ATLAS11], the same sign signature is treated with all the flavour combination ($e^{\pm}e^{\pm}$, $\mu^{\pm}\mu^{\pm}$, $e^{\pm}\mu^{\pm}$) summed. For the opposite sign signatures, final states with leptons from different families are considered separately from final states with leptons of the same family. For the OS signature, results are presented for the change in branching ratios for ($e^{\pm}\mu^{\mp}$) and ($e^{+}e^{-}$) final states. The branching ratios for ($\mu^{+}\mu^{-}$) are identical with those for ($e^{+}e^{-}$).

Same sign production can only occur from decays of two charginos of the same sign: each $\tilde{\chi}^{\pm}$ gives decays to give a lepton $l^{\pm}$. In computing $LP(l^{\pm}l^{\pm})$, which is defined in Eq. (17), all branching ratios to produce exactly one lepton each from $\tilde{A}$ and $\tilde{B}$: $\mathrm{Br}(\tilde{A} \to l^{\pm} + X) \cdot \mathrm{Br}(\tilde{B} \to l^{\pm} + X)$, are multiplied by the production cross section of $\tilde{A} + \tilde{B}$ at the LHC, and summed over:

$$LP(l^{\pm}l^{\pm}) = \sum_{\tilde{A},\tilde{B}} \sigma_{p+p\to\tilde{A}+\tilde{B}} \cdot \mathrm{Br}(\tilde{A} \to \tilde{\chi}_1^{\pm} + X) \cdot \mathrm{Br}(\tilde{B} \to \tilde{\chi}_1^{\pm} + X) \cdot \quad (21)$$

$$\cdot \mathrm{Br}(\tilde{\chi}_1^{\pm} \to l^{\pm} + X) \cdot \mathrm{Br}(\tilde{\chi}_1^{\pm} \to l^{\pm} + X). \quad (22)$$

Here only decay products relevant for the dilepton signature have been written out explicitly. Quarks, neutrinos and $\tilde{\chi}_1^0$ produced in the process have been omitted from the text. The suming is over $\tilde{A}$ and $\tilde{B}$, which are gluinos, squarks and anti-squarks of any flavour in the first two families. The branching ratio for $\tilde{\chi}_1^+$ decay into a e^+ is defined in equation (19). The value is identical with the branching ratio for $\tilde{\chi}_1^-$ decay into e^-.

The relative change in dilepton signature $\Delta LP(ll)$ is defined as

$$\Delta LP(ll) = \frac{LP(ll)_{\text{phenoGrid 2c}} - LP(ll)_{\text{Light Neutralino Grid}}}{LP(ll)_{\text{Light Neutralino Grid}}}. \quad (23)$$

Figure 18 shows the change in the same sign dilepton signature $\Delta LP(l^{\pm}l^{\pm})$ between the Light Neutralino Grid and phenoGrid 2c in units of %.

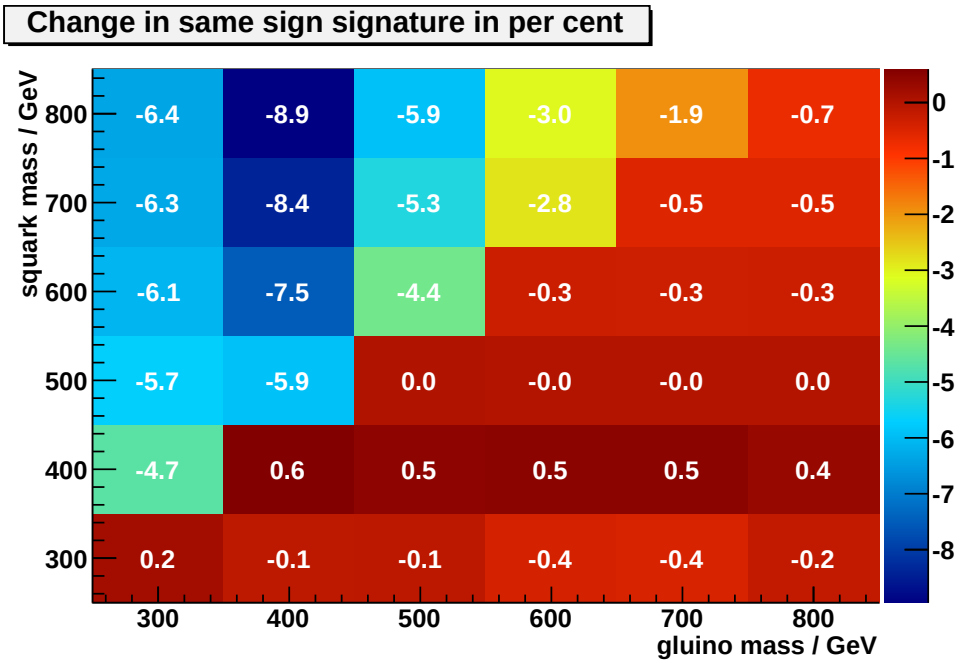

Figure 18: The change in branching ratios $\Delta LP(l^{\pm}l^{\pm})$ in % between the Light Neutralino Grid and phenoGrid 2c. Gluino masses are varied along the x-axis. Squark masses are varied along the y-axis. The numbers in the grid and the colour coding show the value of $\Delta LP(l^{\pm}l^{\pm})$. Blue areas correspond to large negative values (below -5), red areas correspond to small positive or negative values (close to 0%).

One way to obtain the opposite sign signature is from the decay of two oppositely charged charginos. For the opposite sign signature with different lepton families in the final state, the relevant branching ratios are added according to:

$$LP(e^{\pm}\mu^{\mp}) = \sum_{\tilde{A},\tilde{B}} \sigma_{p+p\to\tilde{A}+\tilde{B}} \cdot \mathrm{Br}(\tilde{A} \to \tilde{\chi}_1^{\pm} + X) \cdot \mathrm{Br}(\tilde{B} \to \tilde{\chi}_1^{\mp} + X) \cdot$$
$$\cdot \mathrm{Br}(\tilde{\chi}_1^{\pm} \to e^{\pm} + X) \cdot \mathrm{Br}(\tilde{\chi}_1^{\mp} \to \mu^{\mp} + X). \quad (24)$$

The change in OS dilepton signature of different flavour $\Delta LP(e^{\pm}\mu^{\mp})$ is shown in Fig. 19.

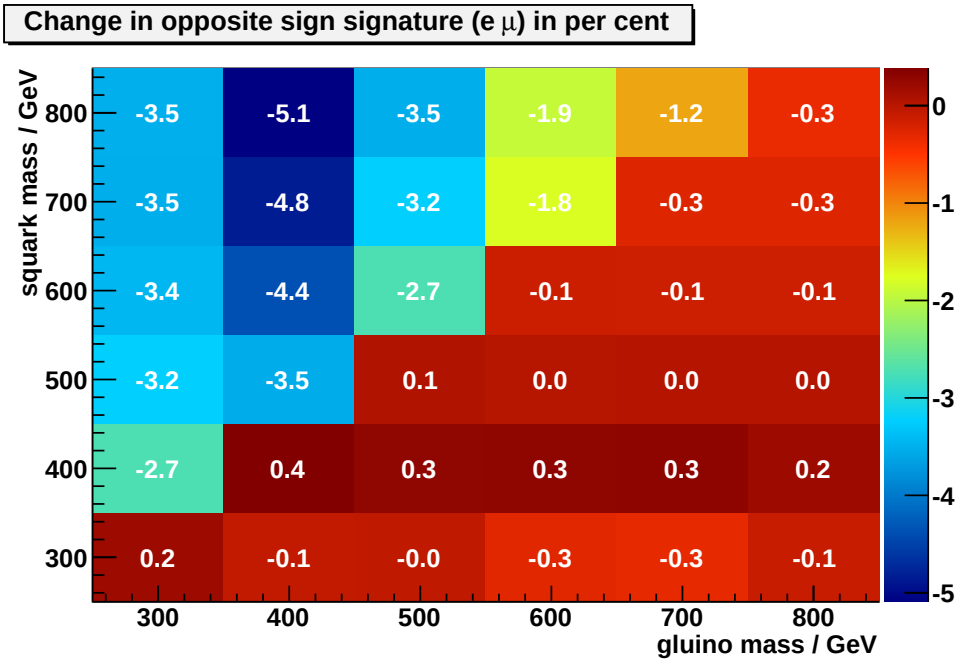

Figure 19: Change in branching ratios in % between the grids for opposite sign signature, different flavours: $\Delta LP(e^{\pm}\mu^{\mp})$. Gluino masses are varied along the x-axis. Squark masses are varied along the y-axis. The numbers in the grid and the colour coding show the value of $\Delta LP(e^{\pm}\mu^{\mp})$. Blue areas correspond to large negative values, red areas correspond to values close to 0%.

Another way to obtain the OS signature is from the decay of $\tilde{\chi}_2^0$, which can result in two leptons of opposite sign from the same flavour leptons. The decay of one sparticle results in the production of two leptons, which means that the other decaying sparticle must produce no leptons to meet the requirement of exactly two leptons in the final state. This branching

ratio is calculated by subtracting branching ratios that result in at least one lepton from 100% for the squark or gluino in question. The expression for opposite sign signature with the same flavour leptons in the final state has contributions from both $\tilde{\chi}_1^{\pm}$ and $\tilde{\chi}_2^0$ decays:

$$\begin{aligned} LP(e^+e^-) &= \sum_{\tilde{A},\tilde{B}} \sigma_{p+p\to\tilde{A}+\tilde{B}}[\cdot \mathrm{Br}(\tilde{A}\to\tilde{\chi}_1^+ + X)\cdot \mathrm{Br}(\tilde{B}\to\tilde{\chi}_1^- + X)\cdot \\ \cdot \mathrm{Br}(\tilde{\chi}_1^{\pm}\to e^{\pm} + X) &\cdot \mathrm{Br}(\tilde{\chi}_1^{\mp}\to\mu^{\mp} + X) + \\ +\mathrm{Br}(\tilde{A}\to\tilde{\chi}_2^0 + X) &\cdot \mathrm{Br}(\tilde{B}\to X)\cdot \mathrm{Br}(\tilde{\chi}_2^0\to e^+e^- + X)]. \end{aligned} \quad (25)$$

In the second term of equation (25), $\mathrm{Br}(B \to X)$ denotes the branching ratio of B to decay into a final state with no leptons. The change in OS dilepton signature of the same flavour leptons $\Delta LP(e^+e^-) = \Delta LP(\mu^+\mu^-)$ is shown in Fig. 20.

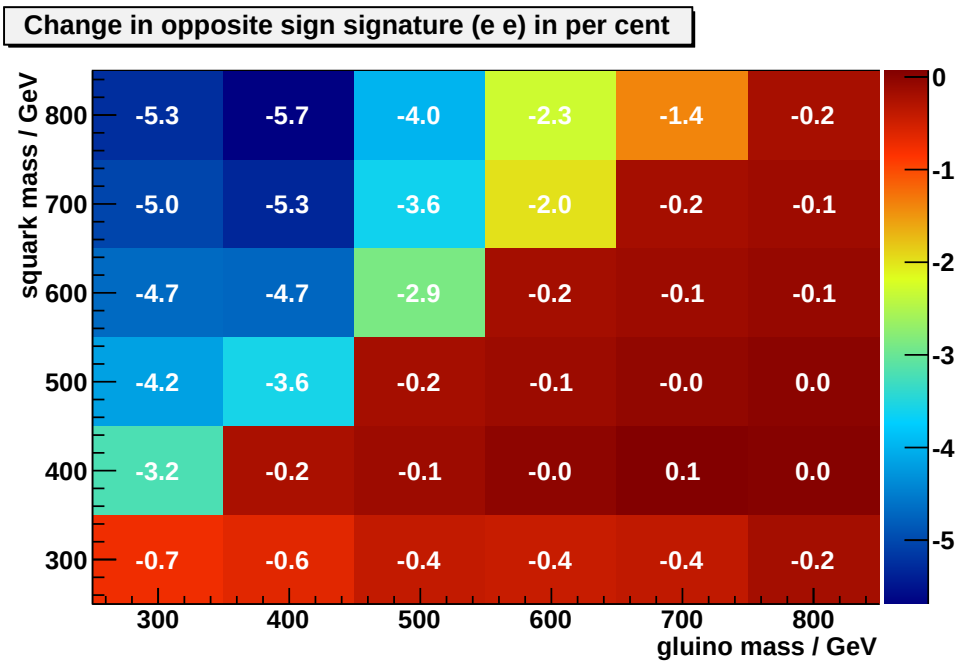

Figure 20: Change in branching ratios in % between the grids for opposite sign signature, same flavour: $\Delta LP(e^+e^-)$. Gluino masses are varied along the x-axis. Squark masses are varied along the y-axis. The numbers in the grid and the colour coding show the value of $\Delta LP(l^{\pm}l^{\pm})$. Blue areas correspond to large negative values, red areas correspond to values close to 0%.

Ideally, Fig. 18 - 20 would show 0% for the change in signature $\Delta LP(ll)$

for each grid point. The red area in the right lower side of the grids has a small change: $|\Delta LP(ll)| < 1\%$ for both for SS and OS signature. This is neglibible compared to the estimated signal uncertainty of $20\% - 30\%$ in the ATLAS analysis. This red region corresponds to gluinos that are heavy compared to squarks.

In the heavy squarks region ($m_{\tilde{q}} > m_{\tilde{g}}$), there is less dilepton production in phenoGrid 2c than in the Light Neutralino Grid: the change in branching ratios $\Delta LP(ll)$ is negative and the colour is blue. A large decrease in dilepton production corresponds to blue areas in the Figs. 18-20. The decrease in lepton production in the heavy squarks region is a result of changing $\tan\beta$, which affects the couplings of gauginos to other sparticles.

For the the SS signature, the model that agrees the worst between the model grids is $m_{\tilde{g}} = 400$ GeV, $m_{\tilde{q}} = 800$ GeV. Here the branching ratios corresponding to SS production in phenoGrid 2c are $|\Delta LP(l^{\pm}l^{\pm})| \leq 8.9\%$ lower than for the Light Neutralino Grid. This number is compared to the cited error in the signal region in Ref. [ATLAS11]: $20 - 30\%$. The lower bound of experimental uncertainty (20%) is added to the largest estimated change in branching ratios $|\Delta LP(l^{\pm}l^{\pm})|$ to give an upper limit of the uncertainty we add by changing model grids. These numbers are added quadratically: $\sigma_{\text{tot}} = \sqrt{20^2 + 8.9^2} = 21.9\%$. The change in the total uncertainty σ_{tot} is considered insignificant compared to the experimental uncertainty. Therefore this branching ratio modification is negligible compared to ATLAS uncertainties.

For the OS signature with different lepton flavours, the same model ($m_{\tilde{g}} = 400$ GeV, $m_{\tilde{q}} = 800$ GeV) also gives the least agreement between the model grids, corresponding to a change of $\Delta LP(e^{\pm}\mu^{\pm}) = -5.1\%$ in the dilepton signature. The total uncertainty from this model and the lowest cited ATLAS uncertainty is $\sigma_{\text{tot}} = 20.6\%$. For the OS signature with the same lepton family, the same model corresponds to the maximum change in dilepton signature of $\Delta LP(e^{+}e^{-}) = -5.7\%$, which gives $\sigma_{\text{tot}} = 20.8\%$. The OS signature shows better agreement of branching ratios between the grids than SS signature.

In conclusion, by changing grids from Light Neutralino to phenoGrid 2c, we introduce a change in the phenomenology that is negligible compared to the uncertainty cited by ATLAS. Judging by the branching ratios, the ATLAS exclusion limits should also apply to phenoGrid 2c.

3.4.4 PhenoGrid 2c and non-LHC constraints

As noted in Sec. 3.4.1, all models tested for in the Light Neutralino Grid imply too much dark matter to be consistent with the world we live in. All models correspond to a Higgs boson mass that has been excluded by LEP. As shown in Sec. 3.4.3.4, the modification of the Light Neutralino Grid into phenoGrid 2c does not affect the dilepton signature significantly,

compared to the experimental uncertainties estimated by ATLAS. Therefore the ATLAS exclusion limits [ATLAS11] also apply to phenoGrid 2c.

In this section, we investigate whether phenoGrid 2c meets the physical constraints on the dark matter density, Higgs boson mass, and $\mathrm{Br}(b \to s+\gamma)$ better than the Light Neutralino Grid does.

The relic dark matter density for the models in phenoGrid 2c is presented in Fig. 21, where the WMAP7 central value is drawn as a blue line and the WMAP7 upper bound is shown as the red line. As seen in Fig. 21, all models in phenoGrid 2c are compatible with the WMAP7 upper bound for cold dark matter density. In fact, there are no models above the central value.

All models in phenoGrid 2c give a relic dark matter density close to the central value, as seen in Fig. 21, meaning that they correspond to $\tilde{\chi}_1^0$ making up almost all the cold dark matter in the Universe. The mass range 100 GeV $< m_{\tilde{l}_R} <$ 111 GeV gives an allowed dark matter density. The upper limit on $m_{\tilde{l}_R}$ has not been systematically studied. It is possible that models with $m_{\tilde{l}_R} >$ 111 GeV do fullfill the relic dark matter constraint as well.

The values for the dark matter density are presented in the form of a two-dimensional grid in Fig. 22. The value for $\Omega_c h^2$ ranges between 0.104 and 0.111 for our models. The central value from WMAP7 is equal to 0.111 to three significant figures.

In Fig. 23, the relic dark matter density for models in phenoGrid 2c is compared to values for the corresponding models in the Light Neutralino grid. The dark matter density is decreased by a factor of 3-30, depending on the point in the squark-gluino mass plane.

The Higgs mass for phenoGrid 2c has been calculated to be 114.8 GeV for all models in phenoGrid 2c, which is found to be consistent with data from LEP. The Higgs mass is 105.4 GeV for all models in Light Neutralino Grid, which is excluded by LEP.

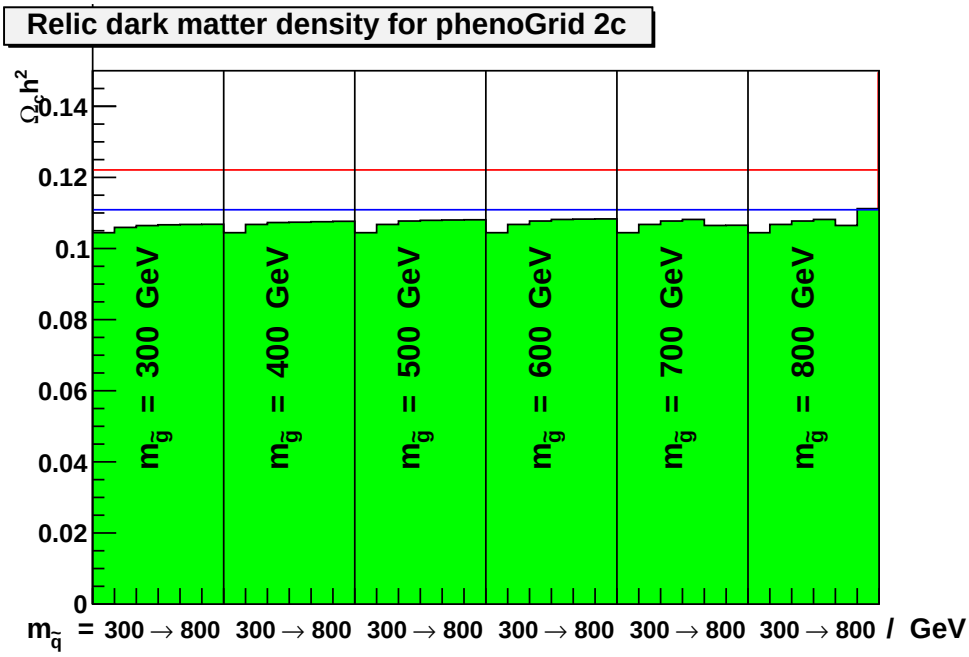

Figure 21: The relic dark matter density corresponding to models in phenoGrid 2c. The blue line shows the central value from WMAP7 for the relic cold dark matter density. The red line shows the upper bound from WMAP7. The wide bins correspond to constant gluino masses. Within each wide bin, the squark mass is varied between 300 GeV and 800 GeV.

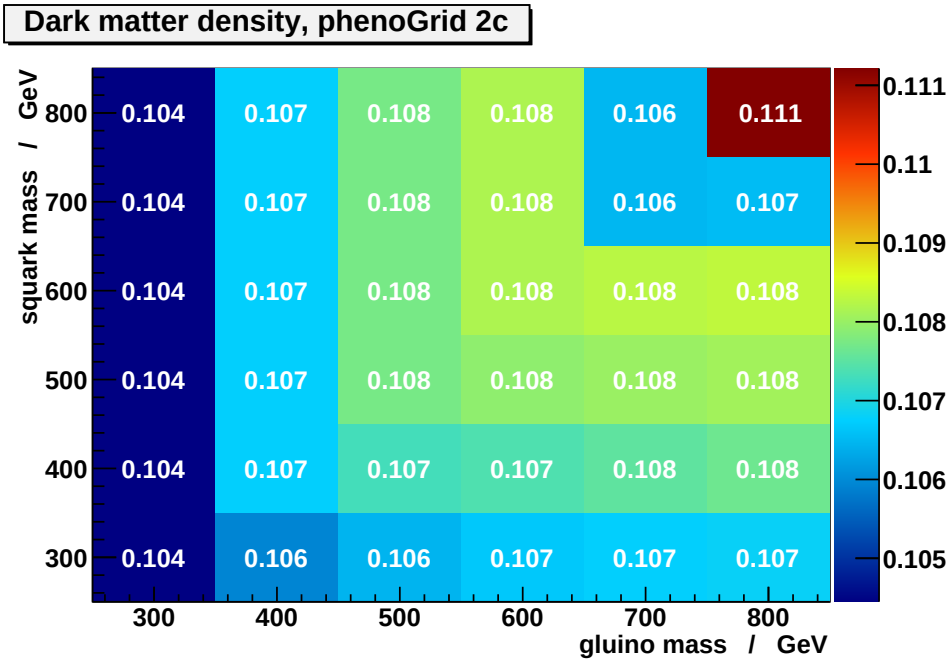

Figure 22: The relic dark matter density for the models in PhenoGrid 2c as a function of gluino mass (on the x-axis) and squark mass (on the y-axis). The numbers and colour coding show the relic dark matter density $\Omega_c h^2$ for the models. Red denotes high values, blue denotes low.

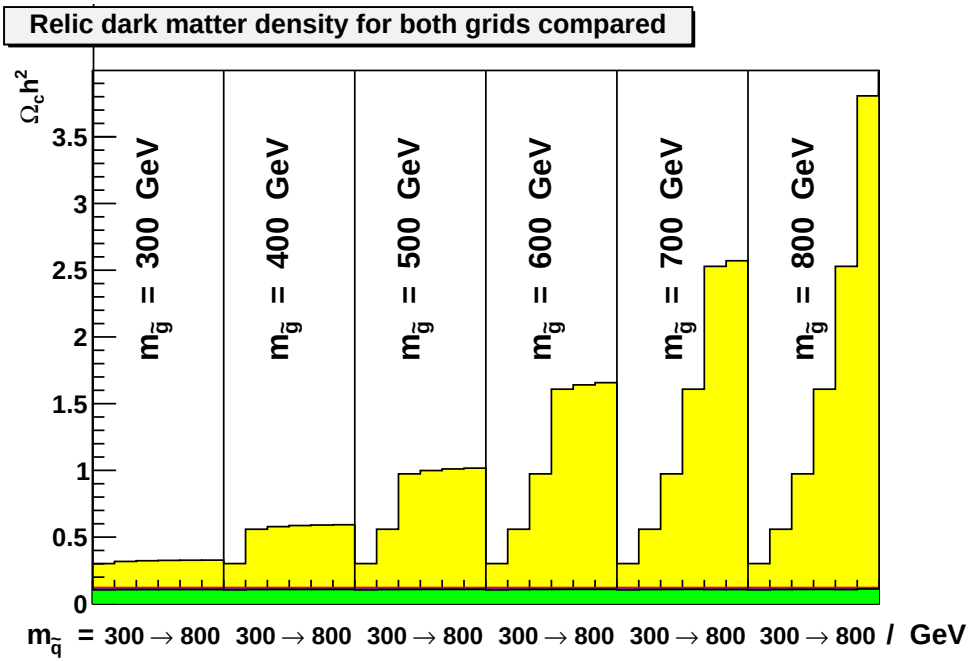

Figure 23: Dark matter density as given by Light Neutralino Grid (yellow) and PhenoGrid 2c (green). The red line shows the WMAP7 upper bound to the relic cold dark matter density. All models in phenoGrid 2c are just below the red line, all models in the Light Neutralino Grid are above it. The wide bins correspond to constant gluino masses. Within each wide bin, the squark mass is varied between 300 GeV and 800 GeV.

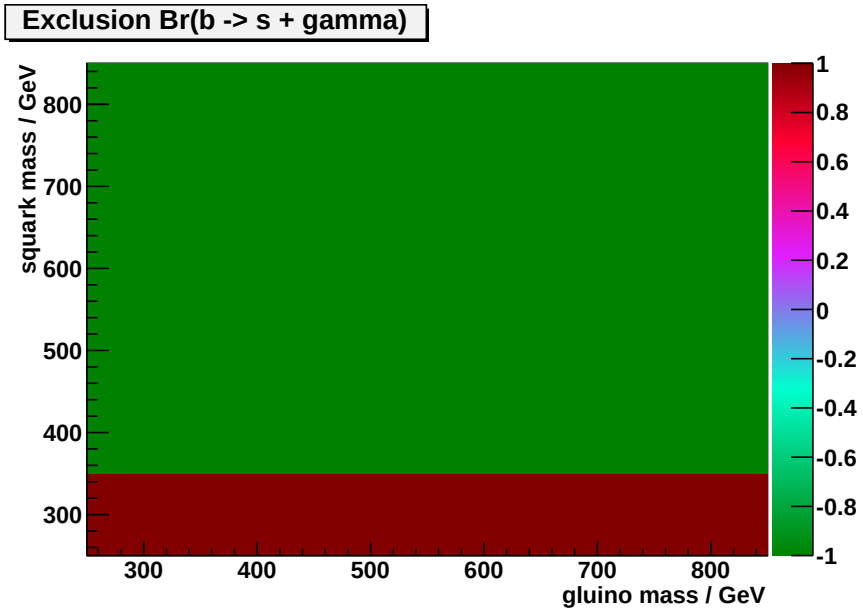

Figure 24: Values for Br($b \rightarrow s + \gamma$) corresponding to the models in phenoGrid 2c. Red denotes forbidden values. Green means allowed values. The gluino mass is varied on the x-axis. The squark mass is varied on the y-axis. A total of 36 models, evenly spaced in this grid, is tested for.

In the Light Neutralino Grid, all models have a value for $\mathrm{Br}(b \to s + \gamma)$ that is compatible with experimental bounds. In phenoGrid 2c, however, the six models with $m_{\tilde{q}} = 300$ GeV gave a forbidden value for $\mathrm{Br}(b \to s+\gamma)$, as shown in Fig. 24. Changing model parameters such as $\tan\beta$ and squark masses, affects this value. The six models excluded by $\mathrm{Br}(b \to s + \gamma)$ for phenoGrid 2c are already excluded by ATLAS, as seen in Fig. 9. All other models in phenoGrid 2c return allowed values for $\mathrm{Br}(b \to s + \gamma)$.

So, by making the modifications to Light Neutralino Grid, we have created a set of models that are consistent with the observed dark matter density and that does not contradict experimental results from LEP of searches for Higgs.

3.5 Conclusions

We started by analysing pMSSM models with a dilepton signature that have been considered by ATLAS in Ref. [ATLAS11] to set exclusion limits on SUSY production. We found that all of them gave a value for the relic dark matter density that was by far excluded by WMAP7 and that the corresponding Higgs boson mass has been excluded by searches at LEP. From these observations we can say that the ATLAS paper [ATLAS11] excluded models that were already excluded elsewhere.

We modified the Light Neutralino Grid and demanded that it would meet constraints on dark matter, Higgs boson mass and $\mathrm{Br}(b \to s+\gamma)$. The mass of right-handed sleptons $m_{\tilde{l}_R}$ was lowered to decrease the corresponding relic dark matter density. To increase the Higgs boson mass, the Higgs fields v.e.v.s ratio $\tan\beta$ and the mass of the third generation sfermions were increased. The resulting model grid was called phenoGrid 2c.

We investigated final states with SS and OS dilepton signatures, corresponding to models in the Light Neutrlaino Grid and phenoGrid 2c. It was shown that the relevant branching ratios have not changed significantly. Therefore we can apply the ATLAS exclusion limits shown in Fig. 9 to our models. The particle kinematics is not affected by our modification of the grid because the only sparticle with changed mass is $\tilde{l}_R$, which does not contribute to the ATLAS dilepton signal region [1]. Changing $\tan\beta$, affected some branching ratios, however, this change was considered insignificant when compared to the ATLAS experimental errors.

All models with $m_{\tilde{q}} \geq 400$ GeV in PhenoGrid 2c are consistent with the experimental Higgs bounds from LEP, WMAP7 dark matter density limits and $\mathrm{Br}(b \to s+\gamma)$. Only models with $m_{\tilde{q}} = 300$ GeV gave a forbidden value for $\mathrm{Br}(b \to s + \gamma)$. These models are already excluded by ATLAS. So, the Light Neutralino grid was modified to provide a grid of models compatible

[1] This was also checked by generating fast simulations of the Light Neutralino Grid and of phenoGrid 2c, but this work was not carried out by the author of this work.

with experimental bounds and with LHC phenomenology unchanged with respect to the grid tested experimentally with ATLAS.

The ATLAS experiment excludes several of the phenoGrid 2c model points. Therefore, although the initial ATLAS paper [ATLAS11] was excluding models already excluded elsewhere, we showed that it also excludes a range of models compatible with the relic dark matter density, Higgs boson mass and $\mathrm{Br}(b \to s + \gamma)$.

4 Complementarity between the LHC and other dark matter detection experiments

4.1 Introduction

In this chapter, three sets of pMSSM models are investigated. The model sets correspond to pair production of i) squarks and gluinos, ii) gauginos, and iii) sleptons at the LHC. These model sets are referred to as "Squark-gluino", "Gaugino", and "Slepton" model sets respectively. They are investigated in Sec. 4.4.1, Sec. 4.4.2 and Sec. 4.4.3. The model parameters are selected based on published LHC projections [BCPT95], [BCPT96], [Pol96], [ATL11], [BCPT94]. The criteria is that these models should be detectable wih an integrated LHC luminosity of around 500 fb^{-1}, corresponding to LHC operation until about 2020. Out of the models that we generate, we keep those that are compatible with experimental constraints on the relic dark matter density, the Higgs boson mass and $\text{Br}(b \to s + \gamma)$. The constraints are described in Sec. 2.4, with three standard deviations from the WMAP central value used as an upper bound, as given by Eq. (7), to be consistent with Ref. [GEU+04]. The remaining models are studied to see whether they can be detected in other experiments. Two things in particular affect the production rate of SUSY particles. The first is the coupling between the SM particle from the proton to the SUSY particle to be produced. Particles that interact by the strong force, such as squarks and gluinos, have higher couplings than those that interact by the weak or electroweak force, such as gauginos and sleptons. The second is the phase space available for SUSY production - lighter SUSY particles would be produced at a higher rate than heavier.

4.2 Detection of dark matter

There are several different strategies for dark matter searches. The two main classes are direct detection and indirect detection. Direct detection experiments aim to measure direct interactions with dark matter particles in the form of the elastic scattering of dark matter off nuclei in the detector. Indirect detection experiments search for products from annihilation of dark matter particles in the galactic halo or in the Sun. Production of dark matter particles at accelerators, such as the LHC, and detection of missing transverse energy can be regarded as a third kind of method.

The overlap between detectability in the LHC with other dark matter detection experiments is investigated below. In this part of the work, the dark matter particles will sometimes be referred to as WIMPs rather as LSPs. WIMPs can denote both SUSY dark matter or other hypothetical weakly interacting elementary particles.

4.2.1 Direct detection

The most convincing evidence for WIMP dark matter would be through direct detection. Hundreds of thousands of WIMPs from the galactic halo should pass through every square centimeter of the Earth each second [JKG96]. WIMPs must have a small but finite coupling to SM particles to explain the observed (low) abundance today, otherwise they would not have annihilated into SM particles in the early Universe. If so, WIMPs will occasionally scatter off nuclei in ordinary matter today. However, interactions with SM particles are rare. The challenge is to measure and distinguish from the background the small amount of energy deposited from the rare collisions of dark matter particles with the detector.

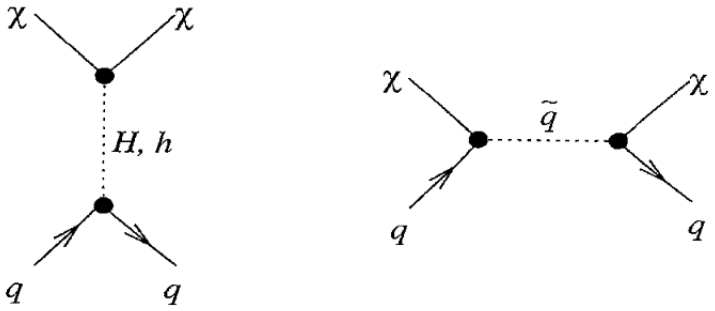

Figure 25: Two Feynman diagrams for interactions of the $\tilde{\chi}_1^0$ with squarks. These processes are important for the spin independent cross section, which is relevant for direct detection experiments. Neutral Higgs bosons or squarks can be exchanged. The image is obtained from [JKG96].

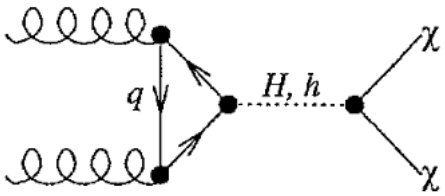

Figure 26: One possible Feynman diagram, representing interaction of $\tilde{\chi}_1^0$ with gluons. This process contributes to the spin independent cross sections, which is relevant for direct detection experiments. SM quarks and neutral Higgs bosons can be exchanged in the process. The image is obtained from [JKG96].

The $\tilde{\chi}_1^0$ can interact with the nucleus in a spin independent way with a cross section σ_{SI}. The spin independent scattering reflects the interaction of

the neutralino with gluons or quarks in the nucleus. Virtual Higgs bosons or squarks may be exchanged in the processes, as shown in Figs. 25 and 26.

The contribution of the spin independent scattering cross section σ_{SI} to the total scattering cross section scales with A^2, where A is number of nucleons in the nucleus [JKG96]. The sensitivity to the spin independent cross section can be increased greatly by increasing the mass of the target nuclei.

4.2.2 Indirect detection

In indirect detection experiments, the annihilation products from LSP annihilation are searched for. One can either look at the flux of gamma rays from neutralino annihilation in the galactic halo and set limits on the quantity $\langle \sigma v \rangle / m^2_{\tilde{\chi}^0_1}$, where σ is the annihilation cross section multiplied by and averaged over v, the LSP velocity and $m_{\tilde{\chi}^0_1}$ is the LSP mass and the brackets denote averaging. Or one can look at high-energetic neutrinos arising from annihilation of neutralinos trapped in the Sun and set limits on the spin dependent scattering cross section σ_{SD}. These two methods are described below.

4.2.2.1 Spin dependent cross section

The total elastic scattering cross section of the a $\tilde{\chi}^0_1$ off protons has a contribution from both the spin independent cross section σ_{SI} and the spin independent cross section σ_{SD}. In the spin dependent process, the $\tilde{\chi}^0_1$ couples to the spin of a nucleus. As the sensitivity for σ_{SI} can be regulated by using heavy nuclei in the detector, better limits for σ_{SI} than for σ_{SD} can be obtained for direct detection experiments. However, more competitive limits on σ_{SD} can be placed from indirect detection experiments [WE09].

The $\tilde{\chi}^0_1$ annihilation rate depends on the square of the $\tilde{\chi}^0_1$ number density [JKG96]. Therefore regions with a high density of dark matter could be a good source for indirect detection experiments. The $\tilde{\chi}^0_1$ particles could become gravitationally captured inside celestial bodies, such as the Sun. Once captured, the particles would scatter and loose energy until they reach thermal equilibrium at the core of the Sun. The capture occurs mainly via spin dependent scattering, as a large part of the nuclei in the Sun are light protons with non-zero spin. With enough WIMPs concentrated at the core, the result could be an annihilation signal strong enough for detection on Earth. Of any annihilation products, the weakly interacting neutrinos would escape the Sun and reach the Earth. Assuming that the $\tilde{\chi}^0_1$ are in equilibrium in the Sun, the $\tilde{\chi}^0_1$ annihilation rate is set equal to the capture rate [WE09]. Thus, measurements of annihilation products from the Sun provides limits for the spin dependent cross section.

In the spin dependent scattering interaction, the neutralino can interact with quarks in the nucleus by exchange of Z^0 bosons and squarks, as is

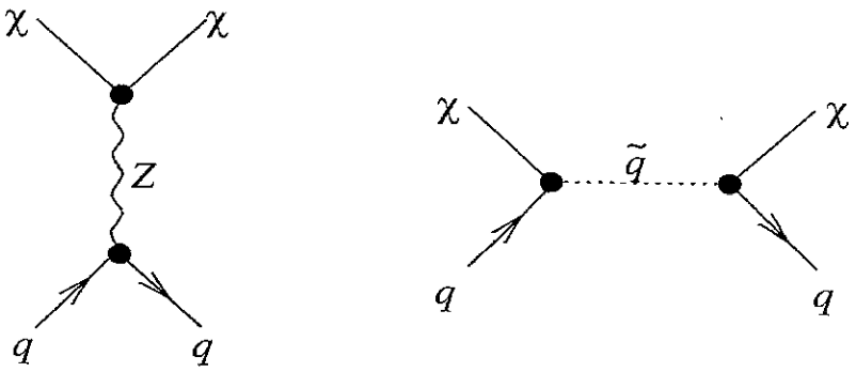

Figure 27: Two possible Feynman diagrams that are important for the spin dependent cross section, which is relevant for indirect detection experiments. The SM Z^0 boson or a squark can act as an intermediate particle. The image is obtained from [JKG96].

shown in Fig. 27.

4.2.2.2 Annihilation cross section

Pair-annihilation of $\tilde{\chi}_1^0$ in the galactic halo would result in gamma rays with the flux proportional to $\langle\sigma v\rangle/m_{\chi^2}$ [Fermi-LAT11]. Here $\langle\sigma v\rangle$ is the velocity averaged annihilation cross section and m_χ is the mass of the $\tilde{\chi}_1^0$. Indirect detection experiment can measure the gamma ray flux from the cosmos and compare with predictions from $\tilde{\chi}_1^0$ annihilation in the galactic halo.

Some Feynman diagrams for $\tilde{\chi}_1^0$ pair annihilation are shown in Fig. 28. An intermediate sfermion, Z^0 boson or a CP-even Higgs boson can mediate the annihilation, which results in two SM fermions.

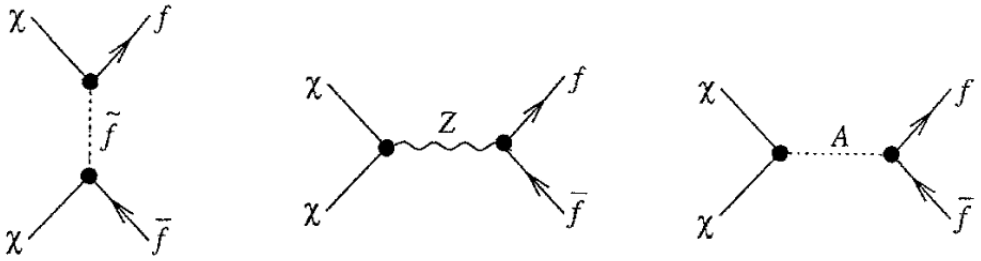

Figure 28: The three main annihilation channels for neutralino $\tilde{\chi}_1^0$ annihilations into fermions. Sfermions, Z^0 bosons or the CP-odd Higgs boson A^0 can be exchanged in the process. The image is obtained from Ref. [JKG96].

4.3 Dark matter experiments

This section provides an overview of the experiments for direct and indirect detection of dark matter that are relevant for this work. Some of the experiments (XENON100, Fermi) are already in operation and have already provided limits on cross sections for the $\tilde{\chi}_1^0$ processes discussed in Sec. 4.2.1 and Sec. 4.2.2. Other experiments (XENON1t, IceCube IC86 and CTA) are in the planning stage and have not yet provided any limits. For these three experiments, sensitivity projections are used to determine if the models generated in this work will be accessible by these planned experiments.

To choose among all dark matter detection experiments and relevant observables, Ref. [BBE11] was used as a starting point. It gives an overview over current and planned experiments for detection of dark matter and presents limits and projected sensitivities for experiments that measure σ_{SI} and $\langle\sigma v\rangle/m^2_{\tilde{\chi}_1^0}$.

A summary of the experiments used and the variable that they measure are given in Table 14 in Sec. 4.5, where the generated models are tested against the limits.

4.3.1 XENON

XENON is a direct detection experiment, setting limits on the spin independent cross section of WIMPs scattering on liquid Xenon. The current phase of the program, XENON100, has a target mass of 62 kg. It is stationed at the Gran Sasso Underground Laboratory, Italy and shown in Fig. 29.

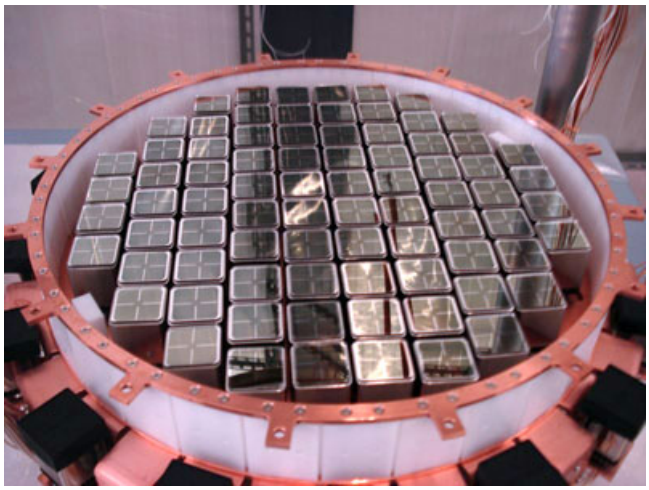

Figure 29: Photomultiplier tube arrays in the XENON100 detector [XEN].

XENON100 limits, computed from 100 days of data [XENON10011], are used in this analysis. The projected sensitivity of the XENON1t upgrade is

also considered. The data for the projected sensitivity is obtained from Ref. [Ni09].

4.3.2 Fermi Large Area Telescope

The Fermi Large Area Telescope (Fermi-LAT) is the main instrument on the Fermi satellite, shown in Fig. 30. It is a telescope that measures gamma ray fluxes and is particularly sensitive in the energy range $20\,\text{MeV} - 300\,\text{GeV}$. Using 24 months of data from 10 dwarf satellite galaxies, the best limits to date on $\langle \sigma v \rangle$ were set, as described in Ref. [Fermi-LAT11]. Out of the different $\tilde{\chi}_1^0$ annihilation channels examined in Ref. [Fermi-LAT11], the two channels with $(b\bar{b})$ or $(\tau^+\tau^-)$ in the final states provide the best limits. Data for these two channels is used in this work.

Figure 30: The Fermi spacecraft shortly before launch into orbit. The image photograph is obtained from Ref. [Fer].

4.3.3 Cerenkov Telescope Array

The Cerenkov Telescope Array (CTA) is a ground based indirect detection experiment in construction. CTA will search for Cherenkov light produced by particle showers created when high-energy cosmic particles hit the atmosphere. CTA has a larger detector area than Fermi and is expected to have better sensitivity than Fermi for high-energy gamma rays, which corresponds to large $\tilde{\chi}_1^0$ masses. The projected sensitivity of CTA is obtained from Fig. 6 in Ref. [BMDG11].

4.3.4 IceCube

IceCube is the largest neutrino detector in the world, situated on Artarctica at the South Pole. A photograph of some Antarctic inhabitants is shown in Fig. 31. The effective volume of IceCube is more than one cubic kilometer of ice. High-energetic neutrinos that interact with nuclei in the ice, in the vicinity of the detector, produce energetic muons. The muons emit Cherenkov light, which is transmitted through the transparent ice and detected by arrays of PMTs.

Figure 31: Antarctic penguins, photographed by an IceCube member [Ice].

IceCube places limits on the spin dependent scattering cross section σ_{SD} in searching for for neutrinos produced in WIMP annihilations inside the Sun.

The sensitivity of IceCube for 180 days of data taking with 86 strings is used from Ref. [IceCube11]. A worst-case and best-case scenario is presented in Ref. [IceCube11]. In this analysis, the best case scenario, called "hard case", is used.

4.4 Model sets

In this section, the generated model sets will be described and examined. As squarks and gluinos interact by the strong force, their production in LHC will be dominant if the masses of SUSY particles are similar. Such models are examined in Sec. 4.4.1. To achieve dominant production of gauginos or sleptons on the GeV scale, these particles need to be considerably lighter than squarks and gluinos [BCPT96]. Models with dominant gaugino production are examined in Sec. 4.4.2. Models with dominant slepton production

are described in Sec. 4.4.3. For each model set, it is examined what fraction of the generated models are compatible with the three experimental constraints, described in Sec. 2.4. Investigations are made into what values of SUSY parameters correspond to models that are compatible with the experimental constraints. In Sec. 4.5, these models are compared with experimental limits from detection experiments described in Sec. 4.3.

4.4.1 Squark-gluino model set

The squark-gluino models are characterized by production of squarks and gluinos at the LHC. With an integrated luminosity of 10fb^{-1} at $\sqrt{s} = 14$ TeV, squarks and gluinos up to 2 TeV should be detectable in the LHC [BCPT96], [Pol96].

4.4.1.1 Model parameters

To produce specific models corresponding to production of squarks and gluinos, several scans over different SUSY parameters are performed. The squark and gluino masses are varied independently of each other in the mass range 400 GeV − 2000 GeV. The $\tilde{\chi}_1^0$ mass is the lowest of the eigenvalues for the neutralino mixing matrix, defined in equation (3). In this model set, both bino-like ($M_1 < M_2$) and wino-like ($M_2 < M_1$) LSPs are explored. The bino mass is scanned up to 1250 GeV. The parameter $\tan\beta$ is varied up to 23. The trilinear top coupling parameter A_t is set to correspond to either $A_t = \mu/\tan\beta$ (minimum stop mixing) [ADK+04], or to $A_t = \mu/\tan\beta + \sqrt{6}m_{\tilde{t}}$ (maximum stop mixing), [Zer10]. The parameter choices for the Squark-gluino model set are summarized in Table 6.

SUSY parameter	Symbol	Scan range
Squark mass	$m_{\tilde{q}}$	$[400, 2000\text{ GeV}]$
Gluino mass	$m_{\tilde{g}}$	$[400, 2000\text{ GeV}]$
Bino mass	M_1	$[20\text{ GeV}, \min(1250\text{ GeV}, M)]$
Higgs parameters	$\mu,\ m_A$	2 TeV
Higgs v.e.v.s ratio	$\tan\beta$	$[3, 23]$
Trilinear couplings	$A_l,\ A_b$	0 GeV
Top trillinear coupling	A_t	$\mu/\tan\beta, \quad \mu/\tan\beta + \sqrt{6}m_{\tilde{t}}$

Table 6: The parameter scans for the squark-gluino models. The scan for M_1 is performed up to the lowest of $M = \min(m_{\tilde{q}}, m_{\tilde{g}})$ and 1250 GeV. The parameter $\tan\beta$ is scanned in steps of 5. The other parameters are scanned in log scale.

In performing the scans, we also vary the masses of sleptons and winos. To keep the number of generated models manageable, five subsets are defined, corresponding to different mass hierarchies for gauginos and sleptons.

Generally, for one given subset, the wino mass is varied and the slepton mass is kept fixed in relation to some other mass, as specified below. The five different subsets are defined in Table 7.

Subset	Wino mass (M_2)	Slepton mass: $m_{\tilde{l}}, m_{\tilde{\nu}}$
(1)	2.5 TeV	2.5 TeV
(2)	$[20\text{ GeV}, \min(M, 1250\text{ GeV})]$	2.5 TeV
(3)	$[20\text{ GeV}, \min(M, 1250\text{ GeV})]$	$\max(M_1, M_2) + 50$ GeV
(4)	$[20\text{ GeV}, \min(M, 1250\text{ GeV})]$	$\max(M_1, M_2) - 50$ GeV
(5)	$[20\text{ GeV}, \min(M, 1250\text{ GeV})]$	$\min(M_1, M_2) + 5$ GeV

Table 7: The five squark-gluino subsets. The parameter M is defined as $M = \min(m_{\tilde{q}}, m_{\tilde{g}})$. The scans for M_2 are performed up to the lowest of $\min(m_{\tilde{q}}, m_{\tilde{g}})$ and 1250 GeV.

The first subset has heavy sleptons and gauginos at 2.5 TeV, which implies that squarks and gluinos decay directly into SM quarks and the $\tilde{\chi}_1^0$. The second subset has heavy sleptons (2.5 TeV) and intermediate gauginos. The wino mass M_2 is scanned (independently) in the same mass range as the bino mass M_1 for subsets (2)-(5). Subset (3) has intermediate sleptons, heavier than all gauginos. Subset (4) has intermediate sleptons, lighter than gauginos. Finally, subset (5) has very light sleptons, only 5 GeV heavier than the LSP-related parameter $\min(M_1, M_2)$.

4.4.1.2 Experimental constraints

Scanning over SUSY parameters as described above, 37 000 models are generated in the Squark-gluino model set. The relic dark matter density for the five subsets is examined.

For model subsets (1), (2) and (3), $1 - 4\%$ of the generated models pass the WMAP7 upper bound on the relic dark matter density. For subsets (4) and (5), a large number of models have been generated with a slepton or sneutrino LSP. These models are discarded. Once the condition that a neutralino is the LSP is applied, no models of subset (4) have an allowed dark matter density; this subset is not considered further. For subset (5), only 4% of 12020 generated models have a neutralino LSP. None of the models from subsets (2) and (5) are consistent with both the dark matter constraint and the Higgs boson mass constraint.

For subsets (1) and (3), 2% or less of the generated models pass both experimental constraints. All remaining models also pass the $\text{Br}(b \to s + \gamma)$ constraint. In conclusion, only subsets (1) and (3) resulted in physical models. These correspond to mass hierarchies with heavy sleptons and gauginos (1), and with intermediate sleptons and gauginos, $m_{\tilde{l}} = \max(M_1, M_2) + 50$ GeV (3).

4.4.1.3 Relation between model parameters and experimental constraints

It is now investigated which parameter values correspond to models that are compatible with the applied experimental constraints. The mass difference between the lightest sfermion and the LSP, called Δm in this text, is investigated. This number is interesting because it may affect the annihilation cross section of the LSP in the early Universe. In fact, we are considering the t-channel interaction that is discussed in Sec. 3.4.2, where it is shown that the cross section for this process is proportional to

$$\sigma \propto \frac{1}{(m_{\tilde{f}}^2 + m_{\tilde{\chi}_1^0}^2)^2}. \tag{26}$$

Expressed in terms of Δm, this value is

$$\sigma \propto \frac{1}{((\Delta m)^2 + 2m_{\tilde{\chi}_1^0}\Delta m + 2m_{\tilde{\chi}_1^0}^2)^2}. \tag{27}$$

So, for a fixed $\tilde{\chi}_1^0$ mass, the annihilation cross section with an intermediate sfermion is large for small values of Δm. While the expression given in Eq. (26) is better theoretically motivated, Δm is more intuitive and easier to implement while generating models. In addition, if the lightest sfermion is a squark, a low Δm value could allow for coannihilations of neutralinos with squarks, which in turn can affect the relic dark matter density [EG97]. Therefore Δm rather than $m_{\tilde{f}}^2 + m_{\tilde{\chi}_1^0}^2$ is examined.

Another relevant mass parameter is the mass difference between the two lightest neutralinos. If the $\tilde{\chi}_2^0$ is close to the LSP $\tilde{\chi}_1^0$ in mass, coannihilations can increase the net annihilation of the LSPs in the early Universe, as discussed in Sec. 2.4.1. A small mass difference $m_{\tilde{\chi}_2^0} - m_{\tilde{\chi}_1^0}$ could imply a lower dark matter density that is consistent with experimental constraints.

For the Higgs mass experimental contraints, criteria for $\tan\beta$ are investigated.

The following criteria can be applied to isolate all the models that pass the dark matter constraint from the models generated in the grids. For subset (1), the only condition for passing the dark matter constraint is $m_{\tilde{q}} - m_{\tilde{\chi}_1^0} < 5$ GeV. Subset (3) has the condition $m_{\tilde{\chi}_2^0} - m_{\tilde{\chi}_1^0} < 9.55$ GeV.

All models with an allowed Higgs mass have $\tan\beta > 3$. At lowest order, the Higgs boson mass is proportional to $|\cos 2\beta|$, which grows with $\tan\beta$, as shown in Fig. 12. Clearly, $\tan\beta = 3$ corresponds to a too low Higgs mass for all of Squark-gluino models. High values of $\tan\beta$, however, correspond to relic dark matter densities incompatible with constraints from WMAP for the subsets (2) and (3). This parameter can affect decay rates, by changing the couplings of the gauginos. As $\tan\beta$ is present in the neutralino

and chargino mixing matrices, Eqs. (2), (3), it can also affect the gaugino masses. For the models generated in subset (2), the lower limit $\tan\beta > 3$ from the Higgs constraint and the upper limit $\tan\beta < 8$ from the relic dark matter constraint overlap, since no models with $3 < \tan\beta < 8$ have been generated. The result is that no models in subset (2) are compatible with both dark matter and Higgs boson mass. The criteria that are compatible with experimental constraints is presented in Table 8.

	Subset (1)	Subset (3)
Survival:	1.1%	2%
Δm (DM)	< 5 GeV	-
$m_{\tilde{\chi}_2^0} - m_{\tilde{\chi}_1^0}$ (DM)	-	< 9.55 GeV
$\tan\beta$ (Higgs)	> 3	> 3
Criteria remove:	76%	100%

Table 8: The criteria found for models that are compatible with the experimental constraints on the relic dark matter density, the Higgs boson mass and $\mathrm{Br}(b \to s + \gamma)$. In parenthesis, it is stated which experimental constraint that constrains the models: "DM" for relic dark matter density and "Higgs" for the Higgs mass. "Survival" is the percentage of all generated models that are compatible with the three experimental constraints. The row "Criteria remove" is a measure of the success of the applied criteria, giving the percentage of models incompatible with experimental constraint that are removed by the criteria.

The region $3 < \tan\beta < 8$ corresponds to a large change in Higgs mass, as demonstrated in Fig. 12. Therefore the region $3 < \tan\beta < 8$ could be explored for models subsets (2) and (3) to find more SUSY models compatible with the physical constraints here.

Generation of the subsets (4) and (5) looked promising at the beginning, seeming to provide a small mass difference between sfermion sleptons and the LSP, which shoul correspond to high annihilation cross sections for the channel with an intermediate sfermion. However, a large part of the models turned out to have a slepton or sneutrino LSP, which is not considered here.

4.4.2 Gaugino model set

If squark masses and gluino masses are much heavier than masses of other SUSY particles, direct production of other lighter sparticles may be significant. In this section, models with dominant direct gaugino production at the LHC are investigated. The gaugino model set is inspired from Ref. [BCPT96].The slepton mass can be either above or below the masses of $\tilde{\chi}_1^+, \tilde{\chi}_2^0$.

4.4.2.1 Model parameters

Given the LHC projections considered in Ref. [BCPT96], charginos up to 400 GeV could be discovered. This sets the mass range for the scans of M_1 and M_2. The other mass parameters are scanned with a common mass in the range $1.5 - 2.5$ TeV. The parameters are specified in Table 9.

SUSY parameter	Symbol	Scan range
Bino mass	M_1	$[20, 400]$ GeV
Wino mass	M_2	$[40, 400]$ GeV
M_{high}	$M_3,\ \mu,\ m_A,\ m_{\tilde{q}},\ m_\tau,\ m_{\nu_\tau}$	$[1.5, 2.5]$ TeV
Higgs v.e.v.s ratio	$\tan\beta$	$[3, 23]$
Tril. couplings	$A_l,\ A_b$	0 GeV
Top tril. coupling	A_t	$\mu/\tan\beta,\ \mu/\tan\beta + \sqrt{6}m_{\tilde{t}}$

Table 9: The scanned parameters for the Gaugino model set. The parameter $\tan\beta$ is scanned in steps of 5. The mass parameters are scanned on a logarithmic scale.

Several subsets are defined to represent different sparticle hierarchies. Within the subsets, slepton masses are locked with respect to gaugino or gluino mass parameters. In subset (1), the slepton mass is set to the same high value as the gluino mass (M_3). In subset (2), the slepton mass is set 50 GeV above the highest of the bino mass M_1 and the wino mass M_2. In subset (3), the slepton mass is instead 50 GeV below this value. In subset (4), the slepton mass is fixed only 5 GeV above the lowest of the bino and wino masses. These subsets are presented in Table 10.

Subset	Slepton mass ($m_{\tilde{l}}$)
(1)	M_3
(2)	$\max(M_1, M_2) + 50$ GeV
(3)	$\max(M_1, M_2) - 50$ GeV
(4)	$\min(M_1, M_2) + 5$ GeV

Table 10: The four subsets of Gaugino models with different mass hierarchies for sleptons and gauginos.

4.4.2.2 Experimental constraints

A total of 18 000 models are generated. It is investigated, which of these are compatible with the physical constraints discussed in Sec. 2.4. Model subsets (3) and (4) contain models with a slepton or sneutrino LSP. These models are discarded from the analysis. Around half of the generated models in each of the model sets (1), (2) and (3) have an allowed dark matter density

and a neutralino LSP. For model set (4), only 6% of the generated models have a neutralino LSP. All of these models are compatible with the dark matter constraint.

For model subsets (1), (2) and (3), most models with allowed dark matter densities correspond to an allowed Higgs mass. The branching ratio $\mathrm{Br}(b \to s + \gamma)$ is allowed for all the models which fullfill Higgs boson mass and dark matter constraints. The total survival rate of each model set is specified in Table 11.

4.4.2.3 Relation between model parameters and experimental constraints

For model subsets (1) and (2) models that fullfill contraints on dark matter can be selected by requiring $M_2 - M_1 < 60$ GeV, $M_1 > 40$ GeV . These criteria remove 93% of the models that are forbidden by dark matter. For subset (3), the condition $M_2 - M_1 < 120$ GeV can be applied to remove 80% of the models with too high relic dark matter densities. In the Gaugino model subsets, most models with a wino-like LSP ($M_2 < M_1$) are compatible with dark matter.

The region where the Higgs boson mass is consistent with LEP limits can be isolated as follows. The low value $\tan\beta = 3$ is forbidden by Higgs boson mass constraints from LEP. Most models with $\tan\beta = 8$ pass Higgs boson mass constraints, except those with the lowest value of m_A: $m_A = 1500$ GeV. For $m_A = 1500$ GeV , the criteria that A_t corresponds to the maximum top mixing must be added. These criteria leave us with all the models in the grids that pass the Higgs mass constraint. The criteria are summarized in Table 11.

Subset:	(1)	(2)	(3)	(4)
Survival:	39%	39%	37%	2%
$M_2 - M_1$ (DM)	< 60 GeV	-	< 120	-
M_1 (DM)	> 40 GeV	-	-	-
$\tan\beta$ (Higgs)	> 3	> 3	> 3	-
Criteria remove:	76%	76%	57%	-

Table 11: The criteria that isolate all models with allowed dark matter density and Higgs boson mass for the Gaugino models are given above. If $\tan\beta = 8$, the constraint $m_A > 1500$ GeV for model sets (1), (2) and (3). "DM" denotes that the dark matter density sets the criteria, "Higgs" that it is the Higgs boson mass. "Survival" denotes the percentage of the generated models within a subset that pass all our constraints. The row "Criteria remove" is a measure of the success of the applied criteria, giving the fraction of models incompatible with experimental constraint that are removed by the criteria.

Clearly, there is a higher survival rate for the Gaugino model set than the Squark-gluino model set. For future extensions of the model set, the region $3 < \tan\beta < 13$ can be explored, since this region corresponds to a significant change in Higgs boson mass.

4.4.3 Slepton model set

For direct slepton production to be a significant source of SUSY events, sleptons (and sneutrinos) need to be much lighter than all other sparticles except the LSP. Sleptons with masses up to 300 GeV should be detectable at the LHC [BCPT96]. Regions corresponding to a physical dark matter density generally have $m_{\tilde{l}_R} \approx 100 - 250$ GeV [BCPT96].

4.4.3.1 Model parameters

The model set generated here is inspired by Ref. [AAD+11]. One set of benchmark models described in Ref. [AAD+11] are models in the pMSSM framework, scanned in the two-dimensional parameter space of LSP mass and slepton mass. The other parameters are kept constant in Ref. [AAD+11]. The left-handed and right-handed slepton masses are set equal.

Following Ref. [AAD+11], the slepton and LSP masses are varied. Only bino-like LSPs ($M_1 < M_2$) are examined, scanning the bino mass M_1 in the range 20 GeV − 300 GeV and the slepton mass $m_{\tilde{l}}$ in 70 GeV − 300 GeV. The leptons produced in the decay $\tilde{l}^{\pm} \to \tilde{\chi}_1^0 + l^{\pm}$ must have a large enough momentum to pass the threshold in the electron and muon triggers in the LHC experiments. Therefore the mass difference between $\tilde{l}$ and the LSP should be at least 30 GeV. In addition, we scan $\tan\beta$ in the range 1-25. All the other sparticle masses are set to M_{high}, which is also varied. The parameter values are given in Table 12. In summary, the sleptons, sneutrinos and the $\tilde{\chi}_1^0$ are light and all other particles heavy. Only these three sparticles would be produced at the LHC. Only one model set is generated. The result is 24 000 direct slepton production models.

LSP	M_1	$[20, 300]$ GeV
Slepton mass	$m_{\tilde{l}}, m_{\tilde{\nu}}$	$[70, 300]$ GeV
M_{high}	$M_2, M_3, m_A, m_{\tilde{q}}, m_{\tilde{\tau}}, m_{\tilde{\nu}_\tau}$	$[1500, 2500]$ GeV
Higgs v.e.v.s ratio	$\tan\beta$	$[1, 23]$
Tril. couplings	$A_l,\ A_b$	0 GeV
Top tril. coupling	A_t	$\mu/\tan\beta, \quad \mu/\tan\beta + \sqrt{6}m_{\tilde{t}}$

Table 12: The parameter scans for the Slepton models. Only one model subset is generated.

4.4.3.2 Experimental constraints

For some of the models generated, the selectron or the sneutrino have masses lower than the lightest neutralino. Once these models are removed from the analysis, 1.0% of the generated models pass the dark matter density constraint. When the Higgs boson mass constraint is added, 0.8% of the generated models remain. All these models pass the $\mathrm{Br}(b \to s+\gamma)$ constraint.

4.4.3.3 Relation between model parameters and experimental constraints

No models with $\tan\beta = 3$ have a Higgs mass compatible with LEP searches. Models with $\tan\beta = 4$ could be examined for further studies.

The parameters that affect the relic dark matter the most for this set, are the LSP mass, the slepton mass $m_{\tilde{l}}$ and the mass difference between the lightest sfermion and the $\tilde{\chi}_1^0$.

The criteria for $\tan\beta$, $m_{\tilde{\chi}_1^0}$, Δm and $m_{\tilde{l}}$ are given in Table 13. The criteria for this model set should be interpreted with particular care, as the Higgs boson mass constraint was found to affect criteria for parameters that do not enter into the Higgs boson mass calculation, as given in Eq. 10. The values in the criteria may be an arbitrary effect of choosing less than 1% from the generated set, as shown in Table 13.

Survival	0.8%
LSP mass (DM + Higgs)	< 80 GeV
Δm (DM+Higgs)	< 55 GeV
$m_{\tilde{l}}$	< 140 GeV
$\tan\beta$ (Higgs)	> 3
Criteria remove:	89%

Table 13: Criteria for Slepton models that are compatible with experimental constraints on relic dark matter density, Higgs boson mass constraints and $\mathrm{Br}(b \to s + \gamma)$. "Survival" denotes the percentage of the generated models that have a neutralino LSP and that pass the experimental constraints. The row "Criteria remove" gives a measure of the success of the applied criteria, giving the fraction of models incompatible with experimental constraint that are removed by the criteria.

In future scans, one could examine wino-like LSPs by scanning the wino mass M_2 in the range $[20, 300]$ GeV and the bino mass M_1 in the range $[1.5, 2.5]$ TeV, especially in view of that models with $M_2 < M_1$ correspond to allowed relic dark matter densities in the Gaugino model set. One could also investigate models with right-handed sleptons with a lower mass than left-handed sleptons to find more models compatible with dark matter.

4.5 Detectability of non-accelerator based experiments

For each of the models presented in Sec. 4.4.1 - Sec. 4.4.3, three observables are computed: the spin independent scattering cross section σ_{SI}, the spin dependent scattering cross section σ_{SD} and the annihilation cross section $\langle\sigma v\rangle$. These three parameters are computed with DarkSUSY [GEU+04] and plotted against the $\tilde{\chi}_1^0$ mass. Limits from current experiments and the projected sensitivity for future dark matter experiments are included in the plots to see if our models could be excluded by planned dark matter experiments of the future, or if the LHC will have sensitivity to models that no other experiment will be able to exclude in this decade.

The search results for from different experiments - direct, indirect and collider, are combined in Sec. 4.5. In combining the experimental result several different situations can occur. A dark matter detection experiment may have excluded models considered. These models would not need to be tested for in ATLAS. If the LHC can access models that other experiments can not, the LHC can contribute with results that would not be possible with the other experiments. However, if a SUSY model would be discovered at the LHC, confirmation that SUSY LSPs constitute dark matter would be needed from cosmological experiments. For this case, an overlap between the LHC and a dark matter detection experiment is desirable.

For current experimental limits, we use data from XENON100 for the spin independent cross section and limits from Fermi for the annihilation rate. For future experiments, we choose XENON1t for expected sensitivity to σ_{SI}, CTA for the annihilation cross section and 1-year and 10-years IceCube projections for the spin dependent cross section. These limits and predictions are compared to the corresponding values for σ_{SI}, σ_{SD} and $\langle\sigma v\rangle$ computed with DarkSUSY for our models. An investigation will be made of which SUSY parameters affect the different cross sections. The experiments used are summarized in Table 14.

Observable	Current experiment	Projected sensitivity
σ_{SI}	XENON100	XENON1t
σ_{SD}	-	IceCube 1 year, 10 years
$\langle\sigma v\rangle/m^2_{\tilde{\chi}_1^0}$	Fermi	CTA

Table 14: The experiments from which limits and the projected sensitivity to different observables are used in this section.

4.5.1 Spin independent cross section

The spin independent scattering cross section of $\tilde{\chi}_1^0$ on protons σ_{SI} is computed for the models considered above. We test whether the generated

models can be detected in direct detection experiments such as XENON. The results are illustrated for the three model sets in Fig. 32 - 34 together with current exclusion limits [XENON10011] from XENON100 (blue) and projected exclusion limits [Ni09] for XENON1t (red). The curves show the experimental upper bounds for the allowed cross section. The areas above the curves are excluded.

In the Squark-gluino model set, shown in Fig. 32, many models with an LSP mass $m_{\tilde{\chi}_1^0} \approx 40$ GeV can be excluded by XENON1t. For the gaugino model set, shown in Fig. 33, most models could be excluded by XENON1t. Many models in the Slepton model set, Fig. 34, can be excluded by XENON1t. For all three model sets, not a single model has been excluded by the direct detection experiment XENON100. One should note that XENON1t should be sensitive to the majority of the models considered in this work.

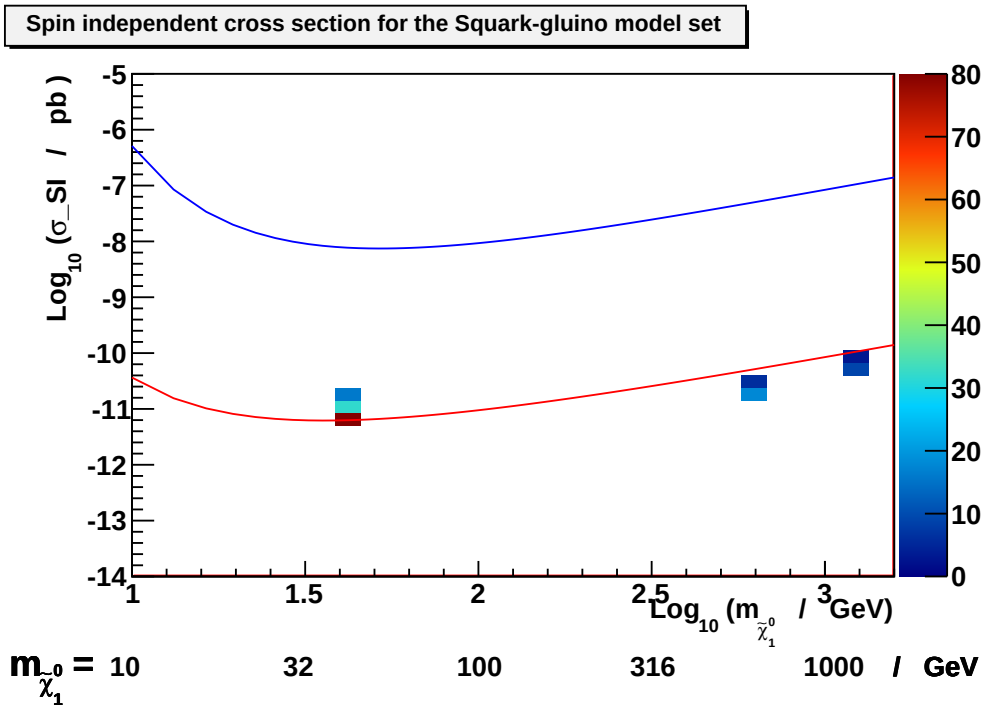

Figure 32: The spin independent cross section $\sigma_{\rm SI}$ as a function of the LSP mass ($m_{\tilde{\chi}_1^0}$) for the Squark-gluino models. Limits from XENON100 are shown as the blue curve. The projected sensitivity of XENON1t is shown as the red curve. The colour coding shows the number of models in each bin.

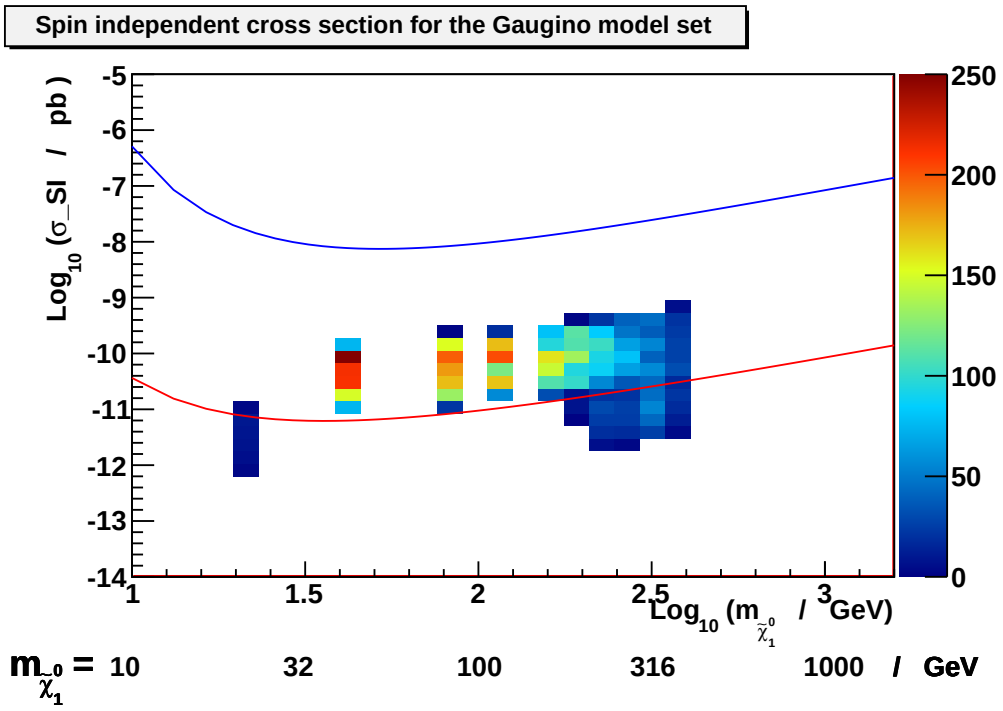

Figure 33: The spin independent cross section $\sigma_{\rm SI}$ as a function of the LSP mass ($m_{\tilde{\chi}_1^0}$) for the Gaugino models. Limits from XENON100 are shown as the blue curve. The projected sensitivity of XENON1t is shown as the red curve. The colour coding shows the number of models in each bin.

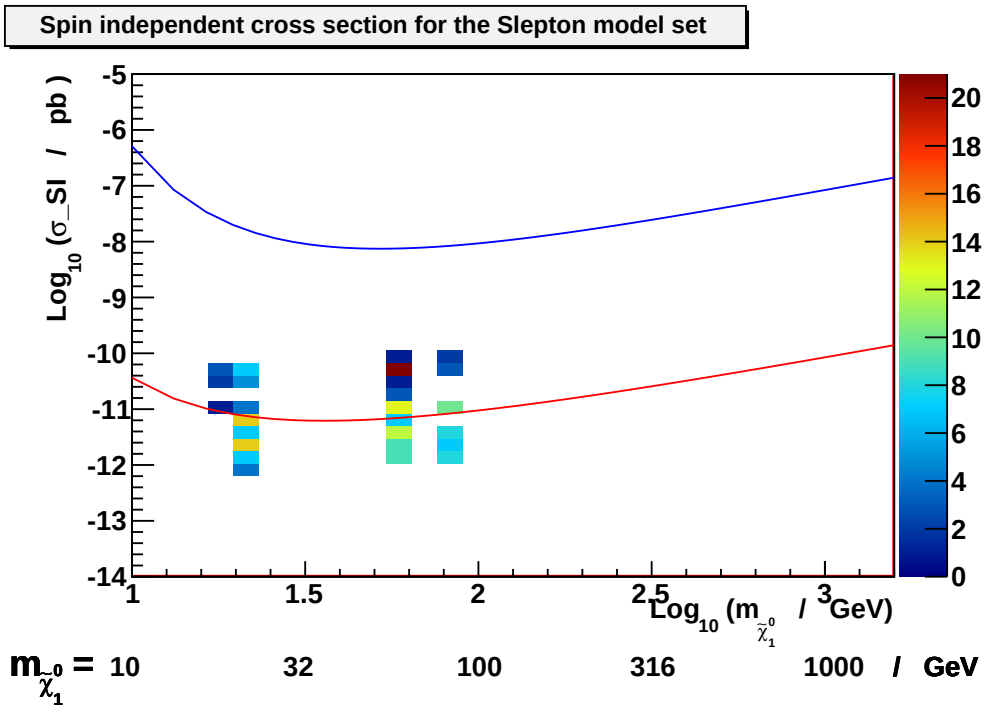

Figure 34: The spin independent cross section σ_{SI} as a function of the LSP mass ($m_{\tilde{\chi}_1^0}$) for the Slepton models. Blue curve: limits from XENON100. Red curve: projected sensitivity of XENON1t. The colour coding shows the number of models in each bin.

4.5.2 Spin dependent cross section

The spin dependent scattering cross section σ_{SD} is examined for the squark-gluino, gaugino and slepton models in Figs. 35 - 37. IceCube limits from one year (180 days) of data-taking are shown as a blue curve. IceCube does not have sensitivity for any of the generated models within one year. By making the experiment run over several years, however, better limits can be set. The projected IceCube sensitivity from 1 year of data-taking is extrapolated to 10 years by dividing σ_{SD}, for which IceCube is sensitive to within one year, by $\sqrt{10}$ (based on Poisson statistics). The black curve in Figs. 35 - 37 corresponds to 10 years of data taking.

After ten years, IceCube will have sensitivity for cross sections within an order of magnitude of the highest σ_{SI} in the Squark-gluino models Fig. 35. As only seven data points are provided in Ref. [IceCube11], there is some uncertainty in where the exclusion curve lies, together with uncertainties in the projections, which could allow for some models (with $m_{\tilde{\chi}_1^0} = 40$ GeV) to be within reach of 10 years of IceCube data taking.

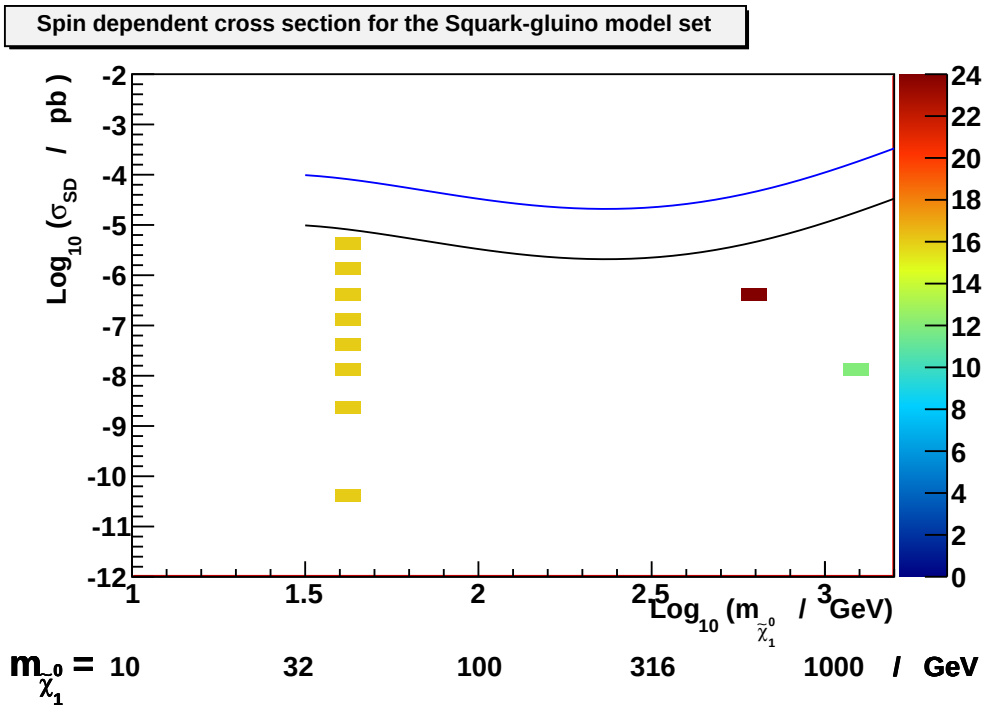

Figure 35: The spin dependent scattering cross section σ_{SD} as a function of the $\tilde{\chi}_1^0$ mass for the Squark-gluino models. The blue line shows the projected upper limit from IceCube for 1 year of data taking. The black line shows the projected upper limit from IceCube, corresponding to 10 years of data taking. The colour coding shows the number of models in each bin.

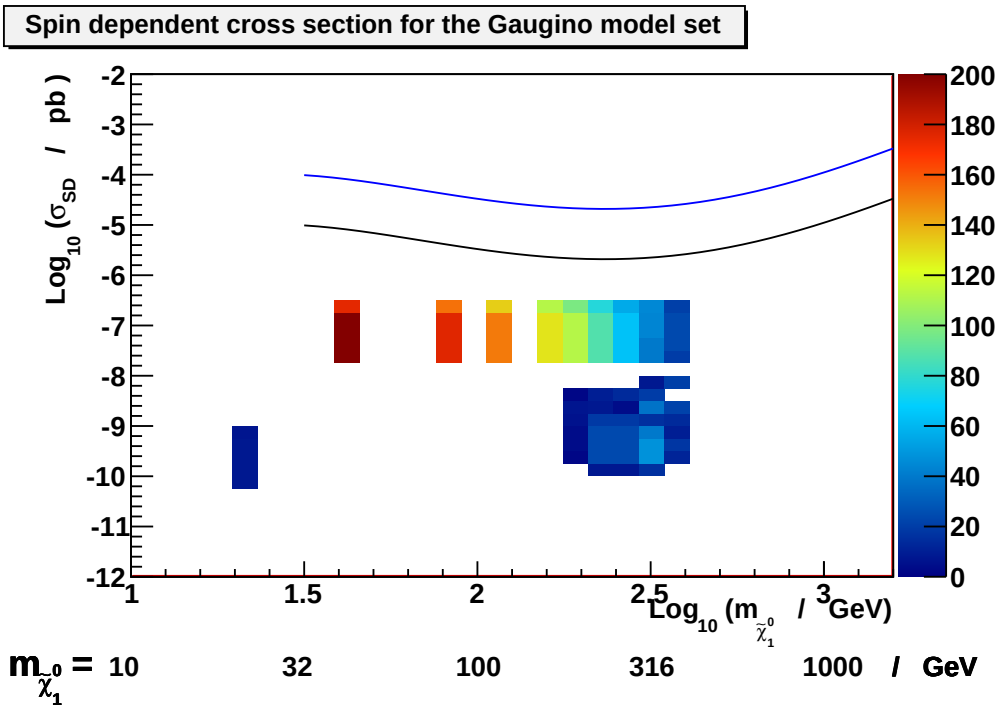

Figure 36: The spin dependent scattering cross section σ_{SD} as a function of the $\tilde{\chi}_1^0$ mass for the Gaugino models. The blue line shows the projected upper limit from IceCube for 1 year of data taking. The black line shows the projected upper limit from IceCube, corresponding to 10 years of data taking. The colour coding shows the number of models in each bin.

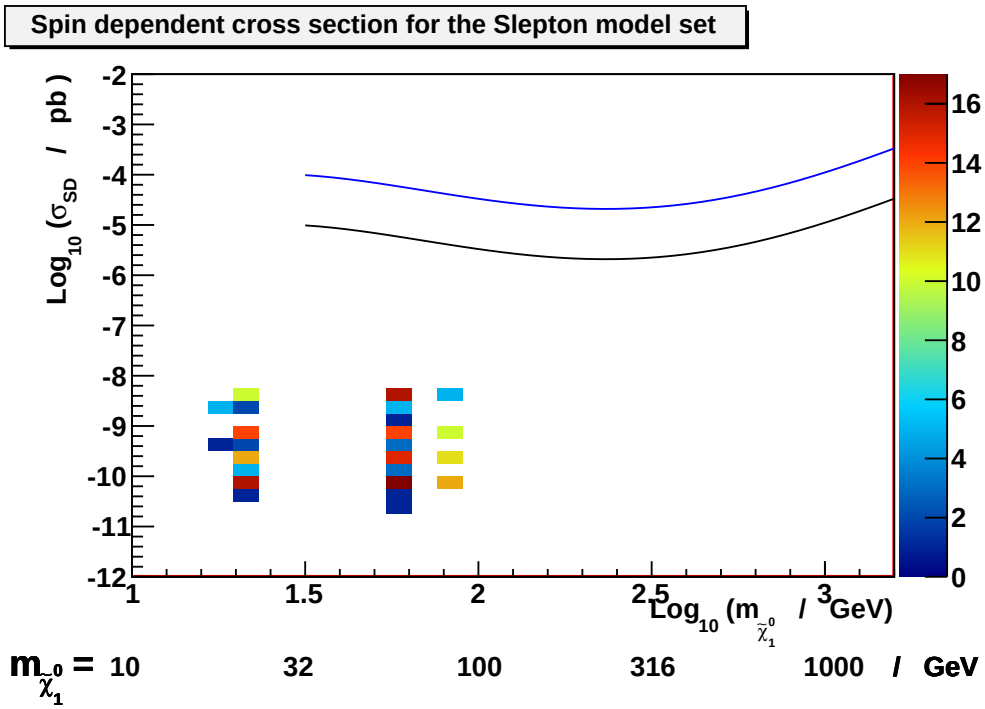

Figure 37: The spin dependent scattering cross section σ_{SD} as a function of the $\tilde{\chi}_1^0$ mass for the Slepton models. The blue line shows the projected upper limit from IceCube for 1 year of data taking. The black line shows the projected upper limit from IceCube, corresponding to 10 years of data taking. The colour coding shows the number of models in each bin.

4.5.3 Annihilation cross section

For indirect detection experiments, the gamma ray flux can provide limits on the annihilation cross section. The flux of gamma-rays from LSP pair annihilation in the galactic halo is proportional to $\langle \sigma v \rangle / m^2_{\tilde{\chi}^0_1}$ [Fermi-LAT11]. This quantity is shown as a function of the LSP mass in Fig. 38 - 40 for the three model sets. The current limits from Fermi [Fermi-LAT11] are shown in blue for the $(b\bar{b})$ annihilation channel and in green for the $(\tau^+\tau^-)$ annihilation channel. The projected limits from CTA [BMDG11] are shown in red.

The Fermi limits are several orders of magnitude above the annilation cross section for the Squark-gluino and Slepton models. For the Squark-gluino and Slepton model sets, no models are within the reach of CTA by several orders of magnitude. However, some of the Gaugino models with $m_{\tilde{\chi}^0_1} \gtrsim 100$ GeV have already been excluded by Fermi. These models are characterized by a very low mass difference between the lightest sfermion, in this case a squark, and the LSP: $\Delta m < 0.5$ GeV. As this only occurs for models with high LSP masses ($m_{\tilde{\chi}^0_1} \gtrsim 100$ GeV), it is difficult to motivate the high annihilation rate by Eq. (27), where the contribution from the sfermion and the LSP is equal. The CTA will be sensitive to more of the the models with high annihilation cross section, high mass and $\Delta m < 0.5$ GeV. However, this is a very constraining condition on the squark mass. One should also note that all these models correspond to squark masses below 400 GeV. Such masses of squarks have been excluded at the LHC for many models sets, for example in Ref. [ATLAS11].

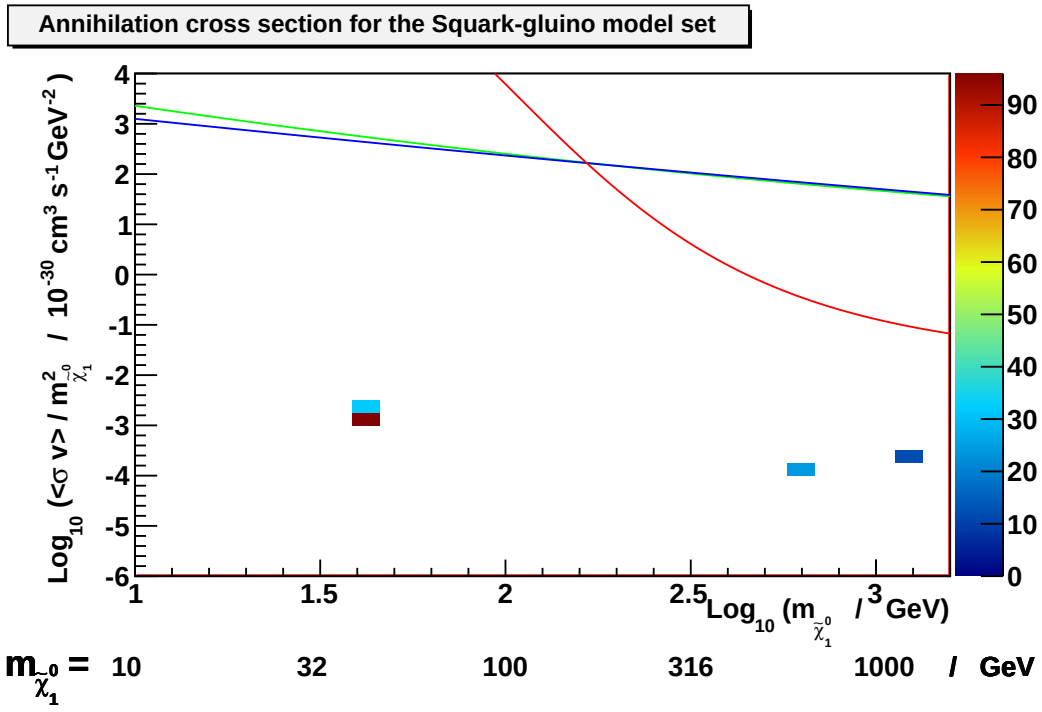

Figure 38: The annihilation cross section $\langle\sigma v\rangle/m^2_{\tilde{\chi}^0_1}$ as a function of the $\tilde{\chi}^0_1$ mass for the Squark-gluino model set. The blue and green curve are current limits from Fermi: the blue for the $b\bar{b}$ annihilation channel, and the green for the $\tau^+\tau^-$ channel. The red curve shows the projected sensitivity of CTA. The colour coding shows the number of models in each bin.

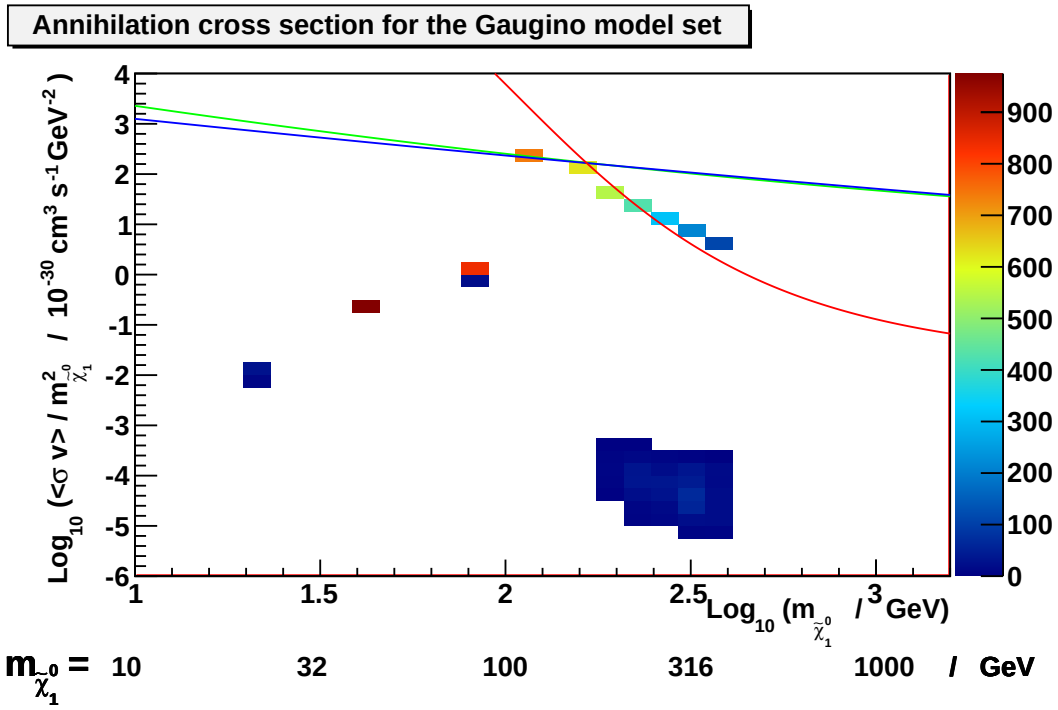

Figure 39: The annihilation cross section $\langle\sigma v\rangle/m^2_{\tilde{\chi}^0_1}$ as a function of the $\tilde{\chi}^0_1$ mass for the Gaugino model set. The blue and green curve are current limits from Fermi: the blue for the $b\bar{b}$ annihilation channel, and the green for the $\tau^+\tau^-$ channel. The red curve shows the projected sensitivity of CTA. The colour coding shows the number of models in each bin.

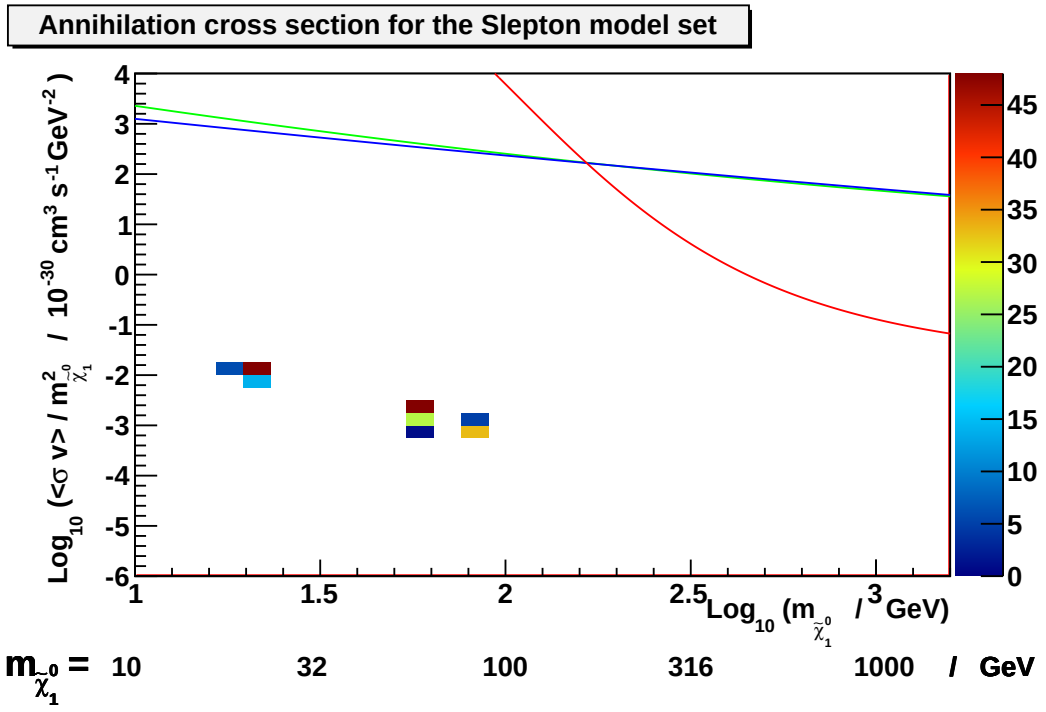

Figure 40: The annihilation cross section $\langle\sigma v\rangle/m^2_{\tilde{\chi}^0_1}$ as a function of the $\tilde{\chi}^0_1$ mass for the Slepton model set. The blue and green curve are current limits from Fermi: the blue for the $b\bar{b}$ annihilation channel, and the green for the $\tau^+\tau^-$ channel. The red curve shows the projected sensitivity of CTA. The colour coding shows the number of models in each bin.

4.5.4 Complementarity between the experiments

The complementarity between the LHC and the dark matter detection experiments is examined for the different model sets in Fig. 41 - 43. Models that are excluded by Fermi are represented by blue circles. Models that both LHC and another experiment will be sensitive to are shown as large red circles. Models that only the LHC will be sensitive to are shown as green pluses.

For the Squark-gluino model set, many models with $\sigma_{\mathrm{SI}} \approx 10^{-11}$ pb can be probed by XENON1t, as shown in Fig. 32. The projected exclusion curve for XENON1t goes up at high $\tilde{\chi}_1^0$ models, as seen in Fig. 32. As a consequence, XENON1t is not sensitive to some models with the same σ_{SI} but a higher $\tilde{\chi}_1^0$ mass. This is reflected by the overlap of the red circles and green pluses in Fig. 41.

For the Gaugino model set, it is shown in Fig. 33 and Fig. 39 that both the direct detection experiment XENON1t and the indirect detection experiment CTA are sensitive to many Gaugino models. As shown in Fig. 42, XENON1t and CTA together will not be sensitive to all the models in the Gaugino model set. At low values of both σ_{SI} and $\langle\sigma v\rangle/m^2_{\tilde{\chi}_1^0}$, only LHC will have sensitivity for the Gaugino models. Models with a high $\langle\sigma v\rangle/m^2_{\tilde{\chi}_1^0}$ are excluded by Fermi, as shown in Fig. 39.

Figure 43 shows the complementarity for the Slepton model set. Models with high σ_{SI} will be accessible by XENON1t, as shown in Fig. 34. Only the LHC will be sensitive to models with a low σ_{SI}.

In Fig. 44, all three model sets have been combined. Defining $x = \log_{10}(\langle\sigma v\rangle/m^2_{\tilde{\chi}_1^0}/[10^{-30}\mathrm{cm}^3\mathrm{s}^{-1}\ \mathrm{GeV}^{-2}])$, all models with an $x > -1$ in the graph belong to the Gaugino model set. These models are either excluded by Fermi, or will be with the reach of XENON1t or CTA. For $x < -1$ in Fig. 44, there are models from all three model sets. Some of them are accessible by XENON1t or CTA, other models only the LHC will have sensitivity to. The region that implies only LHC sensitivity has low values for both σ_{SI} and $\langle\sigma v\rangle/m_{\tilde{\chi}_1^0}$. These two variables are relevant for detection through scattering or through observation of annihilation products. For the LHC, however, it is the mass of the SUSY particles of a certain type that is relevant for production and detection. Ten years of IceCube measurements of σ_{SD} can not detect any of the models considered here.

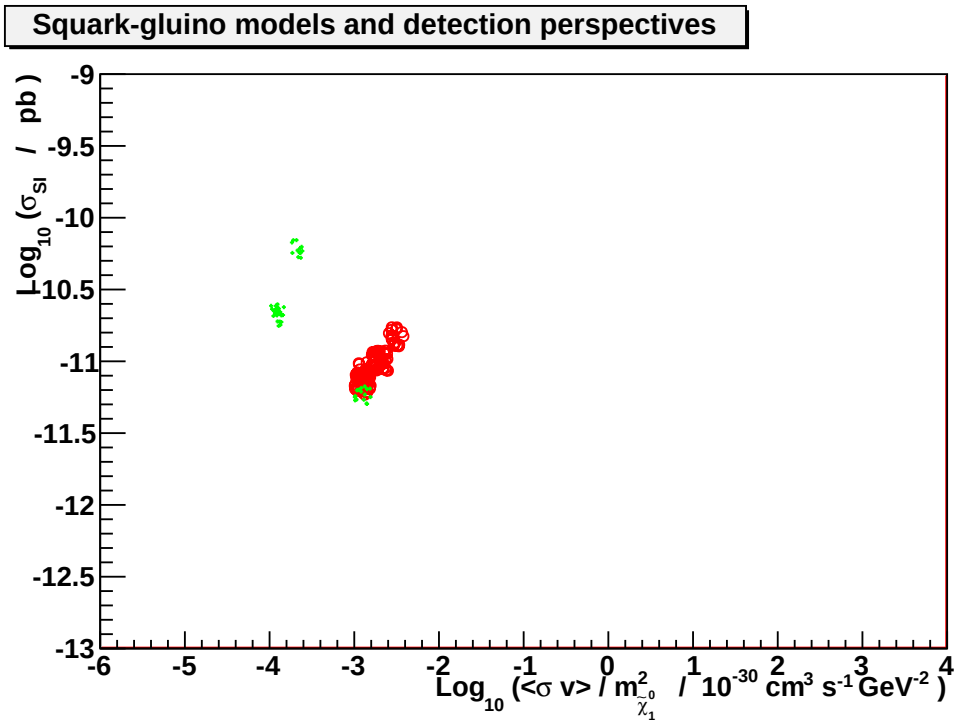

Figure 41: The complementarity of dark matter experiments for the Squark-gluino model set is shown. The green pluses show models that only LHC will be sensitive to. The small blue circles show models that have been excluded by the indirect detection results on measurements of the gamma ray flux by Fermi. The big red circles show models that both the LHC and a planned experiment (XENON1t or CTA) will be sensitive to. On the x-axis, the observable for indirect detection through gamma ray flux $\langle\sigma v\rangle/m^2_{\tilde{\chi}^0_1}$ is varied. On the y-axis, the observable for direct detection experiment $\sigma_{\rm SI}$ is varied.

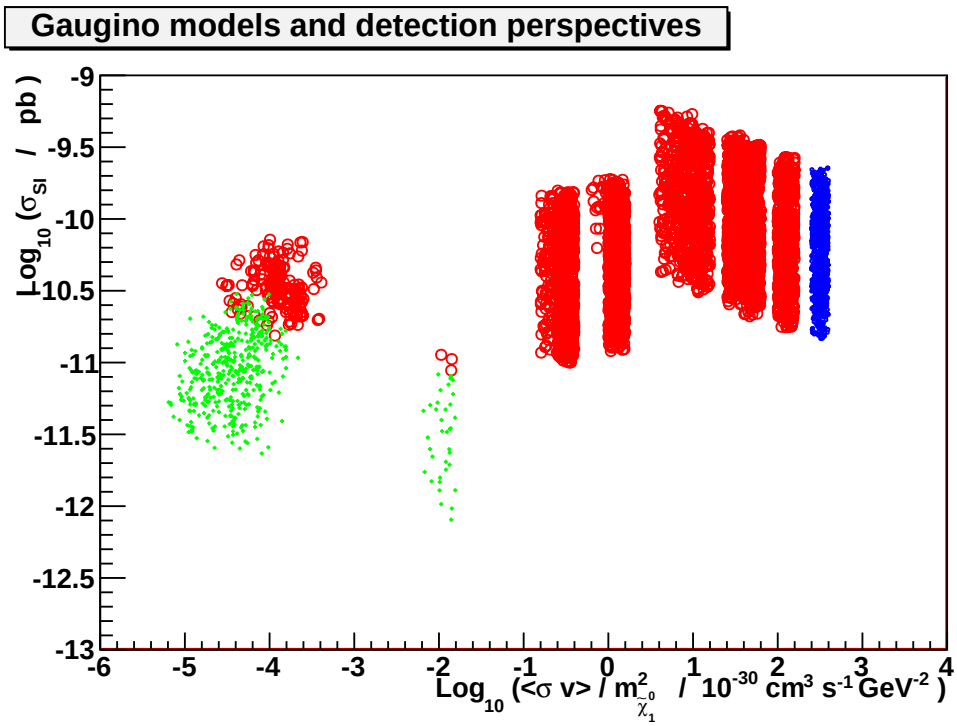

Figure 42: The complementarity of dark matter experiments for the Gaugino model set is shown. The green pluses show models that only LHC will be sensitive to. The small blue circles show models that have been excluded by the indirect detection results on measurements of the gamma ray flux by Fermi. The big red circles show models that both the LHC and a planned experiment (XENON1t or CTA) will be sensitive to. On the x-axis, the observable for indirect detection through gamma ray flux $\langle\sigma v\rangle/m^2_{\tilde{\chi}^0_1}$ is varied. On the y-axis, the observable for direct detection experiment $\sigma_{\rm SI}$ is varied.

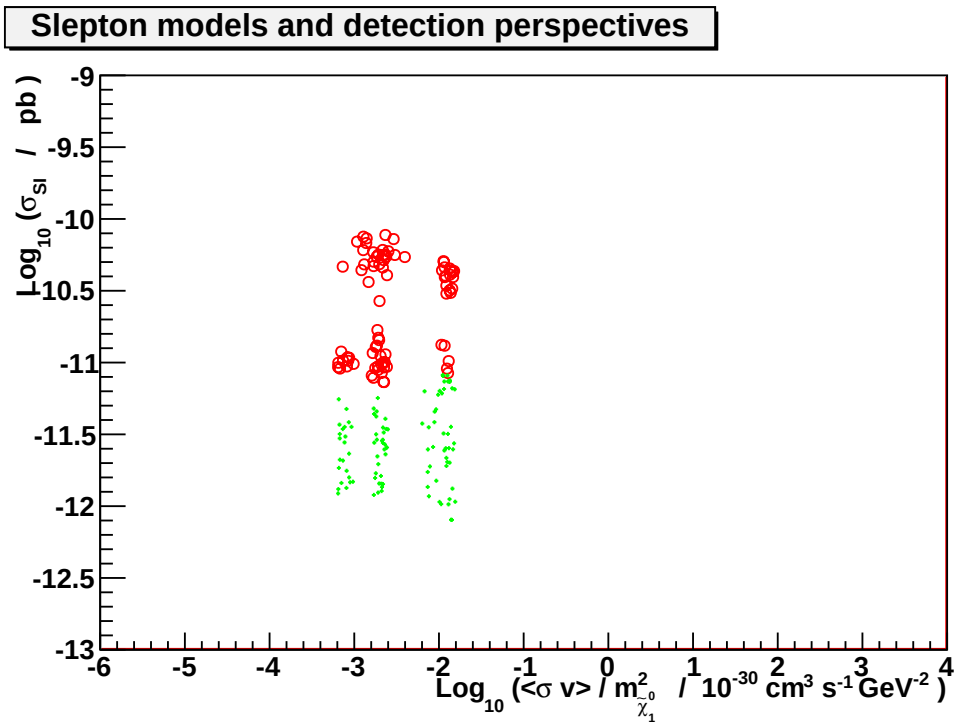

Figure 43: The complementarity of dark matter experiments for the Slepton model set is shown. The green pluses show models that only LHC will be sensitive to. The small blue circles show models that have been excluded by the indirect detection results on measurements of the gamma ray flux by Fermi. The big red circles show models that both the LHC and a planned experiment (XENON1t or CTA) will be sensitive to. On the x-axis, the observable for indirect detection through gamma ray flux $\langle \sigma v \rangle / m^2_{\tilde{\chi}^0_1}$ is varied. On the y-axis, the observable for direct detection experiment $\sigma_{\rm SI}$ is varied.

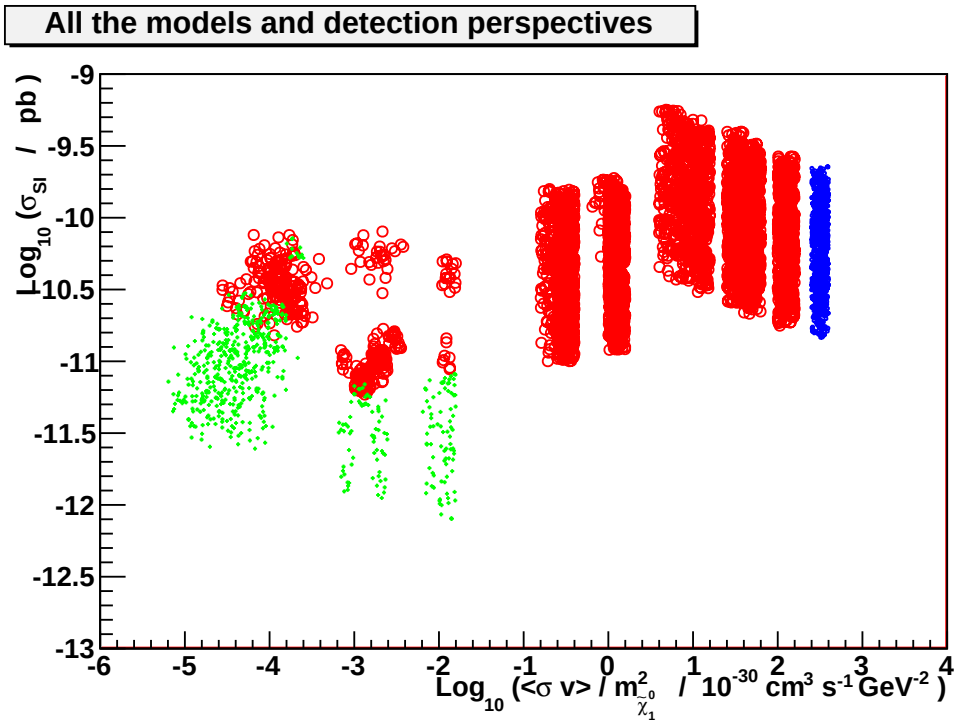

Figure 44: Summary of the complementarity of LHC with experiments for detection of dark matter. The green pluses show models that only LHC will be sensitive to. The small blue circles show models that have been excluded by the indirect detection results on measurements of the gamma ray flux by Fermi. The big red circles show models that both the LHC and a planned experiment (XENON1t or CTA) will be sensitive to. On the x-axis, the observable for indirect detection through gamma ray flux $\langle\sigma v\rangle/m^2_{\tilde{\chi}^0_1}$ is varied. On the y-axis, the observable for direct detection experiment $\sigma_{\rm SI}$ is varied.

4.6 Relationship between model parameters and scattering cross sections

Now the effect on some SUSY parameters on σ_{SI}, σ_{SD} is examined. Within the pMSSM, there are many different SUSY parameters that affect the scattering cross sections σ_{SI} and σ_{SD}. The correlations between different SUSY parameters and σ_{SI}, σ_{SD} are examined qualitatively here for the model sets described in Secs. 4.4.1 - 4.4.3. Only models that are compatible with the experimental constraints described in Sec. 2.4 are considered. Correlations for the parameter $\langle\sigma v\rangle/m^2_{\tilde{\chi}^0_1}$ are not investigated here because they were difficult to find. Any correlations observed here might not apply to the full pMSSM.

The starting point in selecting SUSY parameters is the Feynman diagrams for the processes that are shown in Fig. 25 and Fig. 27. Figure 25 shows that the spin independent cross section σ_{SI} can be mediated by the exchange of squarks or Higgs bosons. The relationship between the masses of these particles and σ_{SI} are examined. Figure 27 shows that a squark can also be exchanged in the spin dependent scattering, so the relationship to the squark mass is explored for σ_{SD} as well.

The effect of the Higgs boson mass on the spin indpenedent cross section is examined in Figs. 45 - 47. The Squark-gluino model set shows no clear dependence of σ_{SI} on the Higgs boson mass, as seen in Fig 45. For the Gaugino and Slepton model sets, Figs. 46 and 47, two separated regions emerge, one with $m_{h^0} < 116$ GeV and one with $m_{h^0} > 116$ GeV. Within each of these regions there appears to be a small negative correlation, based on the negative slope of the red and green areas. For all the models considered, a low Higgs boson mass $m_{h^0} < 116$ GeV is found to correspond to minimum stop mixing, while models with $m_{h^0} > 116$ GeV correspond to maximum stop mixing. The spread in σ_{SI} for a fixed mass of the Higgs boson in the Gaugino model set is by far larger than the dependence of σ_{SI} on the Higgs mass for the models considered here. Adjusting the Higgs boson mass does not appear to be a good strategy for extending this model set in order to find models with either higher or lower σ_{SI} for the Squark-gluino model and Gaugino model sets. The Slepton model set shows a larger negative correlation between the Higgs mass and σ_{SI}, especially for minimum stop mixing ($m_{h^0} < 116$ GeV). Varying the Higgs mass to generate models with other values for σ_{SI} may be a short-lived strategy in view of the expectation of finding or excluding the Higgs boson during 2012.

In Figs. 48 - 50, the mass of the lightest squark is examined in relation to the spin independent scattering cross section. Some negative correlation is observed between the mass of the lightest squark and σ_{SI} for the Gaugino model set (Fig. 49) and the Slepton model set (Fig. 50). No simple dependence was found for the Squark-gluino model set (48). By choosing higher squark masses in the Gaugino and Slepton model sets, models with lower

values for σ_{SI} may be found. The model sets can not be expanded towards lower squark masses as $m_{\tilde{q}}, m_{\tilde{g}} < 400$ GeV are generally already excluded by LHC experiments, such as Ref. [ATLAS11].

The relation of the squark mass to the spin dependent cross section is examined in Figs. 51 - 53. A negative correlation is seen clearly for the Squark-gluino and Slepton model sets. For the Squark-gluino model set, varying the squark mass between 400 GeV and 2 TeV changes σ_{SD} by five orders of magnitude. The spread in σ_{SD} for a fixed squark mass is of the size of the bin height at most. For the Gaugino model set (Fig. 51), there appear to be two groups of negatively correlated models, with different σ_{SD} for the same squark mass. For the Gaugino and Slepton model sets, models with higher squark masses can be generated to give lower spin dependent scattering cross sections. For the Squark-gluino model set, such an expansion is constrained since according to projections of the sensitivity of the LHC [BCPT96], [Pol96], squarks are only expected to be found within this decade if they have masses up to around 2 TeV.

In summary, expanding models with higher squark masses in the Gaugino and Slepton model sets is likely to result in models with lower σ_{SI} and σ_{SD}. In this part of the analysis, no simple way of generating models with higher σ_{SI} and σ_{SD} within the model sets was found. With a greater freedom for parameter values, the correlations should become weaker. As four different mass hierarchies were explored for the Gaugino model set, this may be the reason for the greater spread in σ_{SI} for the parameters explored than for the Slepton model set, which only has one mass heirarchy. The relationships were explored to find some simple guidelines when one wishes to explore the range of models that LHC is sensitive to. Varying the lightest squark mass over a wider range for the Gaugino and Slepton model sets could give new values for $\sigma_{\mathrm{SI}}, \sigma_{\mathrm{SD}}$ that LHC is sensitive to. Input from theoretical expressions relating $\sigma_{\mathrm{SI}}, \sigma_{\mathrm{SD}}$ to the SUSY parameters would be helpful in exploring the parameter space.

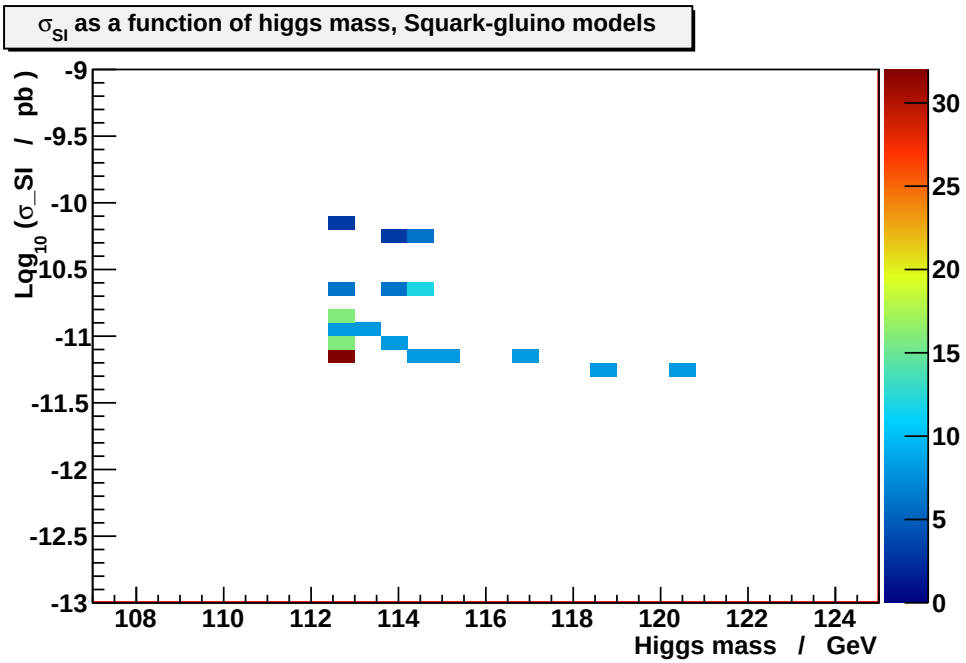

Figure 45: The spin independent cross section σ_{SI} as a function of the Higgs boson mass for the Squark-gluino model set. The colour coding shows the number of models in each bin. The models with a high Higgs boson mass $m_{h^0} > 116$ GeV correspond to maximum stop mixing.

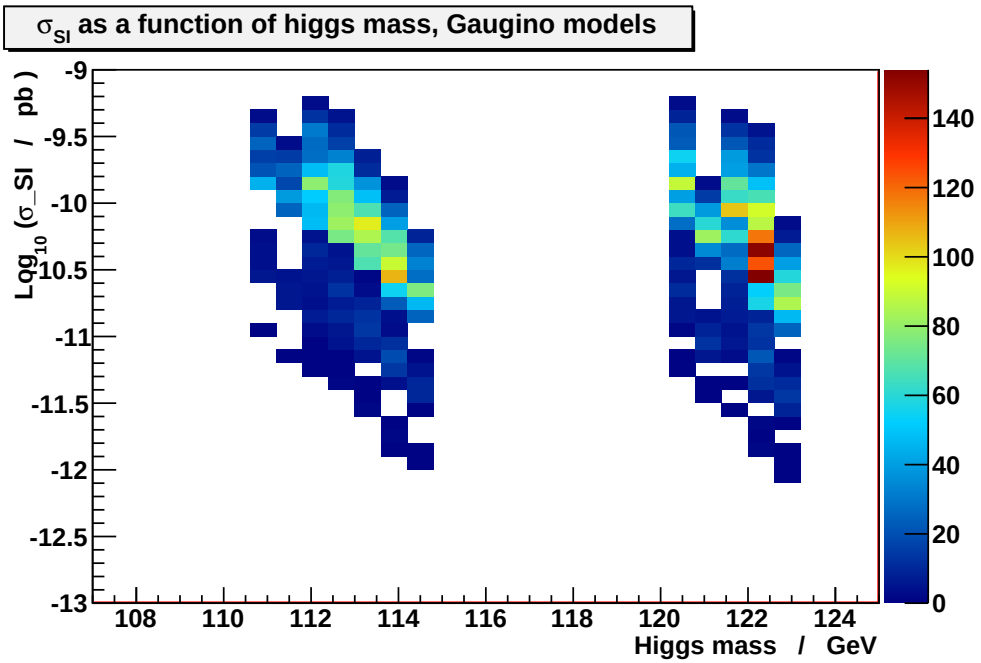

Figure 46: The spin independent cross section $\sigma_{\rm SI}$ as a function of the Higgs boson mass for the Gaugino model set. The colour coding shows the number of models in each bin. The models with a high Higgs mass $m_{h^0} > 116$ GeV correspond to maximum stop mixing.

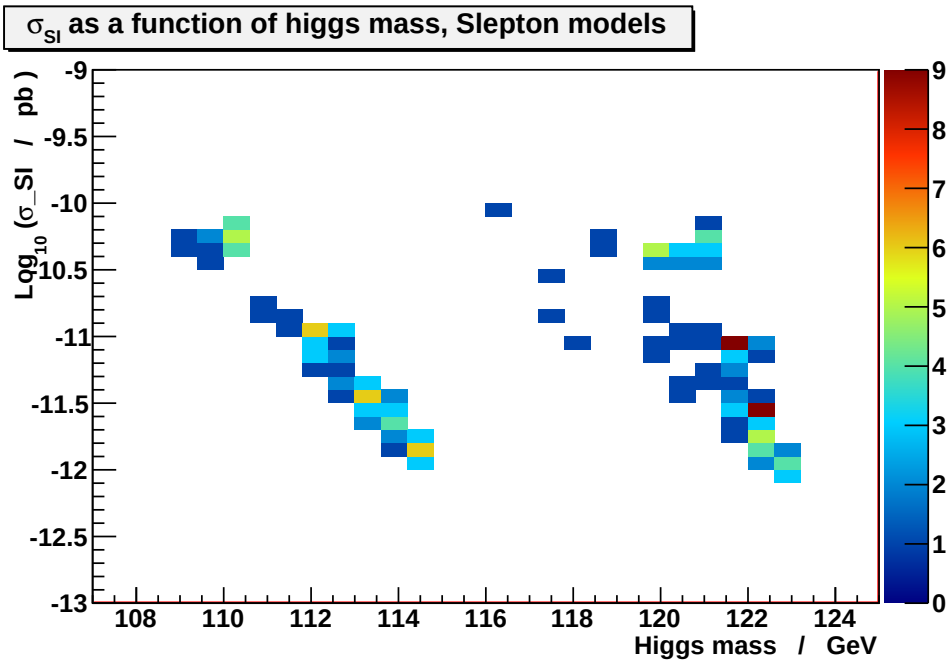

Figure 47: The spin independent cross section $\sigma_{\rm SI}$ as a function of the Higgs boson mass for the Slepton model set. The colour coding shows the number of models in each bin. The models with a high Higgs mass $m_{h^0} > 116$ GeV correspond to maximum stop mixing.

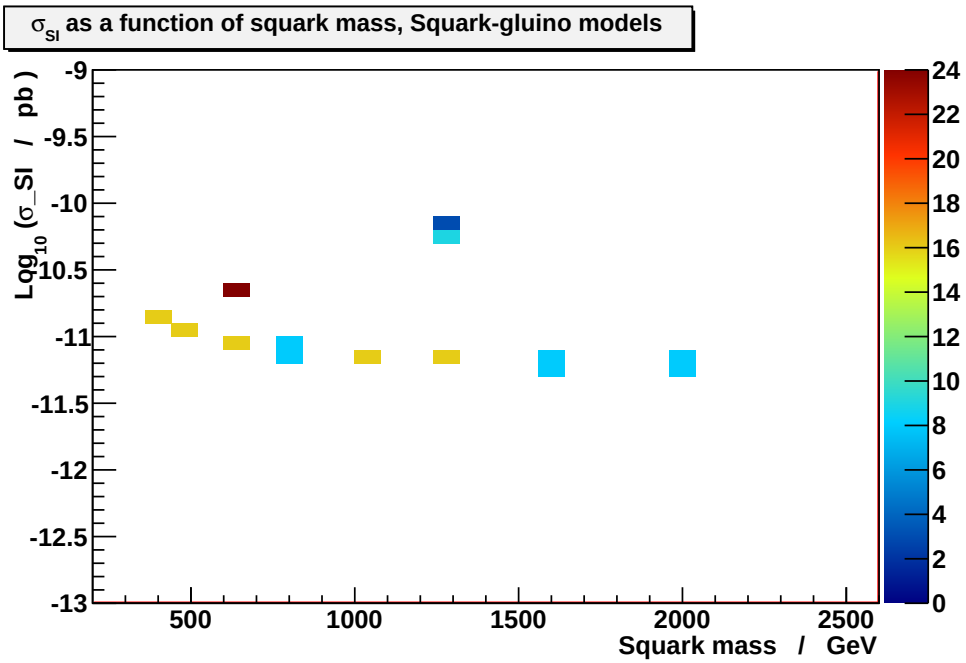

Figure 48: The spin independent scattering cross section σ_{SI} is shown as a function of the squark mass for the Squark-gluino model set. The colour coding shows the number of models in each bin.

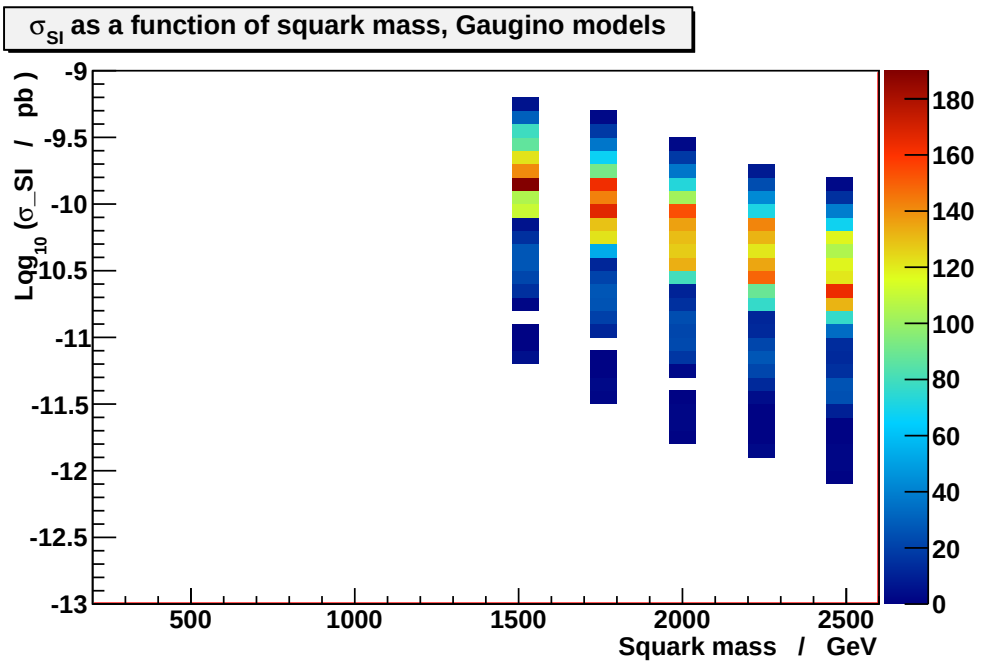

Figure 49: The spin independent scattering cross section σ_{SI} is shown as a function of the squark mass for the Gaugino model set. The colour coding shows the number of models in each bin.

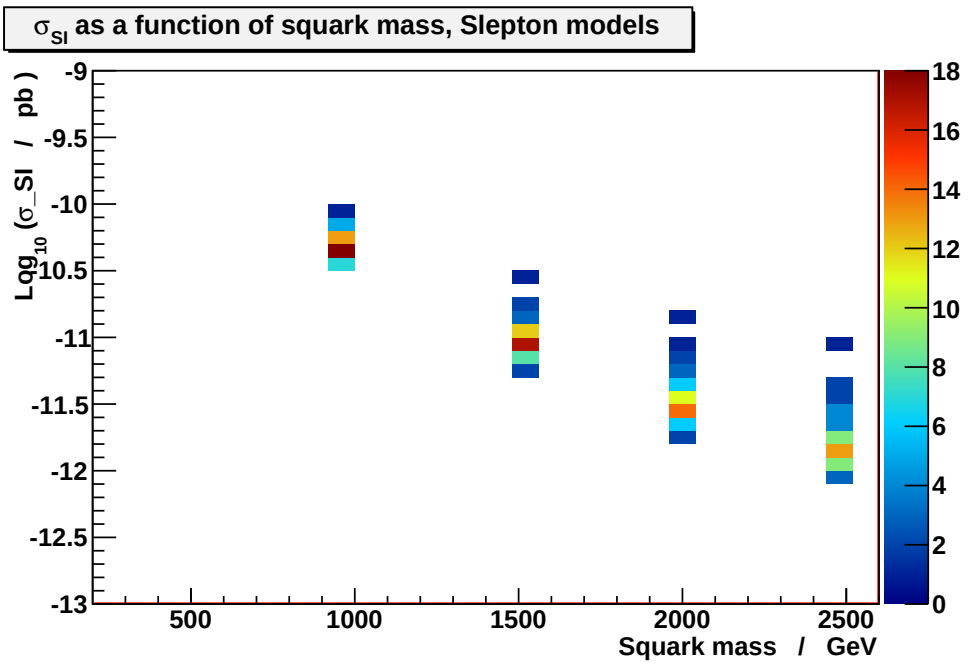

Figure 50: The spin independent scattering cross section σ_{SI} is shown as a function of the squark mass for the Slepton model set. The colour coding shows the number of models in each bin.

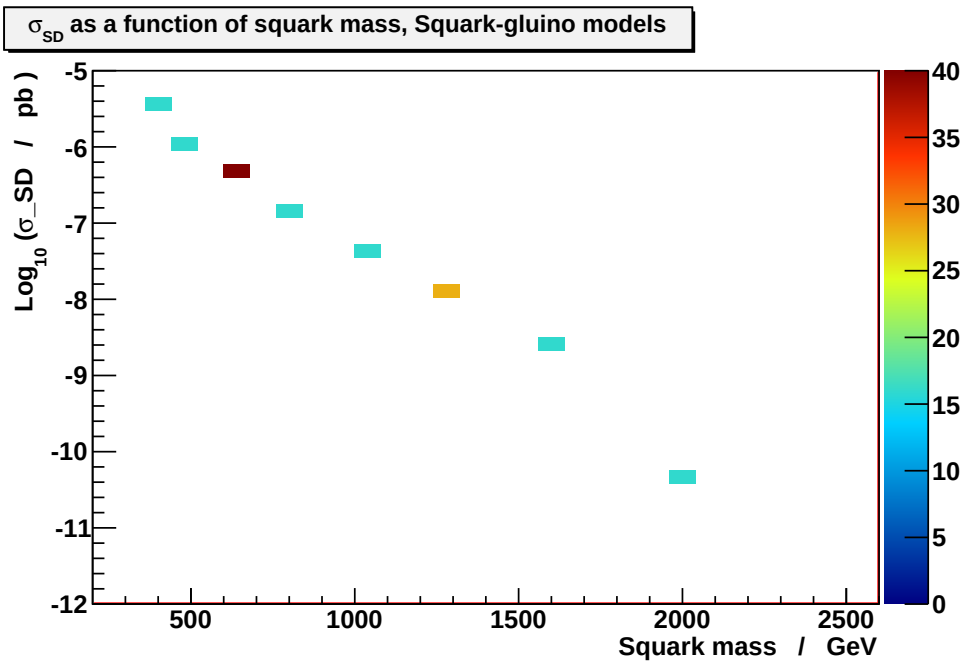

Figure 51: The spin dependent cross section σ_{SD} is shown as a function of the squark mass for the Squark-gluino model set. The colour coding shows the number of models in each bin.

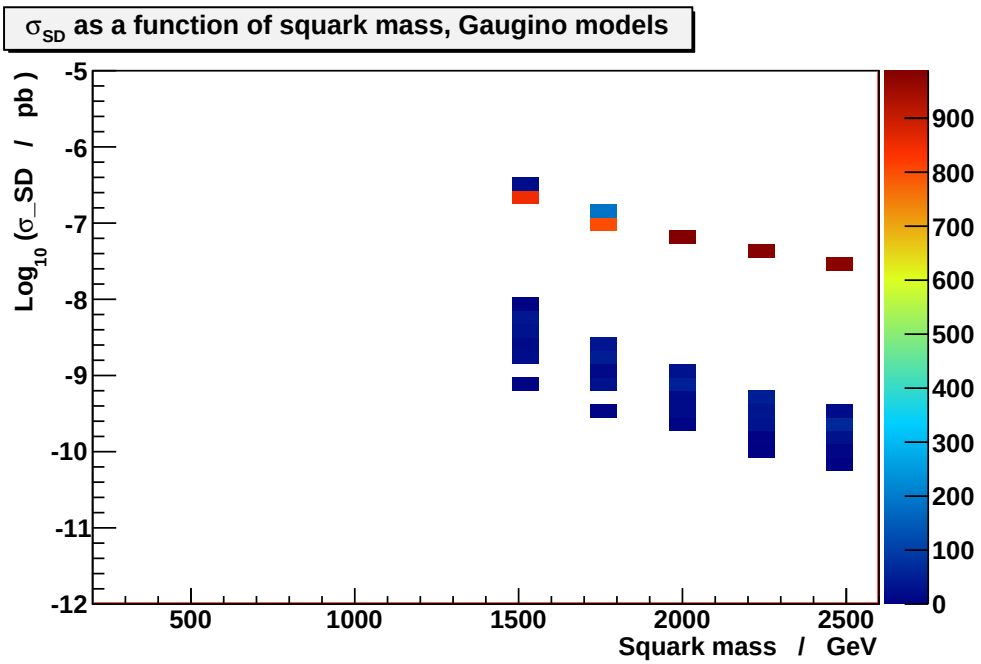

Figure 52: The spin dependent cross section σ_{SD} is shown as a function of the squark mass for the Gaugino model set. The colour coding shows the number of models in each bin.

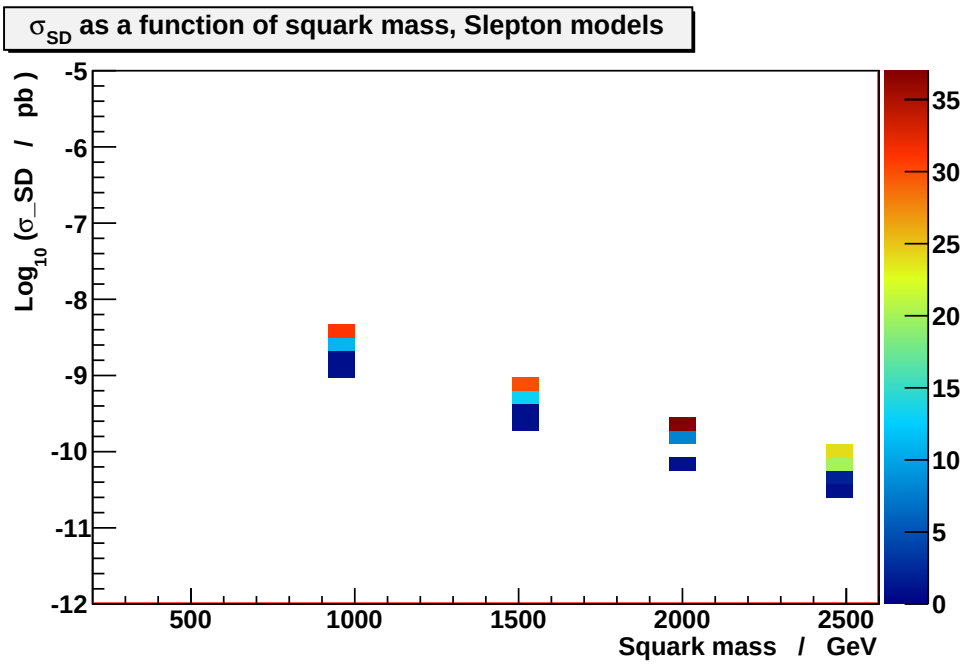

Figure 53: The spin dependent cross section σ_{SD} is shown as a function of the squark mass for the Squark-gluino model set. The colour coding shows the number of models in each bin.

4.7 Conclusions

The main results of the second part of this work is that there is a wide range of SUSY models which are compatible with contraints on relic dark matter density, Higgs boson mass and $\mathrm{Br}(b \to s + \gamma)$, that only LHC experiments should be sensitive to in this decade, as demonstrated in Fig. 44. In addition, there are models that both the LHC and other future experiments should be sensitive to. Some models that could be analyzed at the LHC are already excluded by Fermi. Among the planned experiments examined here, XENON1t will have the greatest overlap with LHC should exclude the majority of models introduced in this work.

In generating models that could be tested against data from the LHC, one could expand the parameter space in the following way, compared to the parameters used here. In the model sets considered in this work, the masses of left-handed and right-handed sleptons are equal. As shown in Sec. 3, a low right-handed slepton mass facilitates meeting constraints on dark matter. To meet Higgs boson mass constraints more easily, the region $3 < \tan\beta < 8$ can be explored for the squark-gluino models and the gaugino models. Low values of $\tan\beta$ generally correspond to a lower Higgs boson mass. Lower squark masses generally correspond to higher spin independent and spin dependent scattering cross sections, as shown in Fig. 49 - 53. A negative value for μ could give lower values for σ_{SI} [BBE11] if one wishes to explore models that are inacccessible by XENON.

Models with low spin independent cross section and low annihilation cross sections will be difficult to access with indirect detection experiments, as shown in Fig. 44. In this region, the LHC has a chance to find or exclude models that no other experiments will be sensitive to. Nevertheless, such a signal at the LHC would require some form of astrophysical confirmation before it can be solidly assigned to dark matter.

A Appendix

A.1 Gaugino production from squarks and gluinos

Production of charginos and neutralinos from squarks and gluinos, described in Sec. 3.4.3.2 occur via the following processes:

1. $\mathrm{Br}(\tilde{g} \to \tilde{\chi}_1^+ + d + \bar{u})$
2. $\mathrm{Br}(\tilde{g} \to \tilde{u}_L + \bar{u}) \cdot \mathrm{Br}(\tilde{u}_L \to \tilde{\chi}_1^+ + d)$

3. $\mathrm{Br}(\tilde{u}_L \to \tilde{\chi}_1^+ + d)$
4. $\mathrm{Br}(\tilde{u}_L \to \tilde{g} + u) \cdot \mathrm{Br}(\tilde{g} \to \tilde{\chi}_1^+ + d + \bar{u})$
5. $\mathrm{Br}(\tilde{u}_R \to \tilde{g} + u) \cdot \mathrm{Br}(\tilde{g} \to \tilde{\chi}_1^+ + d + \bar{u})$

6. $\mathrm{Br}(\tilde{d}_L \to \tilde{g} + d) \cdot \mathrm{Br}(\tilde{g} \to \tilde{\chi}_1^+ + d + \bar{u})$
7. $\mathrm{Br}(\tilde{d}_R \to \tilde{g} + d) \cdot \mathrm{Br}(\tilde{g} \to \tilde{\chi}_1^+ + d + \bar{u})$,

8. $\mathrm{Br}(\tilde{g} \to \tilde{\chi}_1^- + d + \bar{d})$
9. $\mathrm{Br}(\tilde{g} \to \tilde{d}_L + \bar{d}) \cdot \mathrm{Br}(\tilde{d}_L \to \tilde{\chi}_1^- + d)$

10. $\mathrm{Br}(\tilde{u}_L \to \tilde{g} + u) \cdot \mathrm{Br}(\tilde{g} \to \tilde{\chi}_1^- + d + \bar{d})$
11. $\mathrm{Br}(\tilde{u}_R \to \tilde{g} + u) \cdot \mathrm{Br}(\tilde{g} \to \tilde{\chi}_1^- + d + \bar{d})$,

12. $\mathrm{Br}(\tilde{d}_L \to \tilde{\chi}_1^- + u)$
13. $\mathrm{Br}(\tilde{d}_L \to \tilde{g} + d) \cdot \mathrm{Br}(\tilde{g} \to \tilde{\chi}_1^- + u + \bar{d})$
14. $\mathrm{Br}(\tilde{d}_R \to \tilde{g} + d) \cdot \mathrm{Br}(\tilde{g} \to \tilde{\chi}_1^- + u + \bar{d})$

15. $\mathrm{Br}(\tilde{g} \to \tilde{\chi}_2^0 + d + \bar{d})$
16. $\mathrm{Br}(\tilde{g} \to \tilde{\chi}_2^0 + u + \bar{u})$
17. $\mathrm{Br}(\tilde{g} \to \tilde{d}_L + \bar{d}) \cdot \mathrm{Br}(\tilde{d}_L \to \tilde{\chi}_2^0 + d)$
18. $\mathrm{Br}(\tilde{g} \to \tilde{u}_L + \bar{u}) \cdot \mathrm{Br}(\tilde{u}_L \to \tilde{\chi}_2^0 + u)$

19. $\mathrm{Br}(\tilde{u}_L \to \tilde{\chi}_2^0 + u)$

20. $\mathrm{Br}(\tilde{u}_L \to \tilde{g} + u) \cdot \mathrm{Br}(\tilde{g} \to \tilde{\chi}_2^0 + u + \bar{u})$

21. $\mathrm{Br}(\tilde{u}_R \to \tilde{g} + u) \cdot \mathrm{Br}(\tilde{g} \to \tilde{\chi}_2^0 + u + \bar{u})$

22. $\mathrm{Br}(\tilde{u}_L \to \tilde{g} + u) \cdot \mathrm{Br}(\tilde{g} \to \tilde{\chi}_2^0 + d + \bar{d})$

23. $\mathrm{Br}(\tilde{u}_R \to \tilde{g} + u) \cdot \mathrm{Br}(\tilde{g} \to \tilde{\chi}_2^0 + d + \bar{d})$

24. $\mathrm{Br}(\tilde{d}_L \to \tilde{\chi}_2^0 + d)$

25. $\mathrm{Br}(\tilde{d}_L \to \tilde{g} + d) \cdot \mathrm{Br}(\tilde{g} \to \tilde{\chi}_2^0 + d + \bar{d})$

26. $\mathrm{Br}(\tilde{d}_R \to \tilde{g} + d) \cdot \mathrm{Br}(\tilde{g} \to \tilde{\chi}_2^0 + d + \bar{d})$

27. $\mathrm{Br}(\tilde{d}_L \to \tilde{g} + d) \cdot \mathrm{Br}(\tilde{g} \to \tilde{\chi}_2^0 + u + \bar{u})$

28. $\mathrm{Br}(\tilde{d}_R \to \tilde{g} + d) \cdot \mathrm{Br}(\tilde{g} \to \tilde{\chi}_2^0 + u + \bar{u})$

Either gluinos undergo three-body decays, as in term 1, or they decay into gauginos in two steps via intermediate squarks, as in term 2. This is connected to the conservation of charge and baryon number.

Gaugino production from right-handed squarks occurs only if the squark decays into an intermediate gluino. Otherwise, the right-handed squarks decay directly into $\tilde{\chi}_1^0$ without producing leptons.

Production of positively charged charginos $\tilde{\chi}_1^+$ from negatively charged squarks $\tilde{d}$ only occurs if there are intermediate gluinos involved.

Acknowledgements

I want to thank my supervisor Johan Lundberg for finding time to help me, coaching me in programming and good advice. Many thanks to my supervisor Christophe Clement for pushing this project, for all the helpful suggestions and for the effort in the end rush. Thank you, Joakim Edsjö for the discussions and practical help. Tack, Tomas Bylund for all the support, discussions and practical help. Thanks, Yevgeni Bessidski, Tomas Bylund and Simon Tholerus for proof-reading and helpful suggestions. And many thanks to the entire Elementary Particle Physics Group for being awesome.

References

[AAD+11] S. AbdusSalam, B. Allanach, H. Dreiner, J. Ellis, U. Ellwanger et al., *Benchmark Models, Planes, Lines and Points for Future SUSY Searches at the LHC*, Eur.Phys.J. **C71**, 1835 (2011), 1109.3859.

[ADK+04] B. Allanach, A. Djouadi, J. Kneur, W. Porod and P. Slavich, *Precise determination of the neutral Higgs boson masses in the MSSM*, JHEP **0409**, 044 (2004), hep-ph/0406166.

[ADL+06] J. Alcaraz et al. (ALEPH and DELPHI and L3 and OPAL and LEP Electroweak Working Group Collaborations), *A Combination of preliminary electroweak measurements and constraints on the standard model*, (2006), hep-ex/0612034.

[ATL] An image of a collision in the ATLAS detector. Image credit: The ATLAS collaboration. The image is available at http://www.atlas.ch/fact-sheets-view.html.

[ATL11] C. ATLAS, Simple extrapolations for supersymmetry discovery limits at different LHC centre-of-mass energies and luminosities, based on inclusive searches with the ATLAS detector, Technical Report ATL-PHYS-PUB-2011-003, CERN, Geneva, Jan 2011.

[ATLAS11] G. Aad et al. (ATLAS Collaboration), *Search for supersymmetric particles in events with lepton pairs and large missing transverse momentum in $\sqrt{s}$ = 7 TeV proton-proton collisions with the ATLAS experiment*, Eur.Phys.J. **C71**, 1682 (2011), 1103.6214.

[BBE11] L. Bergström, T. Bringmann and J. Edsjö, *Complementarity of direct dark matter detection and indirect detection through gamma-rays*, Phys.Rev. **D83**, 045024 (2011), 1011.4514.

[BBH+10] P. Bechtle, O. Brein, S. Heinemeyer, G. Weiglein and K. E. Williams, *HiggsBounds: Confronting Arbitrary Higgs Sectors with Exclusion Bounds from LEP and the Tevatron*, Comput.Phys.Commun. **181**, 138–167 (2010), 0811.4169, 64 pages, 15 tables, 8 figures/ three typos which made it to the published version corrected/ the code (currently version 3.0.0beta including LHC Higgs search results) is available via: http://projects.hepforge.org/higgsbounds/.

[BCPT94] H. Baer, C.-h. Chen, F. Paige and X. Tata, *Detecting sleptons at hadron colliders and supercolliders*, Phys. Rev. D **49**, 3283–3290 (Apr 1994).

[BCPT95] H. Baer, C.-h. Chen, F. Paige and X. Tata, *Signals for minimal supergravity at the CERN large hadron collider: Multi - jet plus missing energy channel*, Phys.Rev. **D52**, 2746–2759 (1995), hep-ph/9503271.

[BCPT96] H. Baer, C.-h. Chen, F. Paige and X. Tata, *Signals for minimal supergravity at the CERN large hadron collider. 2: Multi - lepton channels*, Phys.Rev. **D53**, 6241–6264 (1996), hep-ph/9512383.

[BG04] L. Bergström and A. Goobar, *Cosmology and particle astrophysics*, Praxis Publishing Ltd, 2004.

[BHS96] W. Beenakker, R. Hopker and M. Spira, *PROSPINO: A Program for the production of supersymmetric particles in next-to-leading order QCD*, (1996), hep-ph/9611232.

[BMDG11] P. Brun, E. Moulin, J. Diemand and J.-F. Glicenstein, *Searches for dark matter subhaloes with wide-field Cherenkov telescope surveys*, Phys.Rev. **D83**, 015003 (2011), 1012.4766.

[BPPT09] H. Baer, F. Paige, S. Protopopescu and X. Tata, ISAJET 7.80, 2009, http://www.nhn.ou.edu/ isajet/.

[CBG+06] D. Clowe, M. Bradac, A. H. Gonzalez, M. Markevitch, S. W. Randall et al., *A direct empirical proof of the existence of dark matter*, Astrophys.J. **648**, L109–L113 (2006), astro-ph/0608407.

[CMB] "The image of the CMB was created by the NASA / WMAP Science Team. It is available at http://map.gsfc.nasa.gov/media/101080/index.html".

[DK98] K. R. Dienes and C. Kolda, Supersymmetry and particle physics: a roadmap of future directions. oai:cds.cern.ch:361414, Technical Report CERN-TH-98-015. IASSNS-HEP-98-04, CERN, Geneva, Feb 1998.

[EG97] J. Edsjo and P. Gondolo, *Neutralino relic density including coannihilations*, Phys.Rev. **D56**, 1879–1894 (1997), hep-ph/9704361.

[Erl10] J. Erler, *Mass of the Higgs boson in the standard electroweak model*, Phys. Rev. D **81**, 051301 (Mar 2010).

[Fay76] P. Fayet, *Supersymmetry and Weak, Electromagnetic and Strong Interactions*, Phys. Lett. **B64**, 159 (1976).

[Fer] "A photograph of photomultiplier tube arrays in the XENON100 detector. Credit: the Fermi collaboration. The photograph is available at glast-isoc.slac.stanford.edu/pages/assets/",.

[Fermi-LAT11] M. Ackermann et al. (Fermi-LAT Collaboration), *Constraining Dark Matter Models from a Combined Analysis of Milky Way Satellites with the Fermi Large Area Telescope*, Phys.Rev.Lett. **107**, 241302 (2011), 1108.3546.

[FF78] G. R. Farrar and P. Fayet, *Phenomenology of the Production, Decay, and Detection of New Hadronic States Associated with Supersymmetry*, Phys. Lett. **B76**, 575–579 (1978).

[Fuc00] B. Fuchs, *The amount of dark matter in spiral galaxies*, (2000), astro-ph/0010358.

[GEU+04] P. Gondolo, J. Edsjo, P. Ullio, L. Bergstrom, M. Schelke et al., *DarkSUSY: Computing supersymmetric dark matter properties numerically*, JCAP **0407**, 008 (2004), astro-ph/0406204.

[(HFAG)07] E. Barberio et al. (Heavy Flavor Averaging Group (HFAG) Collaboration), *Averages of b-hadron properties at the end of 2006*, (2007), 0704.3575.

[HHRW07] S. Heinemeyer, W. Hollik, H. Rzehak and G. Weiglein, *The Higgs sector of the complex MSSM at two-loop order: QCD contributions*, Phys.Lett. **B652**, 300–309 (2007), 0705.0746.

[Ice] "Antarctic penguins, photographed by Hagar Landsman from the IceCube team. The photograph is available at http://icecube.wisc.edu/gallery".

[IceCube11] R. Abbasi et al. (The IceCube Collaboration), *The IceCube Neutrino Observatory IV: Searches for Dark Matter and Exotic Particles*, (2011), 1111.2738.

[JKG96] G. Jungman, M. Kamionkowski and K. Griest, *Supersymmetric dark matter*, Physics Reports **267**(5–6), 195 – 373 (1996).

[LDH+11] D. Larson, J. Dunkley, G. Hinshaw, E. Komatsu, M. Nolta et al., *Seven-Year Wilkinson Microwave Anisotropy Probe (WMAP) Observations: Power Spectra and WMAP-Derived Parameters*, Astrophys.J.Suppl. **192**, 16 (2011), 1001.4635.

[Lid03] A. Liddle, *An Introduction To Modern Cosmology*, WILEY, 2003.

[MAB+07] M. Misiak, H. Asatrian, K. Bieri, M. Czakon, A. Czarnecki et al., *Estimate of BR(B → X_s gamma) at O(alpha$_S^2$)*, Phys.Rev.Lett. **98**, 022002 (2007), hep-ph/0609232.

[Mar97] S. P. Martin, *A Supersymmetry primer*, (1997), hep-ph/9709356.

[MPR98] M. Misiak, S. Pokorski and J. Rosiek, *Supersymmetry and FCNC effects*, Adv.Ser.Direct.High Energy Phys. **15**, 795–828 (1998), hep-ph/9703442, To appear in the Review Volume 'Heavy Flavors II', eds. A.J. Buras and M. Lindner, Advanced Series on Directions in High-Energy Physics, World Scientific Publishing Co., Singapore.

[MS93] F. Mandl and G. Shaw, *Quantum Field Theory, Revised Edition*, Wiley, 1993.

[Nak10] K. e. a. P. D. G. Nakamura, *2011 Review of Particle Physics*, J. Phys. **G 37**, 075021 (2010), with 2011 partial update for the 2012 edition. Cut-off date for this update was January 15, 2011.

[NAS] "A composite image of the matter content in galaxy cluster 1E 0657-56, known as the Bullet Cluster", Composite Credit: X-ray: NASA/CXC/CfA/ M.Markevitch et al.; Lensing Map: NASA/STScI; ESO WFI; Magellan/U.Arizona/ D.Clowe et al. Optical: NASA/STScI; Magellan/U.Arizona/D.Clowe et al.

[Ni09] K. Ni, The data for the projected sensitivity of XENON1t, 2009, originates from a private communication with Kaixuan Ni 090516 and is available at dmtools.brown.edu.

[Pol96] G. Polesello, *Searches for SUSY at LHC*, Acta Physica Polonica B **27**, 3869–3880 (1996), Presented at the XXXVI Cracow School of Theoretical Physics, Zkopane, Poland, June 1-11, 1996.

[PS95] M. E. Peskin and D. V. Schroeder, *"An Introduction to Quantum Field Theory"*, Westview Press, 1995.

[tag03] *Search for the Standard Model Higgs boson at LEP*, Physics Letters B **565**(0), 61 – 75 (2003).

[WE09] G. Wikstrom and J. Edsjo, *Limits on the WIMP-nucleon scattering cross-section from neutrino telescopes*, JCAP **0904**, 009 (2009), 0903.2986.

[WMA] "The illustration of the WMAP leaving the orbit of the earth CMB was created by the NASA / WMAP Science Team. It is available at http://map.gsfc.nasa.gov/media/990387/index.html".

[XEN] "A photograph of photomultiplier tube arrays in the XENON100 detector. Credit: the XENON collaboration. The photograph is available at http://map.gsfc.nasa.gov/media/101080/index.html".

[XENON10011] E. Aprile et al. (XENON100 Collaboration), *Dark Matter Results from 100 Live Days of XENON100 Data*, Phys.Rev.Lett. **107**, 131302 (2011), 1104.2549.

[Zer10] P. Zerwas, Supersymmetry: The Search for the Higgs Boson, in *PreSUSY lecture, 18th International Conference on Supersymmetry and Unification of Fundamental Interactions, Bonn*, 2010, http://susy10.uni-bonn.de/data/zerwas-bonn.pdf.